IOWA STATE UNIVERSITY
Digital Repository

Retrospective Theses and Dissertations

Iowa State University Capstones, Theses and Dissertations

1992

The effect of electrochemical reactions on the surface film composition and corrosion resistance of aluminum in acid solutions

Ching-Feng Lin
Iowa State University

Follow this and additional works at: https://lib.dr.iastate.edu/rtd

 Part of the Chemical Engineering Commons

Recommended Citation

Lin, Ching-Feng, "The effect of electrochemical reactions on the surface film composition and corrosion resistance of aluminum in acid solutions " (1992). *Retrospective Theses and Dissertations*. 10380.
https://lib.dr.iastate.edu/rtd/10380

This Dissertation is brought to you for free and open access by the Iowa State University Capstones, Theses and Dissertations at Iowa State University Digital Repository. It has been accepted for inclusion in Retrospective Theses and Dissertations by an authorized administrator of Iowa State University Digital Repository. For more information, please contact digirep@iastate.edu.

INFORMATION TO USERS

This manuscript has been reproduced from the microfilm master. UMI films the text directly from the original or copy submitted. Thus, some thesis and dissertation copies are in typewriter face, while others may be from any type of computer printer.

The quality of this reproduction is dependent upon the quality of the copy submitted. Broken or indistinct print, colored or poor quality illustrations and photographs, print bleedthrough, substandard margins, and improper alignment can adversely affect reproduction.

In the unlikely event that the author did not send UMI a complete manuscript and there are missing pages, these will be noted. Also, if unauthorized copyright material had to be removed, a note will indicate the deletion.

Oversize materials (e.g., maps, drawings, charts) are reproduced by sectioning the original, beginning at the upper left-hand corner and continuing from left to right in equal sections with small overlaps. Each original is also photographed in one exposure and is included in reduced form at the back of the book.

Photographs included in the original manuscript have been reproduced xerographically in this copy. Higher quality 6" x 9" black and white photographic prints are available for any photographs or illustrations appearing in this copy for an additional charge. Contact UMI directly to order.

U·M·I

University Microfilms International
A Bell & Howell Information Company
300 North Zeeb Road, Ann Arbor, MI 48106-1346 USA
313/761-4700 800/521-0600

Order Number 9302008

The effect of electrochemical reactions on the surface film composition and corrosion resistance of aluminum in acid solutions

Lin, Ching-Feng, Ph.D.

Iowa State University, 1992

U·M·I
300 N. Zeeb Rd.
Ann Arbor, MI 48106

The effect of electrochemical reactions on the surface film composition and corrosion resistance of aluminum in acid solutions

by

Ching-Feng Lin

A Dissertation Submitted to the

Graduate Faculty in Partial Fulfillment of the

Requirements for the Degree of

DOCTOR OF PHILOSOPHY

Department: Chemical Engineering
Major: Chemical Engineering

Approved:

Signature was redacted for privacy.

In Charge of Major Work

Signature was redacted for privacy.

For the Major Department

Signature was redacted for privacy.

For the Graduate College

Iowa State University
Ames, Iowa

1992

TABLE OF CONTENTS

GENERAL INTRODUCTION

Present State of Knowledge on Pitting Corrosion

Aluminum has a passive oxide layer on its surface which protects the metal from corrosion. The role of the passive layer on the metal surface is to reduce the transport rate of reactant species through the layer, therefore, to decrease the corrosion rate (1). Most important technological problems in corrosion involve localized corrosion such as pitting corrosion. Pitting corrosion of passive metals such as aluminum is caused by a local breakdown of the passive oxide film, which exposes the metal to aqueous solution containing aggressive anions (see Figure 1). Usually, the rate of pit initiation is measured by the induction time, that is, the time it takes to form the first pit on a passive metal exposed to a solution containing aggressive anions (e.g., Cl^-). The induction time depends on Cl^- concentration, electrode potential and the quality of the passive film.

During the past three decades, a great deal of work concerning the process leading to the breakdown of passivity has been published. This section will briefly describe the present state of knowledge on localized breakdown of the passive film and pit initiation. Complete reviews of the localized corrosion literature can be found in the works of Galvele (2), Strehblow (3), Szklarska-Smialowska (4) and Bohni (5).

The pitting potential, i.e., the potential at which the passive film begins to break down locally, is one of the most important features characterizing the susceptibility of metals to pitting corrosion. Internal and environmental factors which affect the pitting

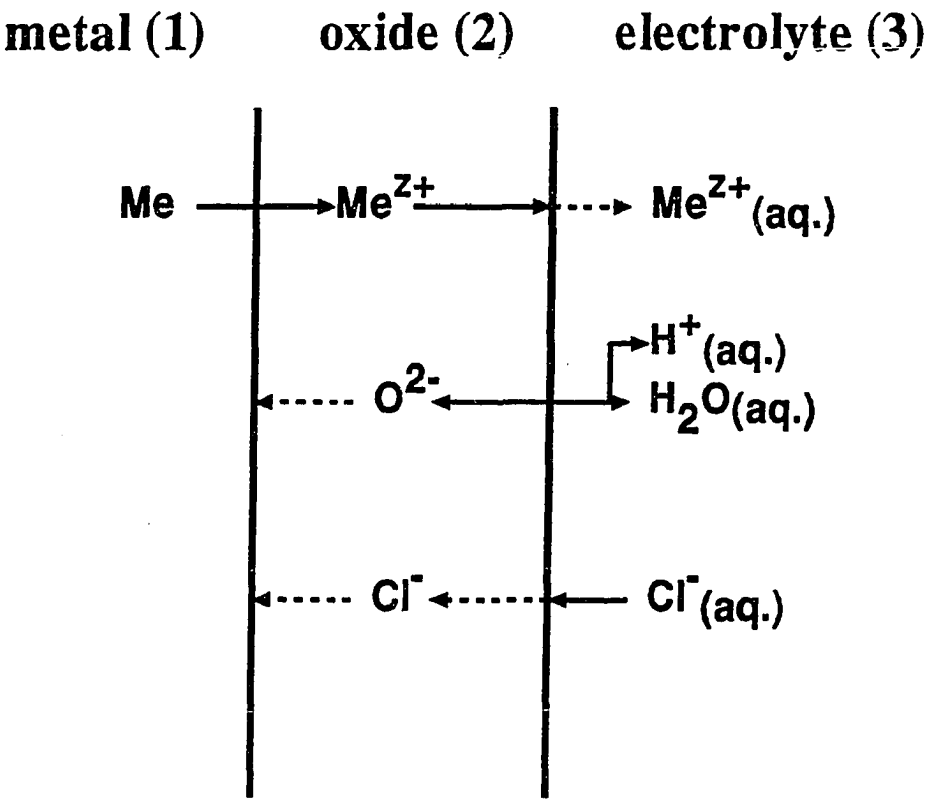

Figure 1. Schematic representation of passive metal in Cl^- ions containing solution.

potential, and therefore pit initiation, have been widely reported in the literature (2-6). Among these factors, halide ions, pH, and nature of passive oxide film have received considerable attention. A simple relationship between pitting potential, E_p, and the concentration of aggressive anion $[C_x]$ has been reported (11-13),

$$E_p = A - B \cdot \log[C_x] \qquad [1]$$

where B is an empirical constant dependent on the electrolyte composition, the measurement technique and the type of metal involved. The dependence of the pitting potential on chloride concentration indicates that chloride ions participate in the film breakdown process. Possible roles for chloride ions include adsorption at the film/solution interface, followed by reaction with the film. Recently, a new variable, prior cathodic polarization, which influences pit initiation on aluminum foil has been studied by Lin and Hebert (7,8). The nucleation rate and the early growth rate of pits are found to be dramatically accelerated by prior cathodic polarization. The role of cathodic charging is to chemically or structurally modify the surface film in some way which promotes anodic pitting. A chemical mechanism, i.e., a cathodic reaction product serving as an anodic reactant, was suggested by the authors for the observed cathodic enhancement.

There have been several models proposed for film breakdown and pit initiation based on observations of effects of various environmental conditions on pitting. The most common mechanisms proposed for pitting are: (a) ion penetration mechanism, (b) mechanical film breakdown mechanism, (c) competitive adsorption theory, (d) flaw and

oxide film defect model and (e) point defect model. These models have been reviewed in detail in the literature (4,5). No complete agreement exists on the essential causes and mechanisms of pit initiation (4), and especially for aluminum, the mechanism of pit initiation is a matter of controversy (9). Recently, a vacancy diffusion mechanism for pitting corrosion of aluminum has been proposed by Wiersma and Hebert (10) to explain observations about early growth of pits during anodic etching of aluminum. This mechanism is able to explain the equivalence between cathodic charge and pit volume found by Lin and Hebert (7).

Cathodic Polarization of Aluminum

It is necessary to investigate the reactions occurring and products produced during cathodic polarization of aluminum before the mechanism of the subsequent anodic pitting can be inferred.

Cathodic hydrogen evolution from acidic solutions has been studied extensively (11-15), and the mechanism has been considered (11) as an initial discharge step (step 1),

$$H_3^+O + e^- + M \rightarrow MH + H_2O \qquad [2]$$

followed by electrochemical desorption (step 2),

$$H_3O^+ + e^- + MH \rightarrow M + H_2 + H_2O \qquad [3]$$

or by atomic recombination (step 3),

$$MH + MH \rightarrow 2M + H_2 \qquad [4]$$

Vijh (11) has studied hydrogen evolution on aluminum in acidic solutions and concluded that the initial discharge step is the likely rate determining step.

The mechanism of the hydrogen evolution reaction on aluminum covered by a "natural" surface oxide film in neutral solutions has been studied by Vijh (16). Tafel slopes much larger than 2.3x2RT/F was obtained by short polarizations, while on long polarizations, some cathodic "activation" is manifested, which also reduces Tafel slops to 2.3x2RT/F approximately. Vijh suggested that the high Tafel slopes observed on oxide-covered aluminum are, most likely, values of 2.3x2RT/F which have been modified by the presence of oxide. A Tafel slope of 0.325V for Al in 0.5N NaCl at pH 5 has been reported by Kunze (17). Kunze has also reported for this system that, at a potential of ~-1.6V, the current increased rapidly while the potential remained appreciably constant. Recently, Tafel slope of 0.11V for potentials more negative than -1.75V *vs.* SCE in neutral solutions of 2M NaCl was reported by Radoševič *et al.* (18), which was attributed to be due to hydration of the oxide layer at potentials more negative than -1.7V, whereupon hydrogen is evolved at the metal/film interface. These authors also concluded that substance other than gaseous hydrogen are produced at cathodic potentials, which are then involved in an oxidation reaction upon return to the original open-circuit potential.

Cathodic polarization of aluminum has received wide attention (19-23) mainly in relation to corrosion of aluminum occurring in the potential region below the open circuit

potential. In this negative potential region, hydrogen evolution due to hydrogen ion reduction and water reduction takes place,

$$H^+ + e^- \rightarrow \frac{1}{2}H_2 \qquad [5]$$

$$H_2O + e^- \rightarrow OH^- + \frac{1}{2}H_2 \qquad [6]$$

resulting the increase of pH at metal surface. Kasesche (19) has observed an increase of aluminum corrosion in sulfate solution caused by the cathodic polarization. Van de Ven and Koelmans (20) have studied the cathodic corrosion of aluminum in NaCl solution and found that the rate of corrosion is limited by the chemical dissolution reaction,

$$Al + OH^- + H_2O \rightarrow AlO_2^- + \frac{3}{2}H_2 \qquad [7]$$

Part of the OH^- ions produced are carried away from the cathode surface into the electrolyte by diffusion and electrical migration (19). It should be noted that the authors stripped the oxide films before weighing the aluminum, and thus could not distinguish solid and dissolved reaction products.

On the other hand, Vedder and Vermilyea (21) studied the oxidation of aluminum in water, and found that the oxidation reaction is continuous and a layer of aluminum hydroxide is formed. In the case of a large cathodic current applied (1 mA/cm^2), the rate of hydroxide formation increases, as measured by both weight change and the OH bend of the infrared spectrum of the oxide film. This result shows that a solid corrosion

product is produced under cathodic polarization. It is possible that cathodically generated hydroxide or water can also participate in the subsequent anodic metal dissolution reaction in the cathodic-anodic etching experiments considered in the present research.

Recently, Radoševič *et al.* (18) have studied the cathodic processes occurring on aluminum in neutral 2M NaCl solution. The authors claimed the presence of some substances other than gaseous hydrogen, formed at potentials more negative than -1.7V *vs.* SCE. The substance, assumed to be aluminum hydride, AlH_3, would possibly participate in the anodic oxidation reaction when the potential was returned to potentials more anodic than -1.7V (18). Despič *et al.* (27) have also studied the cathodic and anodic potential transients of aluminum in 2M NaCl. The observed anodic potential transients after cathodic polarization were attributed to the presence of a substance inside a bulk phase. The substance is concluded to be aluminum hydride whose concentration increases, in a relatively low yield, with the square root of the total amount of cathodic charge passed.

Effect of AC Etching on Nucleation and Early Growth of Pits on Aluminum

AC etching of aluminum is characterized by a high density of pits, uniform depth of corroded metal, and by the presence of a film of oxide or hydroxide within this etched layer. Thompson and Wood (28) have studied the pitting behavior of aluminum in HCl solution under applied alternating voltage. A high density of pits was produced rapidly

($> 10^9$ cm^{-2}) and a thin discontinuous film of hydrated aluminum was present on the metal surface. According to these authors, the film is probably produced on the cathodic half cycle by a dissolution/precipitation mechanism brought about by the local increase in pH due to hydrogen evolution.

Dyer and Alwitt (29) have examined the surface changes during AC etching of aluminum and found that the frequency of an alternating current has a great influence on the size of etch pits. The relationship between the side length of pit (s) and the AC frequency (ω) is found to be $s \propto \omega^{-1/2}$ over the frequency range of 5-100 Hz. Also, the pit density on aluminum under AC etching is found to increase remarkably with decreasing frequency (29). These observations indicate that the applied current waveform determines the initiation and early growth of pits. According to Dyer and Alwitt, the active pits are nucleated during the anodic half-cycle, and are then passivated during the subsequent cathodic half-cycle due to the deposition of a surface oxide film. Thus, for a given anodic charge, a larger total number of pits was obtained for AC etching as opposed to DC etching. On the other hand, a different role of cathodic polarization was reported in the study of anodic pitting on aluminum (7,8), as will be described in the following.

Lin and Hebert (7) have studied the initiation and early growth of pits on aluminum foil through one cycle of cathodic-anodic polarization. The application of only one cycle of AC etching allowed increased fundamental understanding the anodic pitting behavior induced by the prior cathodic process. The pit density on aluminum

during the first 20 ms of anodic etching was found to be as large as $10^7/cm^2$ with a preceding cathodic charge of 10^{-3}-10^{-2} coul/cm^2 in 1M HCl solution at 65°C. About half of the pits are nucleated in the first ms of anodic etching indicating that prior cathodic polarization leads to a burst of pit nucleation within 1 ms. The pit growth rates in the first 20 ms are also enhanced relative to those measured during DC etching. Also, an equivalence between the cathodic charge and the measured anodic pit volume at 20 ms was observed. These observations suggested that the first 20 ms of anodic polarization can be considered as a period during which the initiation and growth of pits are enhanced by preceding cathodic process.

A period of open circuit between cathodic and anodic polarization was found to decrease the cathodic enhancement. The cathodic process had only a slight effect on anodic pitting with an interruption period of one second. The cathodic products may be removed through reaction or by mass transfer during the interruption period. Stirring of the electrolyte solution during interruption had no effect on the anodic current transient suggesting that solution mass transfer is not the cause for the "deactivation" of the electrode surface during the interruption period.

Cathodic-anodic polarization experiments were also carried out at ambient temperature. Similar to the results at 65°C, prior cathodic polarization brought on higher pit initiation rates and early growth rates of pits relative to those during DC anodic etching. However, at ambient temperature, the cathodic polarization is much less efficient in enhancing anodic pitting. It is concluded from the results of ambient

temperature as well as of 65°C that, regardless of temperature, the rate of anodic pit initiation is greatly increased by a preceding cathodic polarization.

The tentative conclusion about the mechanism of cathodic enhancement of pitting made by Lin and Hebert was that cathodic reaction produce species such as hydroxide which is an anodic reactant. The anodic oxidation of aluminum atom would release vacancies into metal which would then diffuse toward localized metal dissolution sites. The rate of pit initiation and growth would then be determined by the rate of vacancy diffusion. Cathodic reactions and products as well as their effect on anodic processes, will be studied directly in the proposed work. The mechanism of pit initiation will also be investigated.

Statement of Purpose

This work attempts to understand the profound effect of prior cathodic polarization on the initiation of pits on aluminum (7,8). Environmental factors affecting pitting behavior have been studied extensively in the literature. However, study of cathodically induced pit initiation has been lacking though AC etching can produce high pit densities on aluminum. The effect of cathodic polarization on pitting is of particular interest because no pits are produced during the cathodic polarization itself; instead, the role of cathodic charging is apparently to modify the surface film in some way which promotes anodic film breakdown. It is believed that study of the effect of prior cathodic polarization on pitting of aluminum will furnish information important to the

understanding of the pitting mechanism. Thus, the objectives of this work are to study the effect of cathodic charging on the composition and structure of surface film, and the effect of surface film modification on the pitting corrosion resistance of aluminum.

Explanation of Dissertation Format

This dissertation is composed of papers prepared for publication. The study of the effect of cathodic charging on natural oxide film on aluminum is contained in Paper I, entitled "The Effect of Cathodic Polarization on the Surface Composition of Aluminum in Acid Solution." Infrared spectroscopy study of the cathodic reaction products is contained in Paper II, entitled "Infrared Spectroscopy of Cathodically Produced Surface Films on Aluminum." The work on cathodically-induced oxidation reaction and mass change, at potentials below the pitting potential, is contained in Paper III, entitled "Study of Cathodically-induced Reactions on Aluminum in Acid Solutions." The study of cathodically-induced pitting corrosion at potentials above the pitting potential appears in Paper IV, entitled "The Effect of Cathodic Charging on Pitting Corrosion Resistance of Aluminum in Acid Solution." Quartz crystal microbalance frequency transients observed during pitting corrosion are presented in Paper V, entitled "Quartz Crystal Microbalance Frequency Transients during Cathodically-induced Pitting Corrosion of Aluminum." Following the last paper is the General Conclusions and that references cited in the General Introduction are listed following the General Conclusions. A thermodynamic model which relates the

relationship between overpotentials is contained in the Appendix. Papers I, III, IV and V under the authorship of Ching-Feng Lin and Kurt R. Hebert, and Paper II under the authorship of Lin, Hebert, and Marc. D. Porter. The investigations were conducted and the manuscripts were written primarily by the Ph.D. candidate, with the advice of the major professor, Dr. Kurt R. Hebert. The style used for each section follows that of *Journal of the Electrochemical Society.*

PAPER I.

THE EFFECT OF CATHODIC POLARIZATION ON THE SURFACE FILM COMPOSITION OF ALUMINUM IN ACID SOLUTION

The Effect of Cathodic Polarization on the Surface Film Composition of Aluminum in Acid Solution

Ching-Feng Lin and Kurt R. Hebert

Department of Chemical Engineering

Iowa State University

Ames, IA 50011

ABSTRACT

Cathodic polarization was found to reduce the hydrogen transport resistance of the surface oxide film on aluminum, at potentials around -1.65V *vs.* Ag/AgCl/4M KCl in 0.1M HCl solution. Five minutes immersion of samples in the electrolyte solution prior to polarization was also necessary for the increase of cathodic current. Reduction of film resistance was shown to be due to change of film composition as a consequence of cathodic charging. Formation of surface film was also found at potentials where the film resistance was reduced. The film, which was shown to contain appreciable amounts of water, was found to be an ohmic proton conductor with the conductivity at the same order of magnitude as precipitated aluminum hydroxide. The mechanism through which the oxide film resistance reduced during cathodic charging in acid solution is discussed.

INTRODUCTION

Cathodic polarization of aluminum has received wide attention mainly in relation to corrosion of aluminum occurring in the potential region below open circuit potential (1-10). Cathodic corrosion is reported to occur on aluminum thin films used as conductors on integrated circuits (10). When hydrogen is cathodically evolved at a metal surface in electrolyte solution, an increase of hydroxide anion concentration at the electrode results. This alkalization effect is thought to be responsible for the cathodic corrosion of an amphoteric metal like aluminum (10).

Cathodic polarization is also found to increase the susceptibility of aluminum surfaces to pitting corrosion (11). Pit densities approaching $10^7/cm^2$ have been observed after single cycles of cathodic and anodic polarization on aluminum. Apparently, cathodic charging of aluminum modifies the oxide film surface in a way which greatly increases the susceptibility of the metal to pitting. An understanding of the nature of this surface modification may yield important insight into the mechanism of passive film breakdown in pitting corrosion.

The mechanism of hydrogen evolution reaction on aluminum covered by a "natural" surface oxide film in neutral solutions has been studied by Vijh (6). Tafel slopes much larger than 2.3x2RT/F were obtained in short polarizations, while on long polarizations, some cathodic "activation" is manifested, which reduces the Tafel slope to 2.3x2RT/F approximately. Vijh suggested that the high Tafel slopes observed on

oxide-covered aluminum are, most likely, values of 2.3x2RT/F which have been modified by the presence of oxide. A Tafel slope of 0.325 for Al in 0.5N NaCl at pH 5 has been reported by Kunze (4). Kunze has also reported for this system that, at a potential of ~-1.6V, the current increased rapidly while the potential remained. Recently, a Tafel slope of 0.11V for potentials more negative than -1.75V *vs.* SCE in neutral solutions of 2M NaCl was reported by Radoševič *et al.* (12), which was attributed to hydration of the oxide layer at potentials more negative than -1.7V, whereupon hydrogen is evolved at the metal/film interface. These authors also concluded that substances other than gaseous hydrogen are produced at cathodic potentials, which are then involved in an oxidation reaction upon return to the original open-circuit potential.

In the present work, the effect of cathodic charging on the resistance of surface aluminum oxide films, during hydrogen evolution, was investigated. The cathodic reaction product was studied using *in-situ* quartz crystal microbalance measurement. The effect of HCl pretreatment on the increase of cathodic current is also reported.

EXPERIMENTAL

Preparation of aluminum film samples.- The aluminum film samples used in this study were approximately 0.25 μm thick evaporated from a pure source (99.99% Al foil, provided by KDK corporation, Japan) onto quartz substrates. The substrates were cleaned with CrO_3/H_2SO_4 solution, deionized water and methanol, and then dried in hot air. The pressure in a cryopumped coating system (Edwards E360A, West Sussex, England) during evaporation was < $1x10^{-6}$ torr and the base pressure was < $4x10^{-7}$ torr. The evaporation rate, which was measured with a quartz crystal thickness monitor, was 1.8-2.0 nm/s. The temperature of the substrate was not intentionally controlled. After the substrates returned to room temperature (~45 min), the evaporator was backfilled with purified N_2, and the substrates removed. The Al films were then exposed in laboratory ambient for 24 hours.

XPS measurement.- The thickness as well as the composition of air-formed aluminum oxide films were measured through the X-ray Photoelectron Spectroscopy (XPS). The XPS spectra were acquired on a PHI 5500 multi-technique system. The spectrometer was equipped with a hemispherical analyzer, using Al Kα x-ray at 300W (14 KeV). The photoelectron detection angle relative to the sample surface was 45^{o}. The surface carbon contamination layer was removed by ion sputter etching with an Ar^{+} beam at an accelerating voltage of 4 keV (~0.4μA).

Electrochemical quartz crystal microbalance (QCM).- The instrumentation for the QCM was the same as that employed in previous studies (13-17). Potentiostatic control and current measurement were accomplished by interfacing the QCM to a personal computer using a data acquisition board (Lab-PC, National Instruments). The frequency was measured with a frequency counter (Hewlett Packard 5334b) interfaced with a GPIB-PCII board. A QuickBasic (Microsoft) program was developed to drive the two boards simultaneously.

Aluminum film electrodes were evaporated onto both sides of planar (1 inch diam), overtone-polished, AT-cut quartz crystals (Valpey-Fisher, Hopkinton, Massachusetts). The films, which were deposited using a standard keyhole design (18) were ca. 0.25 μm thick and 0.34 cm^2 electrode area. The crystals were operated at the fundamental frequency of 5 MHz with the mass sensitivity of 17.67 $ngHz^{-1}cm^{-2}$, according to Sauerbrey relationship (18,19).

$$\Delta f = -2.26 \times 10^{-6} f^2 \Delta m \qquad [8]$$

The crystal was mounted in the wall of the electrochemical cell using an O-ring joint and two O-rings. A Pt wire and a Ag/AgCl/4M KCl electrode were inserted into the cell as counter electrode and reference electrode respectively. In all experiments the electrolyte was 25 ml aqueous 0.1M HCl solution and the temperature was at ambient (25°C). Prior to polarization experiments, the Al film was allowed to contact with the electrolyte for 5 minutes at open circuit. The frequency was measured at the rate of 18 ms per reading during cathodic polarization.

Stripping of Oxide Film. - The cathodically produced oxide film composition was determined by measuring weight loss after stripping the film. At the conclusion of cathodic charging, the cell was switched to open circuit. 25 ml of stripping solution, consisting of 8% CrO_3 and 20% H_3PO_4, was introduced into the cell after 30 seconds of open circuit. The frequency of the crystal was measured at the rate of 0.5s. The time for the frequency to reach a steady value (defined as completion of stripping) varied from three to five minutes.

RESULTS AND DISCUSSION

XPS investigation of air-formed oxide film.- It is interesting to investigate the state of the air-formed oxide film on aluminum since the nature of the film has been shown to influence the cathodic polarization behavior significantly (11). The air-formed oxide film composition as well as the thickness were studied through X-ray Photoelectron Spectroscopy (XPS). In order to determine the O/Al atomic ratio of the oxide layer, the surface carbon contamination layer was removed by ion sputter etching. Figure 1(a) shows the Al(2*p*) spectra of as deposited Al film sample, after ion sputtering at an acceleration voltage of 4.0 KeV for 2 minutes. At this point the C(1s) peak area was 1.8% of the total. Both peaks from the oxide and the metallic states appear indicating that the air-formed oxide layer is thin. The relative peak areas of the Al(2*p*,metal) and Al(2*p*,oxide) peaks were resolved by Gaussian curve analysis. The O/Al atomic ratio in the oxide layer was calculated from the overall O/Al ratio and the Al(2*p*,oxide) peak area. The ratio is 1.95, which is higher than the stoichiometric value of 1.5 for Al_2O_3. According to this atomic ratio, possible film compositions are AlOOH or $Al_2O_3 \cdot H_2O$.

The O(1s) peak of the oxide film shown in Fig. 1(b) is centered at around 533.2 eV. Fuggle *et al.* have reported O(1s) peak centered at 532.4 eV for aluminum oxide obtained by exposure of clean aluminum to oxygen (20). On reaction of

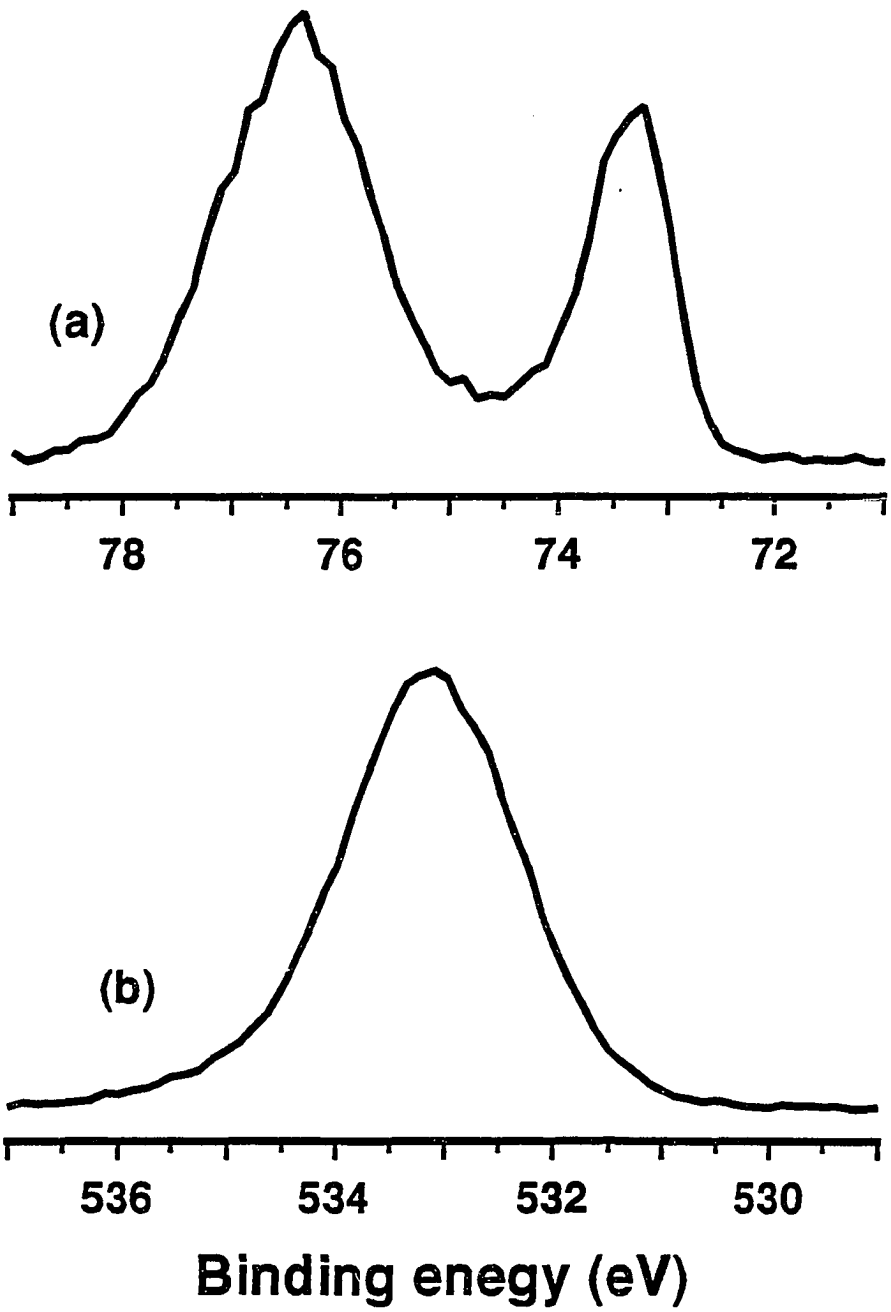

Figure 1. XPS spectra taken on evaporated aluminum film. (a) Al(2p); (b) O(1s).

aluminum with water vapor, a peak centered at 533.3 eV was obtained, which was assigned to hydroxide. The peak is still large at 240 K in UHV which precludes it being adsorbed water unless it is strongly bound (20). Therefore, the O/Al atomic ratio of 1.95 as well as the O(1s) peak position indicates that the air-formed film is hydrated oxide even in vacuum. This observation is in agreement with the broad infrared O-H stretching vibration band found on as deposited Al film sample (21).

The oxide layer thickness was determined to be 3.1 nm, according to Eq.[1](22),

$$\frac{I_2}{I_1} = \frac{D_2\sigma_1}{D_1\sigma_2} \frac{e^{-\sigma_1 x'}}{1-e^{-\sigma_1 x'}} \qquad [1]$$

where I_2 is the intensity of Al(2*p*,metal) (31.8%), I_1 the intensity of Al(2*p*,oxide) (68.2%), D_2 the density of Al atoms in metal (2.7 gm-Al/cm^3), D_1 the density of Al atoms in oxide (1.35 gm-Al/cm^3 for AlOOH), $1/\sigma_2$ the mean free path length in metal (25.5Å), $1/\sigma_1$ the mean free path length in oxide (27.8Å), $x'=\sqrt{2}\,d$ for 45^o angle, and d the film thickness (Å). For the electron mean free path length in Al, Penn's calculated value was used (23). For the calculations of D_1 and $1/\sigma_1$ (see Eqs. [4] and [5] in Ref. (24)), an oxide density of 3.01 g/cm^3 was used (25). In Ref. (24), the electron mean free path length in Al_2O_3 calculated is 27.4 Å.

The average thickness of surface oxide layers on aluminum which were oxidized in pure oxygen at 250^{o}C for 5 hours, has been reported to 2.3 nm (26). The thickness of the oxide layer on as evaporated aluminum films used in the present work is greater. The difference in thickness is probably due to different oxide film compositions.

Cathodic polarization of aluminum.- Cathodic polarization curves as well as weight changes of aluminum were measured simultaneously through the electrochemical quartz crystal microbalance technique (QCM). Figure 2 shows polarization curves measured separately from an anodic potential region as well as from a cathodic potential region. The corresponding current and frequency transients for the cathodic potential region are shown in Fig. 3. As a pretreatment, the sample was immersed in the cell for 5 minutes prior to scanning cathodically at a rate of 10 mV/s. Figure 2 shows that a linear E *vs.* log i portion can be obtained for both potential regions. The Tafel slope for the potentials between -1.2 and -1.5V is -374 mV. No change in the vibration frequency of the electrode in this potential region was obtained. This observation indicates that the mass of the sample remained constant in the high potential region. The slope began to decrease as the potential was driven more cathodically.

Figure 3 shows that the cathodic current rose significantly as the potential became more cathodic than -1.65V. The Tafel slope for the potentials between -1.65V and -1.79V is -127mV. The cell potential includes the overpotential in the metal/film interface (η_H^{12}), the potential drop across the film (η_H^{2}), the overpotential in the film/solution interface (η_H^{23}), and the overpotential between the solution side of the film/solution interface and the reference electrode (η_H^{3}).

$$V = \eta_H^{12} + \eta_H^{2} + \eta_H^{23} + \eta_H^{3} \qquad [2]$$

Where, V=(E_{cell} *vs.* Ag/AgCl/4M KCl) + 0.27, is the total overpotential for hydrogen evolution at the experimental pH of 1.25. η_H^{3}, which is primarily due to ohmic

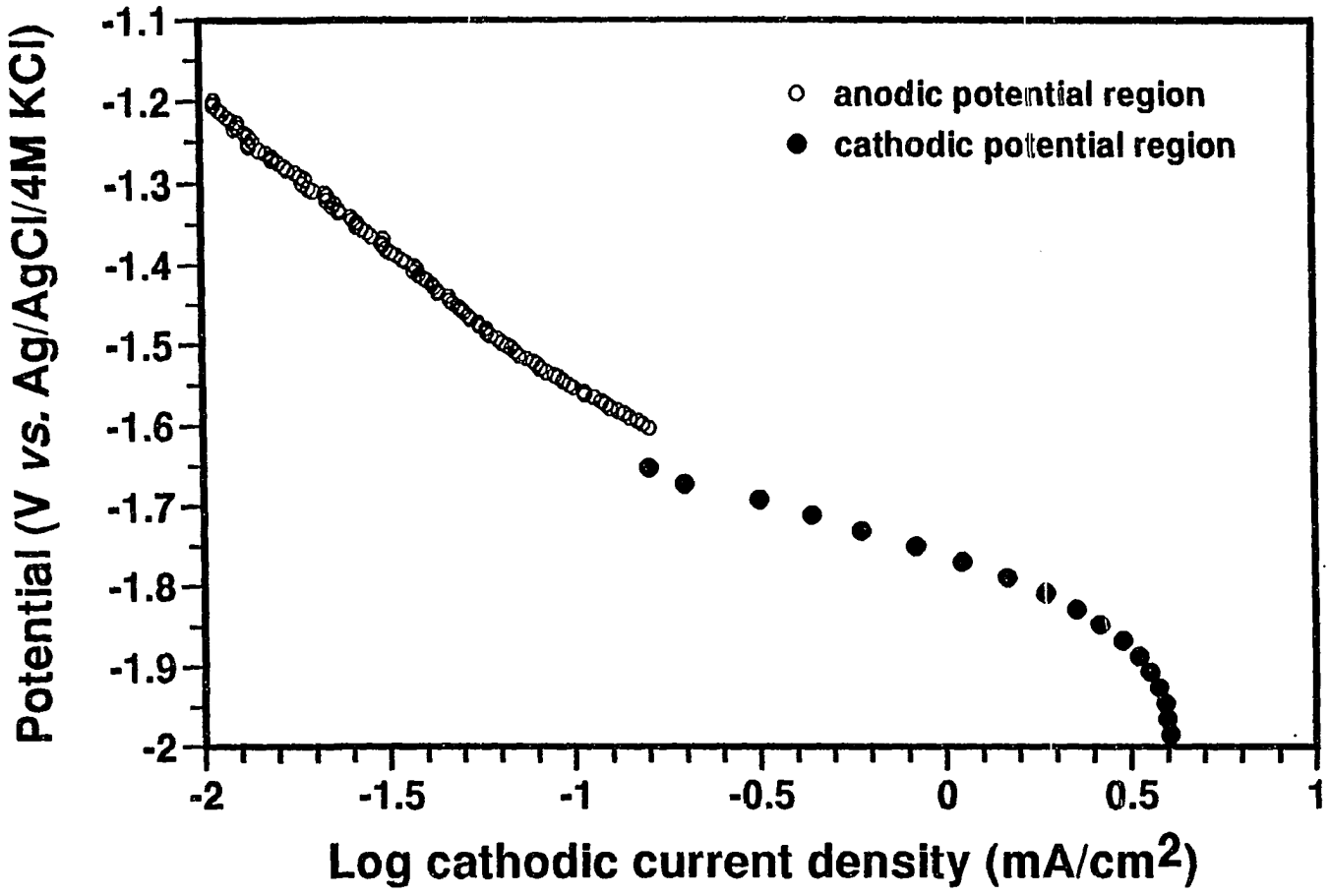

Figure 2. Polarization curves for aluminum in 0.1M HCl at room temperature; pretreatment time 5 minutes. Potential scan rate 10 mV/s; potential regions as indicated. Polarization curves were measured separately for the two regions.

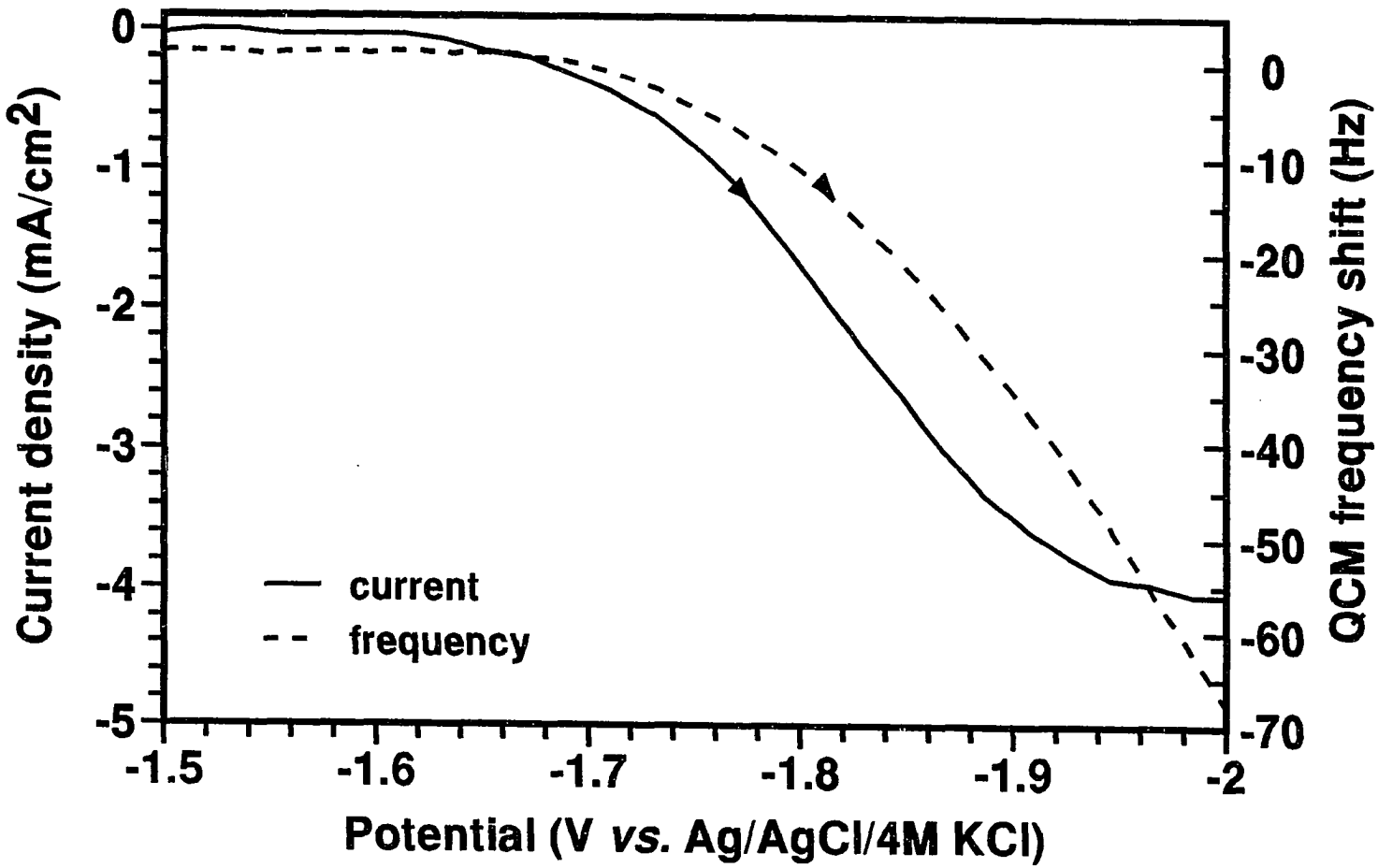

Figure 3. Cathodic polarization curve and quartz crystal frequency shift for the cathodic potential region in Fig. 2. Current and frequency obtained simultaneously.

resistance in the bulk solution, can be calculated from the measured current density and the cell resistance. AR_{Ω}, the cell resistance, was determined to be 37 ohm-cm^2 (27).

$$\eta_H^3 = i \times AR_{\Omega} \qquad [3]$$

The Tafel slope and the exchange current density for the anodic potential region, after correction for $\eta_H{}^3$, are -371 mV and 3.27×10^{-8} A/cm^2 respectively, and are -96 mV and 5.73×10^{-19} A/cm^2 for the cathodic potential region. A Tafel slope of -110 mV for hydrogen evolution reaction (h.e.r.) in acid solution on aluminum, which were considered to be essentially free of surface oxide, has been reported by Vijh (28). This value is reasonably close to the Tafel slope in the negative potential region in Fig. 2. The author suggested that the electrochemical reaction is likely the rate-determining step in the over-all h.e.r. On the other hand, Vijh also found Tafel slopes much larger than $2.3 \times 2RT/F$ on oxide-covered aluminum electrodes (6). Therefore, the reduced Tafel slopes at cathodic potentials can be explained, according to these arguments, by a loss of film resistance to the passage of cathodic current.

By assuming that current flow in the film at anodic potentials obeys an exponential law, the hydrogen current is determined by

$$\begin{aligned} i_H^{12} &= i_H^2 \\ i_{o,H^{12}} \exp(-\beta_{12}\eta_H^{12}) &= i_{o,H^2} \exp(-b_2\eta_H^2) \end{aligned} \qquad [4]$$

where $\beta_{12} = \alpha nF/RT$. The potential drop across the film can be calculated from Eqs. [3-4] by assuming $\eta_H{}^{23}=0$.

$$\eta_H^2 = \frac{1}{\beta_{12}+b_2} \ln\frac{i_{o,H^2}}{i_{o,H^{12}}} + \frac{\beta_{12}}{\beta_{12}+b_2}(V-\eta_H^3) \qquad [5]$$

The hydrogen current is

$$i_H = -i_{o,H^2} \exp^{\frac{-b_2}{\beta_{12}+b_2}\ln\frac{i_{o,H^2}}{i_{o,H^{12}}}} \exp^{\frac{-\beta_{12}b_2}{\beta_{12}+b_2}(V-\eta_H^3)} \qquad [6]$$

$$= i_{o,H} \exp^{-\beta(V-\eta_H^3)}$$

where $i_{o,H}$ the exchange current density for the over-all h.e.r. at anodic potentials. In Eq. [6], β_{12} (24.1) and $i_{o,H}{}^{12}$ (5.73×10^{-19} A/cm^2) were determined from the linear portion of the cathodic potential region in Fig. 2; β (6.19) and $i_{o,H}$ (3.27×10^{-8} A/cm^2) were determined from the anodic potential region, after correction for ohmic resistance. b_2 and $i_{o,H}{}^2$, which were calculated from Eq. [5] are 8.34V^{-1} and 1.72×10^{-4} A/cm^2 respectively. Thus the overall hydrogen kinetics at anodic potentials can be explained if proton conduction in the film obeys an exponential law as in Eq. [4]. Such an exponential law would be expected for high-field conduction,

$$i_H^2 = i_{o,H}^2 \exp\left(B_H\frac{\eta_H^2}{\delta_2}\right) \qquad [7]$$

where δ is the film thickness, 3.1 nm. The value of β_H is $\delta\times b_2=2.6\times10^{-6}$ cm/V. This value compares favorably with field coefficient for high field conduction in films of aluminum, tantalum, and iron oxide, which are all about 5×10^{-6} cm/V (29,30).

The decrease of film resistance is not due to removal of oxide film since no

decrease in mass of the sample was observed at -1.65V. Instead, the mass of the sample began to increase at the potential of -1.67V, which indicates the presence of cathodic reaction products on the sample surface. Radoševič *et al.* (12) also observed dramatic changes in the electrochemical behavior of aluminum below -1.75 V *vs.* SCE, which was attributed to the presence of AlH_3. Results of oxide film stripping experiment presented below and infrared spectroscopy study (21) show, on the other hand, that the mass increase is due to a surface oxide film.

At potentials more negative than -1.8V, the Tafel slope in Fig. 2 began to increase. The mass of the electrode also increased significantly as shown in Fig. 3. The rate of frequency decrease is approximately a constant of 3.2 Hz/s at potentials between -1.9V and -2.0V, which indicates that the film has low resistance for ionic transport. The frequency also decreased continuously at potentials more cathodic than -2.0V (not shown). A total frequency decrease of 665 Hz (11.7 $\mu g/cm^2$) was found after the potential was swept to -3.0V. This potential is well below to the equilibrium potential of -1.663 V *vs.* NHE for Al (31). The overpotential for Al^{+3} transport can be decomposed into

$$E = E^{o}_{Al} + \eta^{12}_{Al} + \eta^{2}_{Al} + \eta^{23}_{Al} + \eta^{3}_{H} \qquad [8]$$

where E^{o}_{Al} is the equilibrium potential for Al. Accordingly, if the film is forming at the potential more negative than E^{o}_{Al}, then $\eta_{Al}{}^{12}$ must be positive. $\eta_{H}{}^{3}$ is -0.33V at the current density of 8.8 mA/cm^2 at -3V. Therefore $\eta_{Al}{}^{2}$, which is controlled by the cathodic reaction, must be large and negative (at least -0.74V at E=-3.0V *vs.*

Ag/AgCl/4M KCl). Thus, film growth at -3.0V can only be explained by appreciable resistance to cathodic current flow in the film. In this case, the high Tafel slope is attributable to increased film resistance.

It is concluded from polarization curves that cathodic charging "activates" the Al surface at the potential around -1.65V, where the hydrogen evolution reaction follows Tafel kinetics. The change in h.e.r. kinetics can be explained by a loss of film resistance to H^+ transport. The mass of the electrode also begins to increase at the potential where the h.e.r. kinetics change. The mass increase was attributed to the formation of surface oxide film. The rate of mass increase was approximately constant suggesting that the film has low resistance for transport of aluminum and oxygen ions. The polarization behavior as well as the cathodically-induced film growth were further studied by a potentiostatic method.

Potentiostatic cathodic charging.- Shown in Fig. 4 are the quartz crystal microbalance frequency transient, as well as the charge applied, during constant potential charging of the evaporated aluminum film at -2.0V. The corresponding cathodic current transient is shown in Fig. 5. Figure 4 shows that there is an initial period of about 2 s during which no frequency change is observed. The corresponding cathodic charge for this initial period is 7.2 mC/cm^2, which is in good agreement with the critical charge for significant film growth found in infrared spectroscopy (21). After this initial period, the frequency decreases linearly with time, suggesting that cathodic products accumulate at a constant rate on the electrode surface.

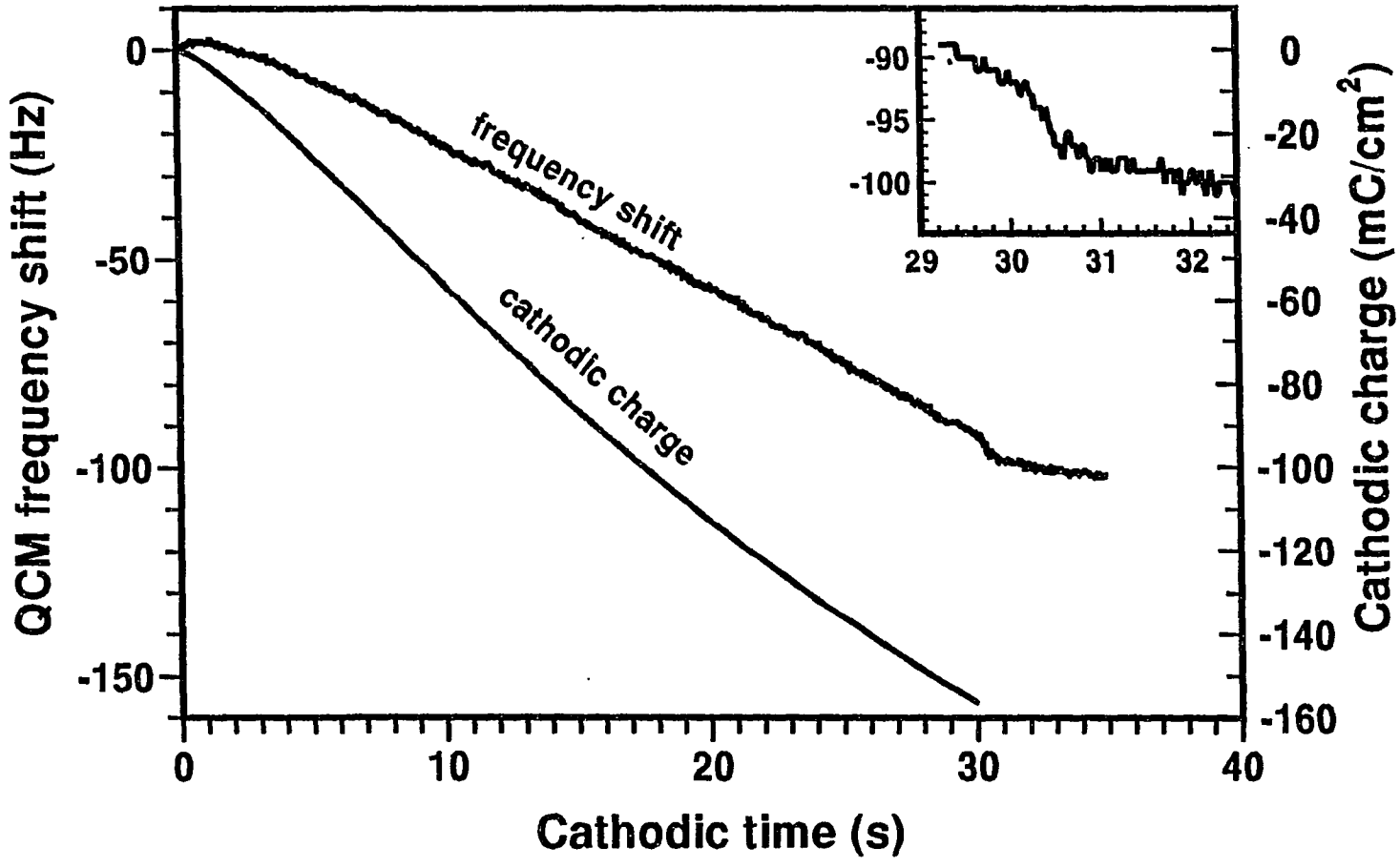

Figure 4. Quartz crystal frequency shift and accumulated cathodic charge obtained during cathodic polarization of Al in 0.1M HCl at room temperature. Cathodic potential -2.0V.

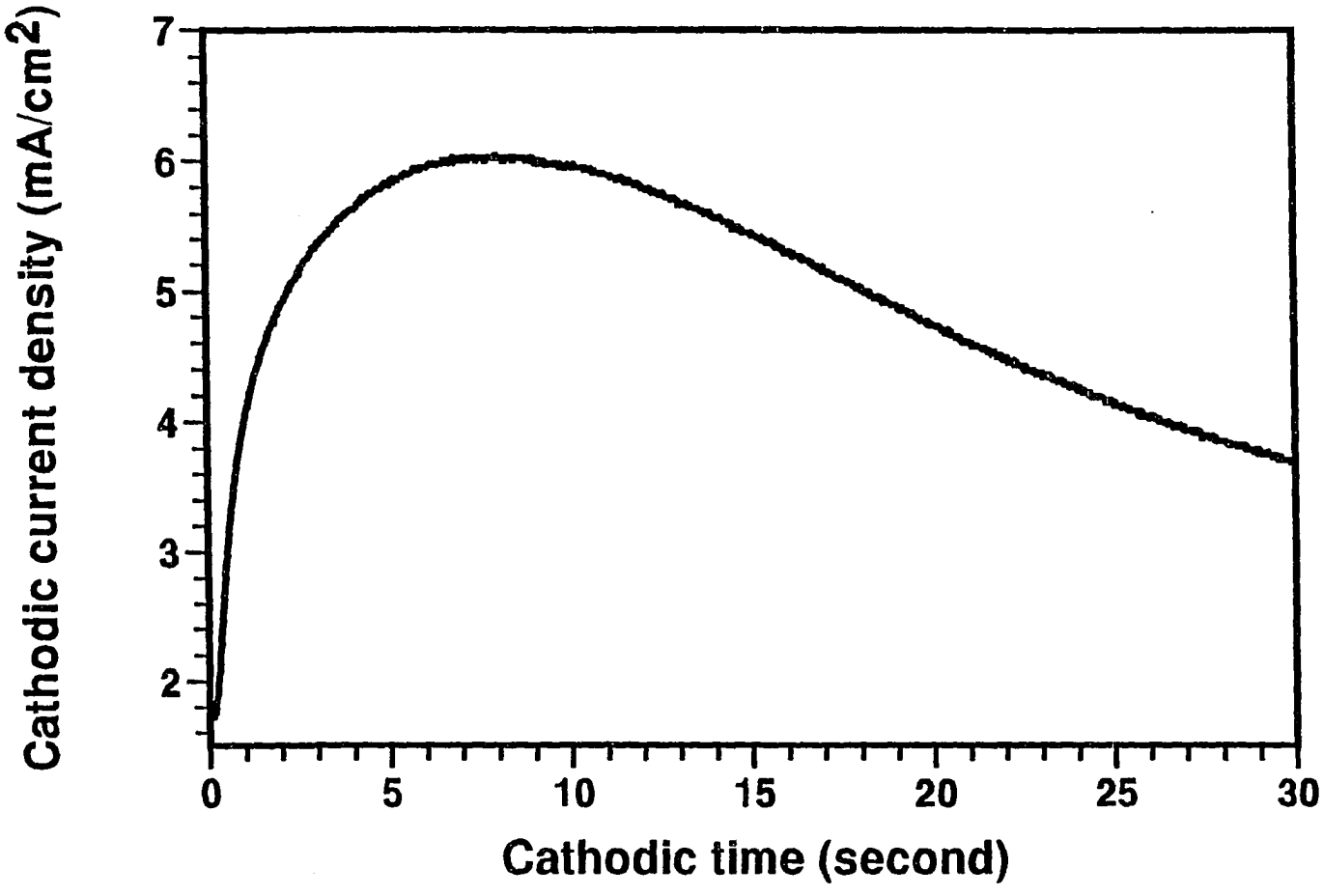

Figure 5. Cathodic current transient obtained during constant potential polarization in 0.1M HCl at room temperature. Cathodic potential -2.0V.

Changes of stress of metal films might also contribute to the frequency shift of the QCM (32,33). Thus, cathodic polarizations were also carried out on 5 MHz BT-cut quartz crystals onto which the aluminum films had been evaporated, to determine any stress effect (33). The frequency measurement on BT-cut quartz crystals gave the same slope as that in Fig. 4, indicating that there was no significant stress change during cathodic polarization. The slope in Fig. 4 is -3.42 Hz/s, which corresponds to a mass increasing rate of 0.06 $\mu g cm^{-2} s^{-1}$, according to the Sauerbrey equation (18,19). The rate of mass increase was approximately constant indicating that the film has little resistance to ionic transport.

The initial cathodic current density in Fig. 5 is 1.7 mA/cm^2, which is only slightly higher than the current density of 1.12 mA/cm^2, calculated from the Tafel kinetic expression found in the anodic potential region in Fig. 2 (with ohmic resistance correction). Therefore, the film had a high resistance initially. The current rose fast during the first 2s, then increased slowly to a maximum current of 6 mA/cm^2 at 7s, and then began to decay. The increase in current during constant potential charging suggests that the resistance of the film decreases. As found in the potential sweep experiment described above, cathodic charging activated the aluminum surface. Assuming that η_H^2 is negligible and the h.e.r. follows the kinetics found in Fig. 2, the cathodic current density for "activated" surface, at the applied potential of -2.0V *vs.* Ag/AgCl/4M KCl (or η_H=-1.73V), can be calculated from Eq. [9],

$$\eta_H = \eta_H^{12} + \eta_H^3 = \eta_H^{12} + (AR_\Omega)(-i_{o,H}^{12})\ \exp^{-\beta_{12}\eta_H^{12}} \quad [9]$$

where the cell resistance and kinetic parameters used are the same as those in Eq. [3] and Eq. [6]. The current obtained is 5.45 mA/cm^2 in good agreement with the experimental maximum current of 6 mA/cm^2. It is thus apparent that "activation" of the Al surface, i.e., the transition between the two kinetic rate laws, took place over the period of 7s in Fig. 5. The mass of the electrode began to increase at 2s while the current was increasing. Therefore, film dissolution is not the cause for surface activation, in stead, the resistance of the existing film decreased due to a chemical or structural transformation.

After the current maximum, the cathodic current decayed slowly while the rate of mass increase stayed constant. Thus, the decrease of current was considered due to build up of low resistance surface oxide film. The rate law for conduction in the film at these times was determined from the current transient in Fig. 5, as will be described in the next section.

Figure 4 (inset) also shows a frequency transient below the pitting potential, after cathodic charging. The frequency decreased by about 7 Hz, in a time of 1-2s, after the potential was stepped at 30 seconds to -0.9V. A linear relationship was found between frequency decrease and anodic charge during this transient (27). Therefore, the frequency transient at open circuit can be associated with a film growth process. Anodic film growth induced by cathodic charging will be discussed in more detail in a

subsequent paper (27).

Determination of film conduction rate law.- The constant rate of mass increase together with the decrease of cathodic current is interesting. If conduction in the film follows Ohm's law, the current in the film is

$$i_2 = \kappa \frac{\eta_H^2}{\delta} \qquad [10]$$

where $\eta_H{}^2$ the potential drop in the film (volt), κ the conductivity of the film ($ohm^{-1}cm^{-1}$), and δ the film thickness (cm). Assuming $\eta_H{}^{23}$ is negligible, the overpotential for the h.e.r is

$$V = \eta_H^{12} + \eta_H^2 + \eta_H^3 \qquad [11]$$

where $\eta_H{}^3 = iAR_\Omega$ the IR drop in the electrolyte solution. Therefore,

$$\delta = \frac{\kappa}{i}(V_H - \eta_H^{12} - iAR_\Omega) \qquad [12]$$

The film thickness can be calculated from the mass increase Δm (g/cm^2) and the density of the film ρ (g/cm^3).

$$\Delta m = \frac{\kappa\rho}{i}(V_H - \eta_H^{12}) - \rho(\kappa AR_\Omega + \delta_o) \qquad [13]$$

where δ_o is the original oxide thickness before film growth. Figure 6 shows the relationship between mass change (Δm) and 1/i for times between 7-30s in Fig. 5. The mass changes calculated from the measured frequency changes in Fig. 4, and the stripping ratio of 1.38 (see next section). The cathodic currents used were from Fig. 5.

Since the current varies from 5.7 mA/cm^2 to 3.7 mA/cm^2 over the linear portion (t=13s-30s), the variation for $\eta_H{}^{12}$, calculated from the kinetic parameters obtained from Fig. 2, is only about 0.017V. Thus the term (V -$\eta_H{}^{12}$) in Eq. [13] is approximately a constant. Fig. 6 shows that the linear relationship between Δm and 1/i in Eq. [13] is obeyed, which indicates that the film at these times is an ohmic proton conductor. The slope and intercept extracted from Fig. 6 are -1.74×10^{-8} g-A/cm^2 and -1.47×10^{-6} g/cm^2 respectively. The conductivity of the film κ and the potential drop $\eta_H{}^{12}$ calculated from Eq. [13] are 1.12×10^{-8} $ohm^{-1}cm^{-1}$ and -1.18V respectively. The parameters used are ρ=2.4 g/cm^3 for hydroxide film (25), AR_Ω=37 Ω-cm^2 for cell resistance (27), δ_o=3.1 nm for the original film thickness, and V=-1.73V. It must be noted here that the conductivity calculated by using the value of δ_o=3.1 nm was underestimated since the initial film thickness should be smaller due to film thinning which occurs during pretreatment (see below).

Dzimitrowicz *et al.* showed that precipitated $Al(OH)_3 \cdot H_2O$ is an ohmic proton conductor, with a conductivity of 6×10^{-8} $ohm^{-1}cm^{-1}$ (34). The aluminum hydroxide studied by these authors was gibbsite obtained by neutralization of $Al(NO_3)_3$ solution; it has low crystalline order and very small particle size (35). The basic structural element for gibbsite is that of double layers of OH ions, with Al ions occupying two-thirds of the octahedral interstices within the layers (35). Additional water molecules occupy the inter-particle spaces to produce a connected, viscous-liquid region through the composite "solid". Since proton transport through the particles is expected to be poor,

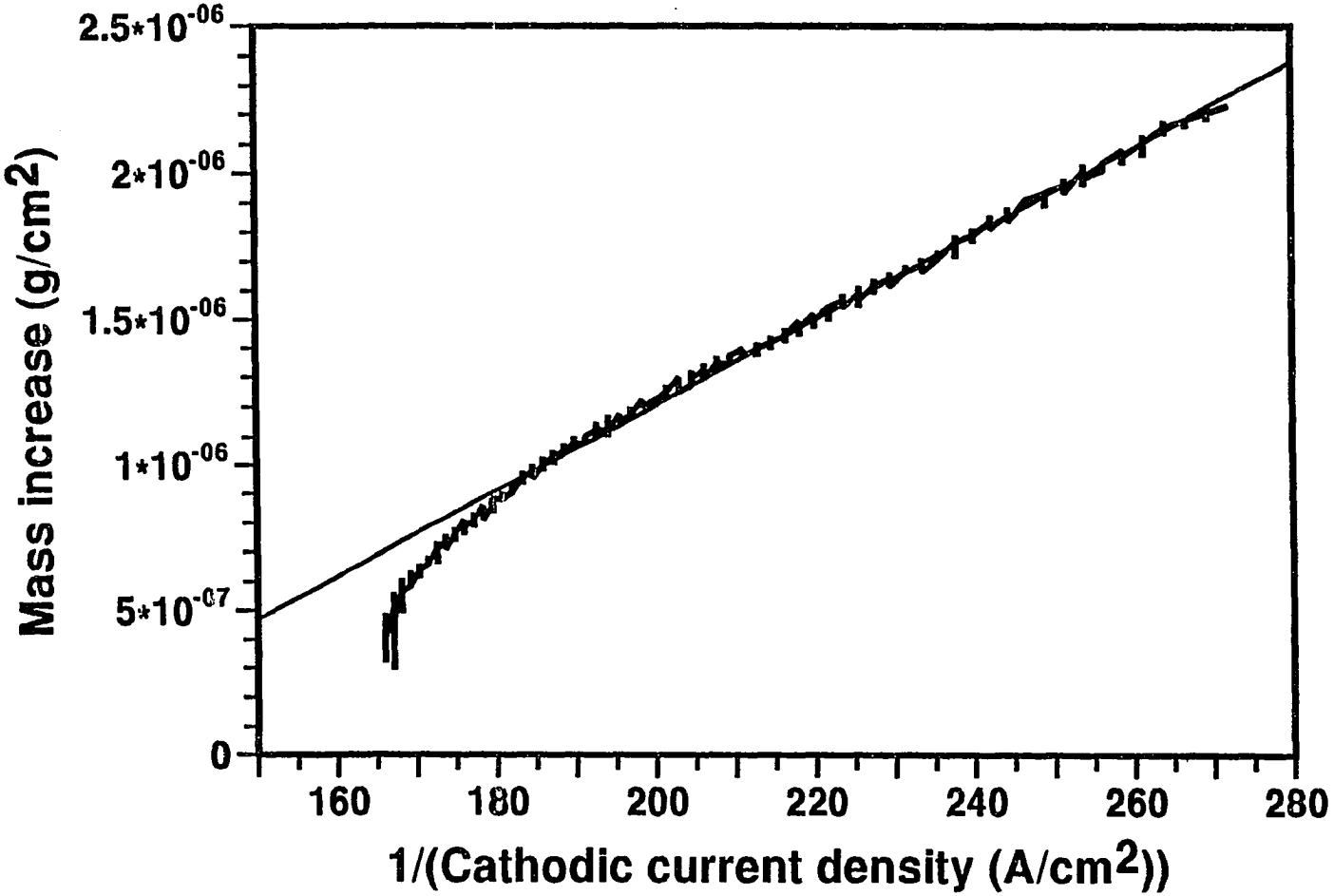

Figure 6. Plot of cathodic mass increase *vs.* 1/(cathodic current density). Cathodic period shown: 7-30s. Cathodic mass increases were calculated from QCM frequency shift in Fig. 4.

Dzimitrowicz *et al.* considered the bulk of the conductivity to arise from motion around the particles. The conductivity for the cathodically produced film has the same order of magnitude as the precipitated hydroxide film, suggesting that both materials have similar structures and both contain appreciable amounts of water. The cathodic current at the beginning of film formation, i.e., $\Delta m=0$, calculated from the slope and intercept of Fig. 6 is 8.4 mA/cm^2. The maximum cathodic current at a time of 7s in Fig. 5 is similar, at 6 mA/cm^2, indicating that the initial resistive oxide film at this point had entirely converted to the conductive structure.

Determination of film composition.- The QCM was applied during immersion of cathodically charged Al in oxide stripping solution. In this way the relation between cathodic frequency shift and oxide growth was determined. The measurement of the frequency decrease due to cathodic charging and the frequency increase in stripping solution gives information about the film composition.

Figure 7 shows a typical quartz crystal microbalance frequency transient during the course of film dissolution. The frequency decreased by about 20 Hz after the cell was switched to open circuit. As mentioned before, this open circuit mass increase is probably associated with an uniform oxidation reaction induced by prior cathodic charging. Total frequency decrease (Δf_c) due to cathodic charging and open circuit mass was 345 Hz. Upon introducing CrO_3/H3PO_4 solution, the frequency decreased further by about 260 Hz, which was probably due to increase of solution mass. After this transient period, the frequency stayed constant for about 5 seconds, and then began

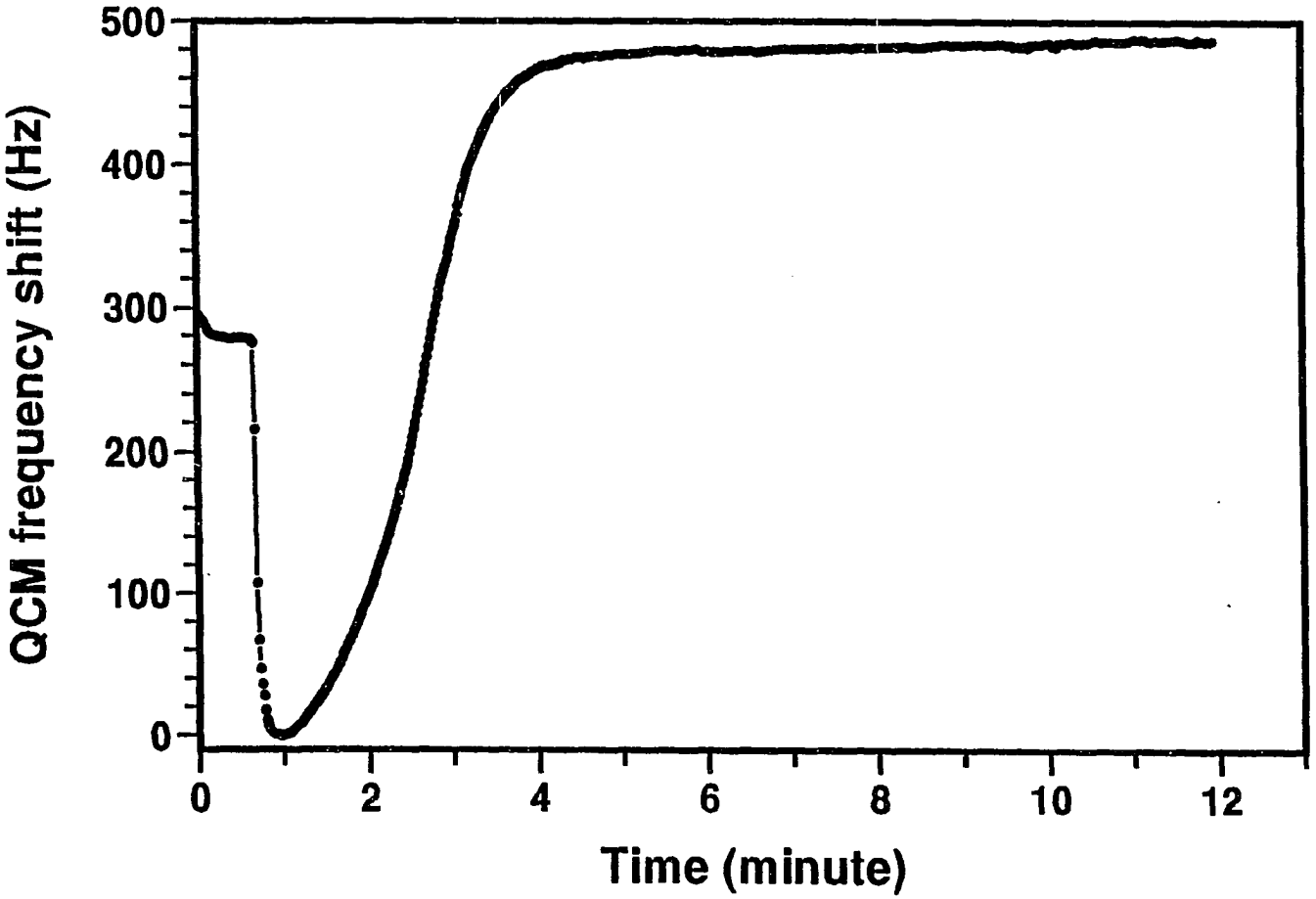

Figure 7. Open circuit quartz crystal frequency shift obtained after cathodic charging of Al in 0.1M HCl solution. Cathodic time 120s; potential -2.0V. Cathodic frequency decrease 325 Hz. Open circuit frequency decrease 20 Hz. CrO_3/H_3PO_4 solution was introduced at 30s of open circuit.

to increase indicating oxide dissolution. The time needed to dissolve the oxide was about 4 minutes.

Figure 8 shows that the amount of frequency increase due to stripping, Δf_s, is a linear function of Δf_c, the cathodic frequency shift. The stripping ratio, i.e., the slope of the data (line 1) in Fig. 8, is 1.38. Points with filled square markers in Fig. 8 are frequency increases when the samples were left in the electrolyte solution (0.1 M HCl) after cathodic charging, without introducing stripping solution. The time for the frequency to arrive at constant values in 0.1 M HCl solution was 45 minutes, which was much longer than when stripping solution was introduced. The decrease of mass in 0.1M HCl indicates that the cathodically produced oxide film is not stable in acid solution. Line 2 in Fig. 8 was drawn through the origin, by using the slope obtained from line 1. The line passes through the frequency shifts which were obtained without stripping solution introduced. Therefore, the intercept found in line 1 (-41 Hz) is probably due to a residual chromium oxide film on the electrode surface.

The weight loss due to stripping (Δf_s) includes mass incorporated into the oxide film during cathodic charging, and aluminum from the metal. Assuming that no Al^{+3} dissolved during cathodic charging, the weight percent of aluminum in the film can be calculated from the stripping ratio,

$$\frac{\Delta f_c}{\Delta f_s} = 1 - (\textit{weight fraction of Al}) \qquad [14]$$

where Δfc is the cathodic frequency shift. The weight fraction of Al from Eq. [14] is

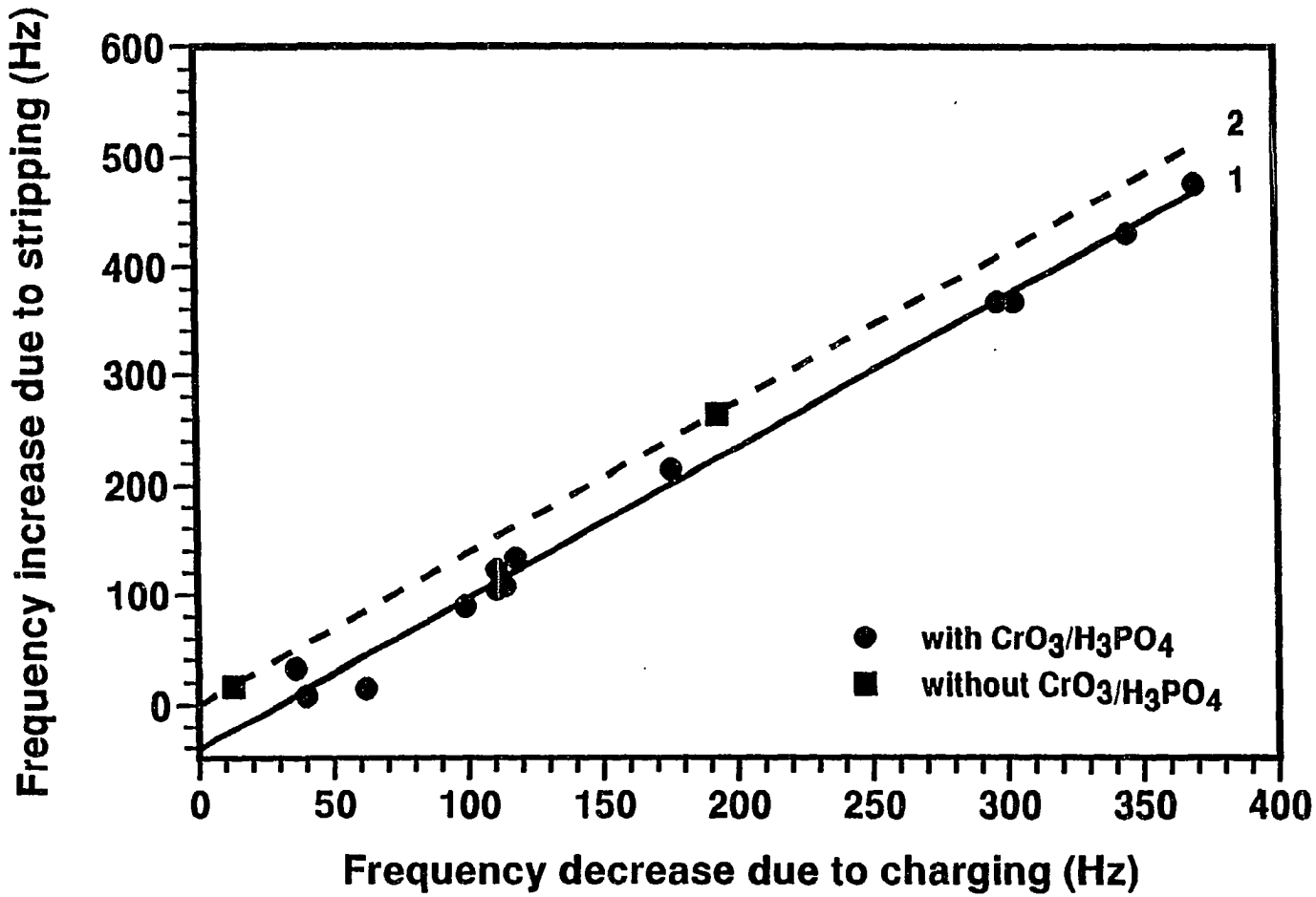

Figure 8. Plot of quartz crystal frequency increase due to stripping *vs.* frequency decrease during cathodic charging and open circuit reaction. Cathodic potential -2.0V.

0.275. This weight percent indicates that four oxygen atoms are associated with one aluminum atom (Al/(Al+4O)=0.296). Possible oxide film compositions are: $AlO_{1.5}$• $2.5H_2O$, AlOOH• $2H_2O$, $Al(OH)_3$•H_2O, or mixtures of these. This composition refers to the film after both cathodic charging and open circuit oxidation. Since part of the Al in the film was introduced by open circuit oxidation, the O/Al ratio during cathodic charging must be higher. Furthermore, if Al^{+3} dissolution occurred during cathodic charging, then mass increase due to incorporation of oxygen and H_2O must be greater than that obtained from the frequency shift. Under this circumstance, the weight fraction for Al would also be smaller than 0.275. It is concluded from these measurements that cathodically produced oxide film contains at least four oxygen atom for every aluminum atom, including at least one water molecule per Al. Since true O/Al ratio of the film during cathodic charging is expected to be higher, the film probably contains even more water. Significant amount of water are consistent with the structure suggested by the proton conductivities calculated above.

It is concluded from the above observations that a surface film was produced during cathodic charging. The composition of the film was determined from the QCM measurement to contain appreciable amounts of water, which would provide small film resistance for ionic transport.

Effect of HCl pretreatment.- Results from polarization studies indicate that cathodic charging dramatically reduces the oxide film resistance for ionic transport. It was also reported in a previous study that immersion of samples in HCl solution, prior

to applying polarization, is necessary to obtain significant cathodic charge, which will then promote pitting corrosion (11). Results concerning role of HCl pretreatment are presented in this section.

Figure 9 shows the effect of HCl pretreatment on cathodic polarization curves. The scan rate was 20 mV/s, which was two times faster than that used in Fig. 2. For the sample without pretreatment, the Tafel slope is -372 mV for potentials between -1.4V and -2.0V. This value agrees with the slopes, for the samples with HCl pretreatment, found in the potential region before surface "activation" (see Fig. 2 and Fig. 9). For the pretreated sample in Fig. 9, the "activated region", i.e., the region where the Tafel slope decreases, is displaced to more cathodic potentials at the higher potential sweep rate. However, without pretreatment, the Tafel slope remained constant at the initial high value. It is concluded that the role of HCl pretreatment is to modify the oxide film in some way, which allows cathodic polarization to "activate" the film.

Since the constituents of HCl electrolyte solution are H^+, Cl^- and H_2O, experiments were conducted to test which of these constituents are necessary during pretreatment. The pretreatment procedure was to immerse Al samples in these solutions for 5 minutes prior to transfer into the etching solution. For this purpose, Al samples were 99.99% pure foil. The etching solution was 1M HCl and the temperature was 25°C. Figure 10 shows the cathodic current transients for samples pretreated with different electrolyte solutions. The initial currents were between 30-40 mA/cm^2 and increased with cathodic time, for samples pretreated with low pH solutions, independent

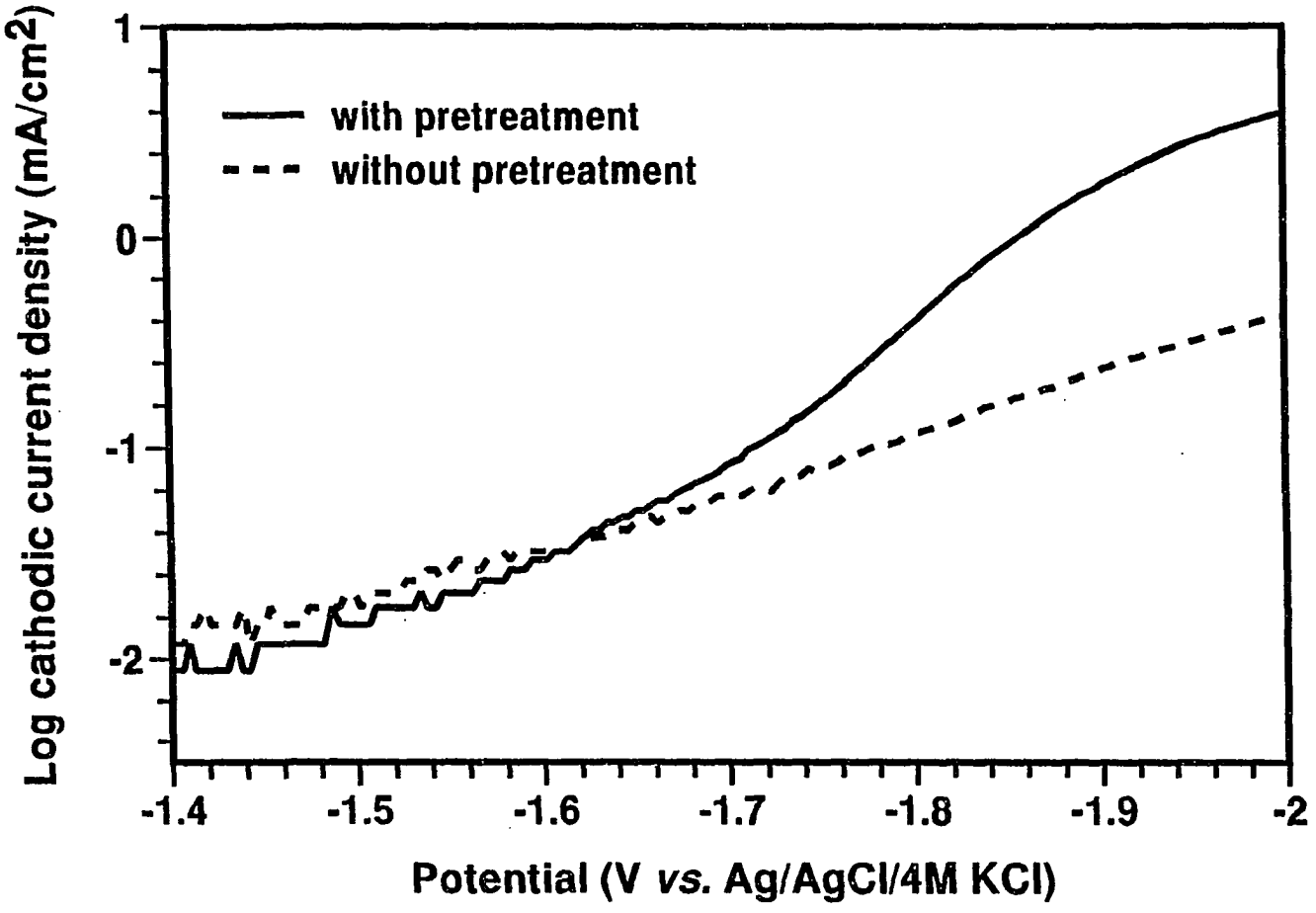

Figure 9. Effect of HCl pretreatment on cathodic polarization curves of Al in 0.1M HCl at room temperature. Potential scan rate 20 mV/s; pretreatment conditions as indicated.

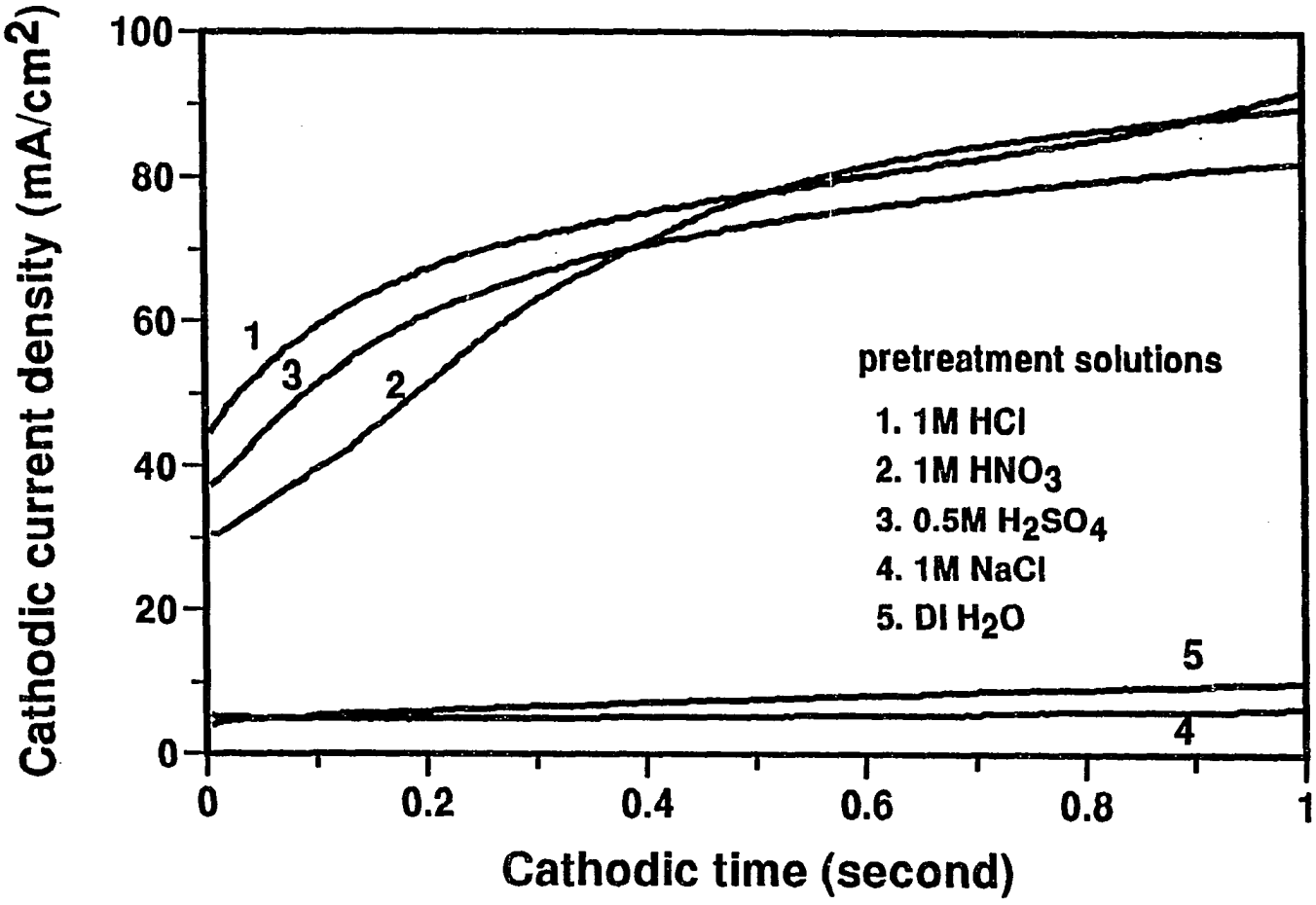

Figure 10. Effect of pretreatment solution on cathodic current transients in 0.1M HCl solution; pretreatment time 5 minutes. Cathodic potential -2.0V, cathodic time 1s. Pretreatment solutions as indicated.

of the anion of the acid. In contrast, the currents for the samples pretreated with H_2O or 1M NaCl were comparatively small and only increased slowly with time. These current transients indicate that pH, instead of the anion, is responsible for the effect of pretreatment on cathodic current transients. Since aluminum oxide films dissolve at pH lower than about 3 (31), the role of pretreatment may be to simply thin the surface film. This possibility was studied with measurements of potential and QCM frequency during the 5 minutes open circuit immersion.

Figure 11 shows typical QCM and potential transients recorded during the pretreatment period. The frequency transient during the first minute is considered to be due to introduction of electrolyte solution into the cell. After the initial transient, the frequency began to increase slowly while the open circuit potential decreased at approximately a constant rate. The total frequency shift during the 5 min pretreatment was about 12 Hz. In the study of infrared spectroscopy, decreases in intensity for the Al-O band were found for samples after HCl pretreatment (21). The ir peak intensity decrease, together with the mass decrease measured through QCM, indicates that film dissolution took place during pretreatment. By assuming a density of 3.0 g/cm^3 (AlOOH) (25) for air-formed oxide film, an oxide thickness of 7Å would be removed for the frequency increase of 12 Hz during the pretreatment (17.67 $ng/cm^2/Hz$). The constant rate of potential decrease may be the result of a constant electric field being maintained while the film thinned. It is concluded from pretreatment studies that the surface oxide layer was thinning during pretreatment.

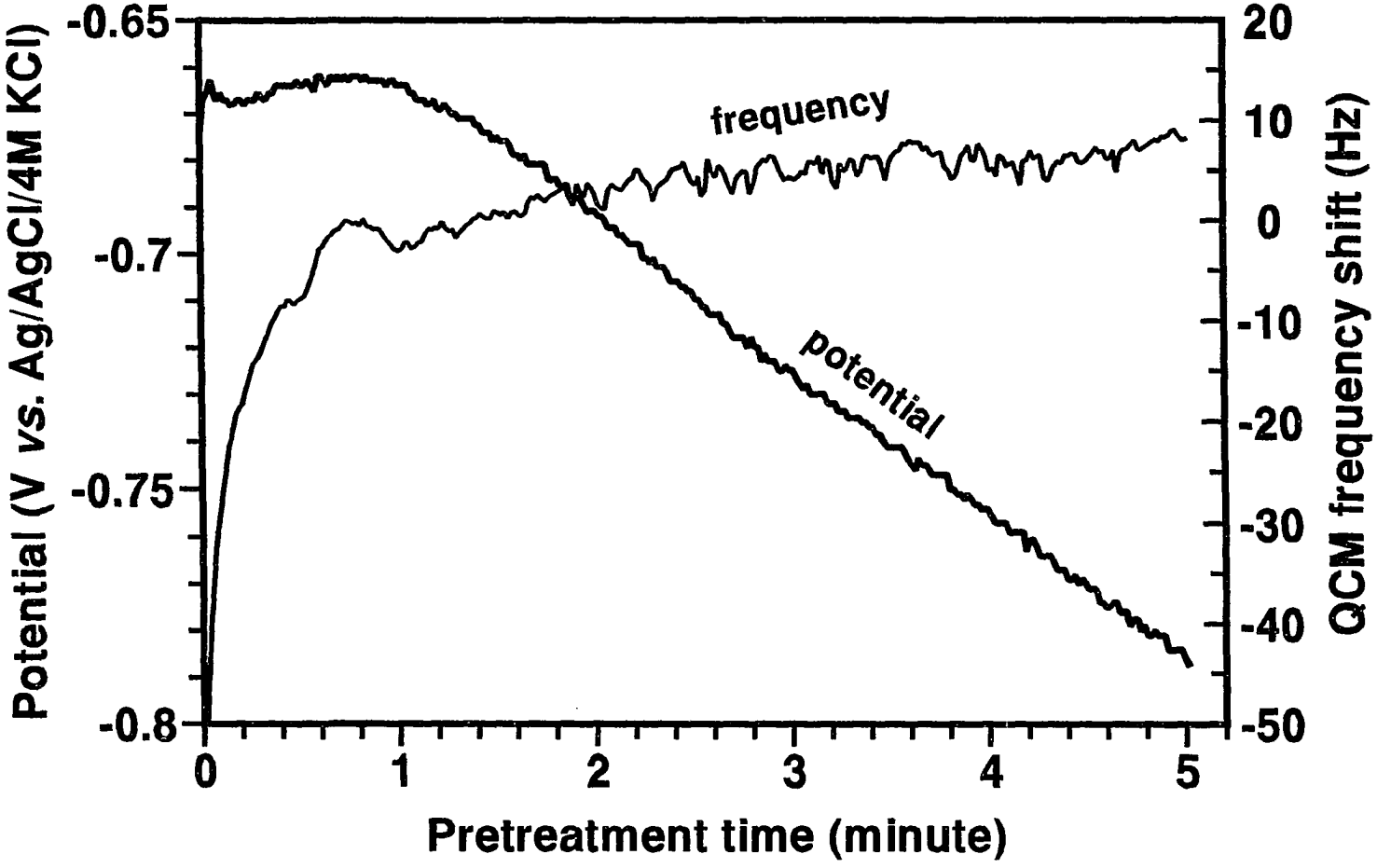

Figure 11. Open circuit potential and quartz crystal frequency shift obtained during immersion of Al in 0.1M HCl solution.

The ion conduction behavior of Al before cathodic charging was studied using the method of Kirchheim (30). The electrolyte used was 0.05M H_2SO_4 solution (pH~1.35). Initially, the cell current was kept at a stationary corrosion current density (i_{co}, ε_2^o) of 13.6 $\mu A/cm^2$, which was obtained from Våland and Heusler's results (27,36). The current was changed to a value i (ε_2^i) and remained at this value for a time period of t_o, during which film formation and metal dissolution occurred and the cell potential increased to ε_2. The current was then decreased to the original stationary value (i_{co}, ε_2^f). During the instationary period the potential changed first instantaneously by $\Delta\varepsilon_i$ ($\Delta\varepsilon_i=\varepsilon_2^i - \varepsilon_2^o$) and then linearly by $\Delta\varepsilon_2$ ($\Delta\varepsilon_2=\varepsilon_2 - \varepsilon_2^i$). After the current was changed at time t_o to i_{co}, a permanent potential change of $\Delta\varepsilon_2^o$ ($\Delta\varepsilon_2^o=\varepsilon_2^f - \varepsilon_2^o$). A linear relationship between $\Delta\varepsilon_i - \eta_O^{23}$ and $\ln(i/i_{co})$ was obtained (see Fig. 12). The high field conduction constant B, calculated from the slope of Fig. 12 and Eq. [15] (Eq. [14] in Ref. (30)), was 4.86×10^{-6} cm/V.

$$\Delta\epsilon_i - \eta_O^{23} = \frac{\delta_o}{B} \ln \frac{i}{i_o} \qquad [15]$$

Where η_O^{23}, the overpotential for film formation, was calculated from i according to Eqs. [4-6] in Ref. (30), and δ_o is the original film thickness (3.1 nm). The prefactor i_o in a high field conduction equation (see Eq. [18]) was calculated from $\Delta\varepsilon_2^o$, according to Eqs. [16] and [17] (Eqs. [25] and [10] in Ref. (30)).

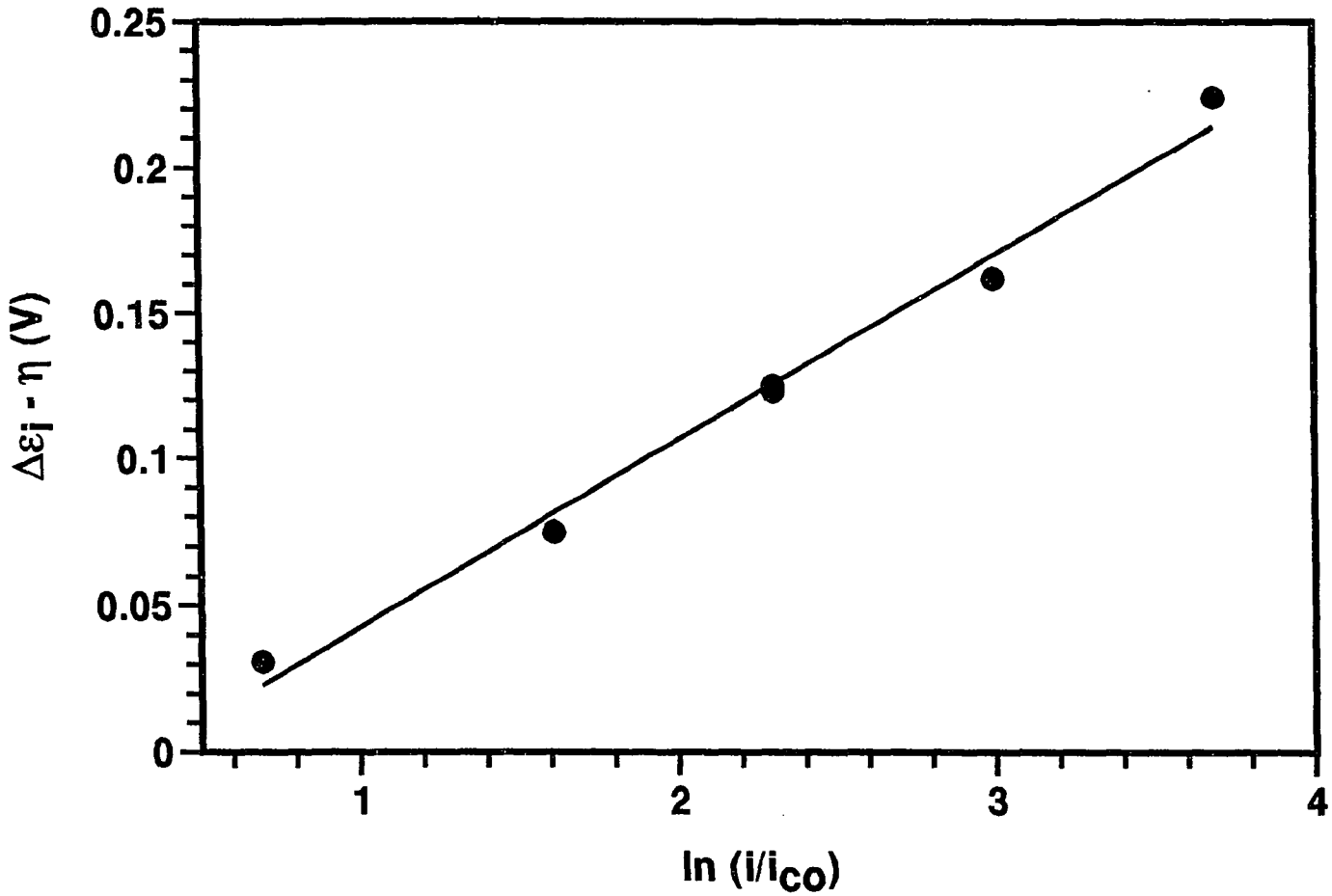

Figure 12. Plot of $\Delta\varepsilon_i$-η *vs.* ln (i/i_{co}) according to Eq. [15]. 0.05M H_2SO_4 solution.

$$\Delta\epsilon_2^o = \frac{\epsilon_2^o}{\delta_o}\frac{V_{ox}}{nF}\, i_l\, t_o \qquad [16]$$

$$\epsilon_2^o = \frac{\delta_o}{B}\ln\frac{i_{co}}{i_o} \qquad [17]$$

Where V_{ox} is the molar volume of the oxide (20 $cm^3\ mol^{-1}$ for AlOOH), and i_l was calculated from i according to Eqs. [4-6] in Ref. (30). The averaged value for stationary electric field ($\varepsilon_2{}^o/\delta_o$) was 3.04×10^6 V/cm, and was 9.8×10^{-12} A/cm^2 for i_o. It is concluded from the above results that the ion conduction rate in the film obeys the high field conduction equation,

$$i = i_o\, e^{\frac{B\eta_{Al}^2}{\delta}} \qquad [18]$$

Where i_o was 9.8×10^{-12} A/cm^2 and B was 4.86×10^{-6} cm/V. Therefore, film thinning due to pretreatment may assist the transport of ions in the film.

Discussion.- The relationship between the overpotentials for aluminum oxidation and hydrogen evolution, at the m/f interface, can be related through consideration of thermodynamics (Appendix)

$$3F\eta_H^{12} = 3F\eta_{Al}^{12} + (\mu_{Al_2O_3}^{21} - \mu_{Al(OH)_3}^{21}) \qquad [19]$$

By assuming the resistance to aluminum oxidation at the m/f interface is small and can be neglected, and that the film is an ideal mixture of Al_2O_3 and $Al(OH)_3$ (Appendix),

Eq. [19] becomes

$$\eta_H^{12} = \frac{1}{3F}\left(\mu^o_{Al_2O_3} - \mu^o_{Al(OH)_3}\right) + \frac{RT}{3F}\ln\left(\frac{X_{Al_2O_3}}{X_{Al(OH)_3}}\right)$$
$$= -1.57V + (8.56\times10^{-3}V)\ln\left(\frac{X_{Al_2O_3}}{X_{Al(OH)_3}}\right) \qquad [20]$$

where $\mu^o_{Al_2O_3}$ = -380,500 cal/mole, and $\mu^o_{Al(OH)_3}$ = -271,900 ca/mole (31). According to Eq. [20], $X_{Al_2O_3}/X_{Al(OH)_3}$ varies from 100 at -1.53V to 0.01 at -1.61V. The thermodynamic transition from Al_2O_3 to $Al(OH)_3$ thus occupies a narrow potential range around η_H^{12}=-1.57V. The critical η_H^{12} of -1.57V for transition between oxide and hydroxide can be compared to the potential of about -1.75V in Fig. 3 at which the hydrogen evolution is "activated" and film growth begins. Neglecting solution ohmic drop and the potential drop through the low-resistivity film, the value of η_H^{12} corresponding to the experimental potential of -1.75V is -1.48V, in very good agreement with Eq. [20]. Thus the markedly decreased film ion transport resistance below -1.75V coincides with the thermodynamic expectation of a hydroxide, rather than oxide film at these potentials. Also, as noted above, the proton conductivity at the cathodic potentials is characteristic of aluminum hydroxide.

The cell potential can be decomposed into a series of overpotentials for Al^{+3} transport as indicated in Eq. [8]. The potential drop at the m/f interface (η_{Al}^{12}) depends on the film composition according to Eq. [19]. Immediately after the potential step from open circuit (V~ -0.53V) to cathodic value (V=-1.73V), the film composition is

unchanged since there has been no time for reactions to take place. Assuming that $\eta_H{}^{12}$ is the dominant potential drop at open circuit, $\eta_{Al}{}^{12}$ decreases from 0V to -0.93V at the beginning of cathodic charging. According to Eq. [8] and neglecting solution ohmic drop and the potential drop at the f/s interface, the potential drop in the film ($\eta_{Al}2$) is 0.86V. Positive $\eta_{Al}{}^{2}$ suggests transport of Al^{+3} from the film outward to the solution, while negative $\eta_{Al}{}^{12}$ implies that no oxidation of Al to Al^{+3} take place. As a consequence, the ratio of O/Al in the film increases, and, to preserve electrical neutrality, protons are incorporated into the film. Therefore, the film composition is changed from oxide to hydroxide as a consequence of Al^{+3} transport. Since $\eta_{Al}{}^{12}$ is related to the film composition through Eq. [19], when the film is converted from oxide to hydroxide, $\eta_{Al}{}^{12}$ becomes less negative, and eventually approach zero. Thus, film growth is possible when the Al surface is "activated".

As described in the above section, the film was found thinning during pretreatment. Therefore, film thinning may be necessary for cathodic activation; Fig. 9 shows that the cathodic "activation" event do not occur on the sample without 5 minutes pretreatment, even the potential was swept to -2.0V. Film thinning due to pretreatment may assist the transport of Al^{+3} ions since the ion transport current is very sensitive to the electric field in the oxide. For example, the current density calculated from the measured electric field and exchange current density is 25.6 $\mu A/cm^2$ at the film thickness of 3.1 nm. By using the same value of potential drop, the current will increase to 428 $\mu A/cm^2$ if the film thickness is reduced by 5Å.

Previous investigators (37-39) have ascribed the formation of amorphous $Al(OH)_3$ during AC etching in HCl solution, to increase of pH at the electrode surface during the cathodic half cycle. For example, at room temperature the pH of a saturated $AlCl_3$ solution is about 0.15 and increasing the pH above 3 causes some $Al(OH)_3$ to precipitate (39). Therefore, it is necessary to examine whether the surface pH is high enough to precipitate $Al(OH)_3$ for the experimental conditions used in this work. The surface H^+ concentration change can be calculated by considering diffusion and migration of H^+ in the HCl binary electrolyte, from bulk solution to the electrode surface

$$\frac{i(1-t_-)}{F} = D_{HCl}\left[\frac{\partial C_{HCl}}{\partial X}\right]_{X=0} \qquad [21]$$

The concentration at the electrode surface (x=0) for constant current electrolysis is (40)

$$C_{HCl\,(o,\,t)} = C_{HCl,\,bulk} - \frac{2it_-^o}{F\sqrt{D\pi}}t^{1/2} \qquad [22]$$

With the values of $C_{HCl,\,bulk}$=0.1M, D_{HCl}=3.05x10^{-5} , t_-^o=0.169 (41), t=5s and i=5.8 mA/cm^2 (the current in Fig. 5 where Δf=-7 Hz), the surface HCl concentration change is only 0.005 M which is negligible by comparison with the bulk HCl concentration of 0.1 M. The solubility product for amorphous hydroxide $Al(OH)_3$ is $10^{-32.34}$ (31). Therefore, a Al^{+3} concentration of $10^{6.4}$ M is required to precipitate $Al(OH)_3$, at the surface HCl concentration of 0.095 M. This result shows that the film

formed during cathodic charging is unlikely produced by precipitation.

CONCLUSIONS

The effect of cathodic charging on the surface aluminum oxide film have been studied through polarization curves as well as *in-situ* weight change measurements. Results from polarization curves studies showed that cathodic charging "activate" the aluminum surface at the potential around -1.65V, where the hydrogen evolution reaction follows Tafel kinetics and film growth begins. The effect of cathodic charging is to reduce the oxide film resistance for ion transport, through change of film composition from oxide to hydroxide. A 5 minutes immersion of the sample in the electrolyte solution, prior to cathodic charging, is also necessary for the cathodic activation. It was shown that pH, instead of the anion, is responsible for the effect of pretreatment on cathodic activation.

The mass of the electrode begins to increase at the potential where the hydrogen evolution kinetics changed. The mass increase was shown due to formation of surface oxide film. Change of pH on the electrode surface was shown to be insignificant, which indicates that the film is unlikely produced through a precipitation mechanism. The film conduction rate law for proton conduction was found to follow Ohm's law, and the conductivity of the film has the same order of magnitude as precipitated aluminum hydroxide. The composition of the cathodically produced film was determined to be containing at least four oxygen atoms for every aluminum atom, which indicates that at least one water molecule per Al atom. Appreciable amounts of water in the film was attributed to be responsible for the increase of film conductivity.

ACKNOWLEDGMENTS

Financial support for this work was provided by KDK Corporation (Takahagi, Japan) through a fellowship to Mr. Lin. The authors appreciate Dr. James Anderegg for carrying out XPS measurement. The authors thank M. D. Porter for supplying the Edwards coating system.

REFERENCES

1. M. J. Pryor and D. S. Krie, *J. Electrochem. Soc.*, **102**, 605 (1955).

2. F. H. Haynie and S. J. Ketcham, Corrosion, **19**, 403t (1963).

3. C. W. Goulding and T. C. Downie, *Metallurgia*, **68**, 93 (1963).

4. J. Krunze. *Corros. Sci.*, 7, 723 (1967).

5. J. W. Diggle, T. C. Downie and C. W. Goulding, *Corros. Sci.*, **8**, 907 (1968).

6. A. K. Vijh, *J. Phys. Chem.*, **73**, 506 (1969).

7. H. Kaesche, in "Localized Corrosion," R. W. Staehle *et al.* Editors, p. 516, NACE, Houston (1974).

8. K. Nisanciouglu and H. Holtan, *Corros. Sci.*, **19**, 537 (1979).

9. W. Vedder and D. A. Vermilyea, *Trans. Faraday Soc.*, **65**, 561 (1969).

10. E.P.G.T. ven de Ven and H. Koelmans, *J. Electrochem. Soc.*, **123**, 143 (1976).

11. C.-F. Lin and K. R. Hebert, *J. Electrochem. Soc.*, **137**, 3723 (1990).

12. J. Radoševič, M. Kliškič, P. Dabič, R. Stevanovič and A. Despič, *J. Electroanal. Chem.*, **277**, 105 (1990).

13. G. S. Ostrom and D. A. Buttry, *J. Electroanal. Chem.*, **256**, 411 (1988).

14. P. T. Varineau and D. A. Buttry, *J. Phys. Chem.*, **91**, 1292 (1987).

15. D. Orata and D. A. Buttry, *J. Am. Chem. Soc.*, **109**, 3574 (1987).

16. O. Melroy, K. Kanazawa, J. G. Gordon II, and D. A. Buttry, *Langmuir*, **2**, 697 (1986).

17. L. A. Larew, J. S. Gordon, Y.-L. Hsiao, D. C. Johnson, and D. A. Buttry, *J. Electrochem. Soc.*, **137**, 3071 (1990).

18. S. Bruckenstein and M. Shay, *Electrochim. Acta.*, **30**, 1295 (1985).

19. G. Sauerbrey, *Z. Phys.*, **155**, 206 (1959).

20. J. C. Fuggle, L. M. Watson, D. J. Fabian, and S. Affrossman, *Surface Science*, **49**, 61 (1975).

21. C.-F. Lin and K. R. Hebert, and M. D. Porter, to be submitted.

22. T. A. Carlson and G. E. McGuire, *J. Electron Spectrosc.*, **1**, 161 (1972).

23. S. Tanuma, C. J. Powell, and R. Penn, *Surface and Interface Analysis*, **17**, 911 (1991).

24. S. Tanuma, C. J. Powell, and R. Penn, *Surface and Interface Analysis*, **17**, 927 (1991).

25. D. R. Lide, "CRC Handbook of Chemistry and Physics," 71st ed., p. 4-41, CRC press, Boston (1990).

26. I. Olefjord, H. J. Mathieu and P. Marcus, *Surface and Interface Analysis*, **15**, 681 (1990).

27. C.-F. Lin and K. R. Hebert, to be submitted.

28. A. K. Vijh, *J. Phys. Chem.*, **72**, 1148 (1968).

29. L. Young, "Anodic Oxide Films," p.93, p.219, p.238, Academic Press, New York (1961).

30. R. Kirchheim, *Electrochim. Acta*, **32**, 1619 (1987).

31. M. Pourbaix, "Atlas of Electrochemical Equilibria in Aqueous Solutions," p. 168, Pergamon Press, Oxford (1966).

32. E. P. EerNisse, *J. Appl. Phys.*, **43**, 4 (1972).

33. G. T. Cheek and W. E. O'Grady, *J. Electroanal. Chem.*, **277**, 341 (1990)

34. D. J. Dzimitrowicz, J. B. Goodenough, and P. J. Wiseman, *Mat. Res. Bull.*, **17**, 971 (1982).

35. K. Wefers and C. Misra, "Oxides and Hydroxides of Aluminum,", p. 3, Alcoa Laboratories, ALCOA (1987).

36. T. Våland and K. E. Heusler, *J. Electroanal. Chem.*, **149**, 71 (1983).

37. H. Terryn, J. Vereecken, and G. E. Thompson, *Corros. Sci.*, **32**, 1173 (1991).

38. G. E. Thompson and G. C. Wood, *Corros. Sci.*, **18**, 721 (1978).

39. C. K. Dyer and R. S. Alwitt, *J. Electrochem. Soc.*, **128**, 300 (1981).

40. A. J. Bard and L. R. Faulkner, "Electrochemical Methods," p253, John Wiley & Sons, New York (1980).

41. F. King and M. Spiro, *J. Solu. Chem.*, **12**, 65 (1983).

PAPER II.

INFRARED SPECTROSCOPY OF CATHODICALLY PRODUCED SURFACE FILMS ON ALUMINUM

Infrared Spectroscopy of Cathodically Produced Surface Films on Aluminum

Ching-Feng Lin and Kurt R. Hebert
Department of Chemical Engineering

and

Marc D. Porter
Ames Laboratory-USDOE and Department of Chemistry

Iowa State University
Ames, IA 50011

ABSTRACT

Cathodic polarization of aluminum in acid solution produces a solid surface product which was studied using Fourier transform infrared reflectance spectroscopy. The cathodic product detected by infrared spectroscopy is an aluminum oxide or hydroxide which contains water. The critical charge for the cathodic film to be detected by *ex-situ* infrared spectroscopy is between 4.7-10 mC/cm^2. The peak areas for three major bands increased linearly with cathodic charge suggesting that the film maintains an approximately uniform composition as it become thicker. The spectra for the cathodic products compare most favorably to that of the porous, amorphous oxide films formed by anodizing in acid solution. Aluminum ions in the film are highly coordinated to hydroxyl groups. The OH groups or H_2O molecules of the film are readily accessible to exchange by D_2O indicating that the film has an "open" structure.

INTRODUCTION

Cathodic polarization of aluminum has received wide attention (1-4) mainly in relation to corrosion of aluminum occurring in the potential region below the open circuit potential. In this negative potential region, hydrogen evolution due to hydrogen ion reduction and water reduction takes place. Cathodic polarization is also found to increase the susceptibility of aluminum surfaces to pitting corrosion (5). Pit densities approaching $10^7/cm^2$ have been observed after single cycles of cathodic and anodic polarization on aluminum. Apparently, cathodic charging of aluminum modifies the metal surface in a way which greatly increases the susceptibility of the metal to pitting.

Kasesche (1) has observed an increase of aluminum corrosion in sulfate solution caused by cathodic polarization. Van de Ven and Koelmans (2) have studied aluminum metal dissolution during cathodic polarization. These authors measured weight loss from aluminum due to cathodic corrosion after stripping the surface oxide films; thus, they were unable to distinguish between solid and dissolved corrosion products. In experiments at similar conditions to those of van de Ven and Koelmans, Vedder and Vermilyea (3) did not strip the surface oxide after cathodic corrosion, and measured a weight gain after cathodic polarization, thus indicating that a solid corrosion product was formed. They also observed an increase in intensity of the OH stretch in the infrared spectrum of the oxide film. Vedder and Vermilyea concluded that film growth during cathodic polarization was by reprecipitation from solution.

In a previous study, cathodic polarization was found to reduce the hydrogen evolution resistance of surface aluminum oxide film in acid solution, at potentials around -1.65V *vs.* Ag/AgCl/4M KCl (6). Formation of surface film was also found by the *in-situ* quartz crystal microbalance technique, at the potential where the film resistance was reduced. The film, which was shown to contain appreciable amounts of water, was found to be an ohmic proton conductor with conductivity at the same order of magnitude as precipitated aluminum hydroxide. In the present work, *ex-situ* infrared reflection spectroscopy is employed to further study the cathodic film composition and to infer structural information about the film. Infrared spectroscopy is a sensitive technique for identifying the various oxyhydroxides and hydroxides; it may also provide evidence for the presence of nonstructural hydroxide, as in adsorbed water (7).

EXPERIMENTAL

The aluminum film samples used in this study were approximately 0.25 μm thick evaporated from a pure source (99.99% Al foil, provided by KDK corporation, Japan) onto1x3 inch microscope glass substrates. The substrates were cleaned with CrO_3/H_2SO_4 solution, deionized water and methanol, and then dried in hot air. The pressure in a cryopumped coating system (E360A, Edwards, West Sussex, England) during evaporation was < $1x10^{-6}$ torr and the base pressure was < $4x10^{-7}$ torr. The evaporation rate, which was measured with a quartz crystal thickness monitor, was 1.8-2.0 nm/s. The temperature of the substrates was not intentionally controlled. After the substrates returned to room temperature (~45 min), the evaporator was backfilled with purified N_2, and the substrates removed. The Al films were then exposed in laboratory ambient for 24 hours.

Prior to cathodic polarization, the Al films were pretreated at ambient temperature by immersion in 0.1M aqueous HCl solution for five minutes. After pretreatment, the films were removed, rinsed with deionized water, dried on a spin coater, and placed in the sample chamber of the infrared spectrometer.

Infrared spectra were acquired with a Nicolet 740 FT-IR spectrometer using p-polarized light incident at 80^{o} and a liquid nitrogen cooled MCT detector. A home-built sample holder was used to position reproducibly the substrates in the spectrometer (8). The spectrometer was purged with boil-off from liquid N_2. Spectra

are obtained by referencing 1024 sample scans to 1024 background scans at 2 cm^{-1} resolution (zero filled) with Happ-Genzel apodization. All spectra are reported as $-\log(R/R_o)$ where R is the reflectively of the sample after cathodic polarization and R_o is the reflectivity of the sample after 5 minutes HCl pretreatment (except noted).

After the reference spectrum was acquired, the Al film was removed from the spectrometer and placed in an electrochemical cell, exposing an area of 12 cm^2 to the electrolyte solution (0.1M HCl). The reference electrode was an Ag/AgCl/4M KCl electrode (Fisher), and the counter electrode was a Pt wire. A CV-27 Voltammograph (Bioanalytical System Inc.) was used for potential control. The amount of cathodic charge passed during polarization was monitored through the coulometer of the CV-27. Cathodic polarization was at -2.0V *vs.* Ag/AgCl/4M KCl reference electrode at ambient temperature. This cathodic potential has been shown to enhance anodic pit initiation on Al foil significantly (5). A polarization experiment was terminated when a desired cathodic charge was attained. The Al film was then removed from the cell, and rinsed with deionized water. After drying in a spin coater, the film was placed in the spectrometer and the spectrum was recorded.

Deuterium exchange experiments were carried out as supplement to the assignment of infrared spectra. For this purpose, some cathodic polarized Al films having had their spectra recorded were immersed in liquid D_2O (Fisher, 99.8%) for three hours. The films were then removed and placed immediately into the sample chamber of the spectrometer. After allowing the film to dry completely in the

N_2-purged chamber, the sample spectrum was recorded. This step was necessary to obtain a completely deuterium exchanged spectrum. Only slight changes in spectra were noted if the films were allowed to dry in the spin coater after removal from D_2O. This result suggests that the rate of exchange between H and D is fast.

RESULTS

Infrared spectrum of air-formed oxide film. - The infrared external reflection spectrum of the as-evaporated aluminum film is shown in Fig. 1. Fig. 1 is a difference spectrum referenced to an evaporated Au film. The broad band at around 3389 cm^{-1} represents an O-H stretching vibration, while the band at 1613 cm^{-1} represents the H-O-H bending vibration (7,9). The O-H stretching vibration is associated with H_2O or hydroxide ions. The band at 949 cm^{-1} has been noted in the reflectance spectra of anhydrous films produced by air oxidation or anodic oxidation in neutral solutions (12). It has been assigned to the Al-O stretching vibration of barrier-type oxide (3,12-14). To further confirm this assignment, high temperature air oxidation of aluminum films was carried out in furnace at 380°C for various times. Figure 2 shows that the only significant absorbance band in the infrared spectra of these oxide films was at 948 cm^{-1}; the absorbance in this band increased with time at 380°C. Therefore, the band at 940-950 cm^{-1} is related to Al-O bonds. The peak at 828 cm^{-1} was assigned as the stretching vibration of Al-OAl bonds (10,11).

The structure of air-formed oxide layer on aluminum has been reported to be "amorphous" γ-Al_2O_3 (15,16) containing some aluminum hydroxide and bound water (17-19). The O/Al atomic ratio for the oxide layer on as-evaporated aluminum, measured through XPS, is 1.95 (6), which suggests that some hydroxide or

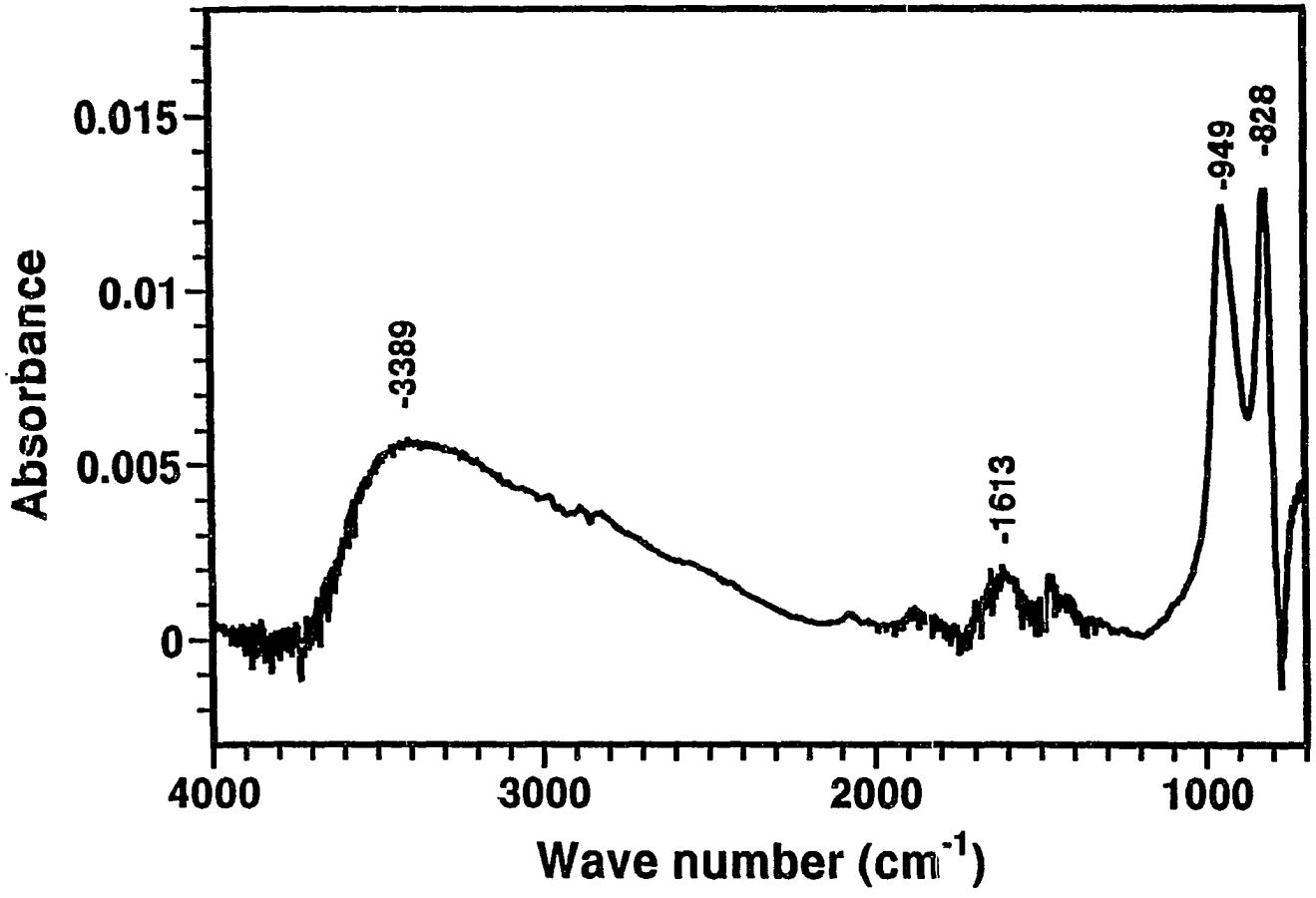

Figure 1. Infrared external reflection spectrum for as deposited Al film; Au film as reference spectrum. The p-polarized light was incident at 80°.

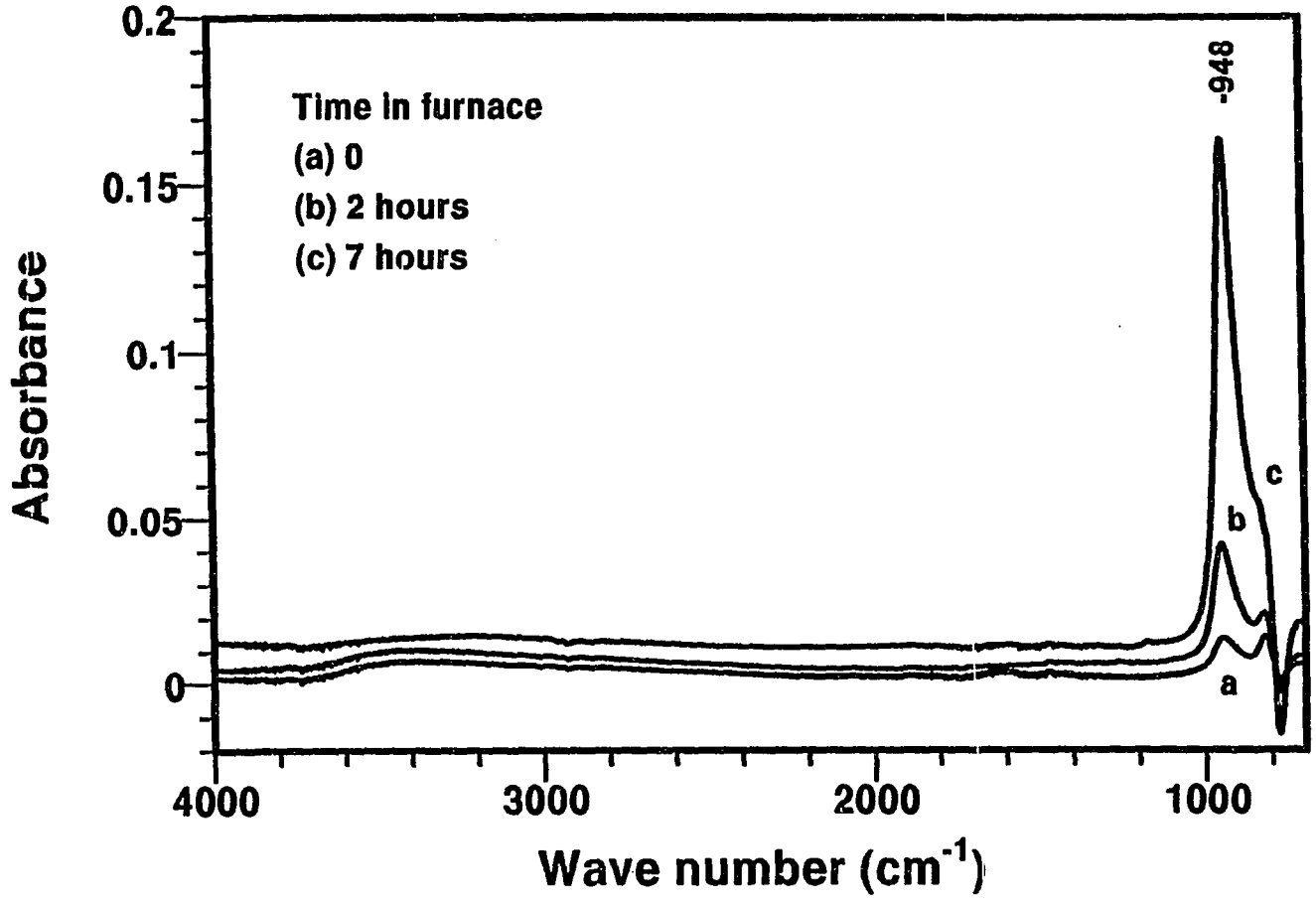

Figure 2. Infrared external reflection spectra for heat treated Al films; Au film as reference spectrum. Temperature 380°C; time in furnace (a) zero (b) 2 hours (c) 7 hours.

water is present. The hydroxide stretch band is very wide (1500 cm^{-1}) and is at lower wavenumber than the O-H stretch for "free water" hydroxyl (3600-3700 cm^{-1}). Thus it appears that much of the hydroxide is in a "bound" state, as would be the case for a film incorporating hydroxide or chemisorbed water. On the other hand, one cannot rule out the possibility that both the O-H stretch and the H-O-H bending vibrations in Fig. 1 may be simply due to gas-phase or physically adsorbed water on the film surface.

Effect of HCl pretreatment.- As discussed in a previous paper, HCl pretreatment promoted the cathodic hydrogen evolution reaction when the electrode potential was stepped to below a critical potential (6). Therefore, the effect of HCl pretreatment on the air-formed oxide film was also examined. Shown in Fig. 3 are the infrared spectra of aluminum films after immersion in 0.1 M HCl at room temperature for 5 and 20 minutes, using the spectra of the films before immersion as references (as in Fig. 1). All the major peaks decrease in intensity, indicating film dissolution. The intensity for the Al-O peak at 961 cm^{-1} decreased continuously during the HCl pretreatment. The peak area for the Al-O band decreased 4.1% at 5 minutes and 9.7% at 20 minutes. Mass loss during immersion of samples in 0.1M HCl was also noted from *in-situ* quartz crystal microbalance measurement. The mass loss measured during 5 min pretreatment was about 210 ng/cm^2 (6), which is much greater than 4.1% (38 ng/cm^2) of the oxide dissolved. Thus it appears that both metal dissolution and oxide film thinning occurred during pretreatment. The effect of pretreatment on the increasing cathodic current was attributed primarily due to oxide film thinning (6).

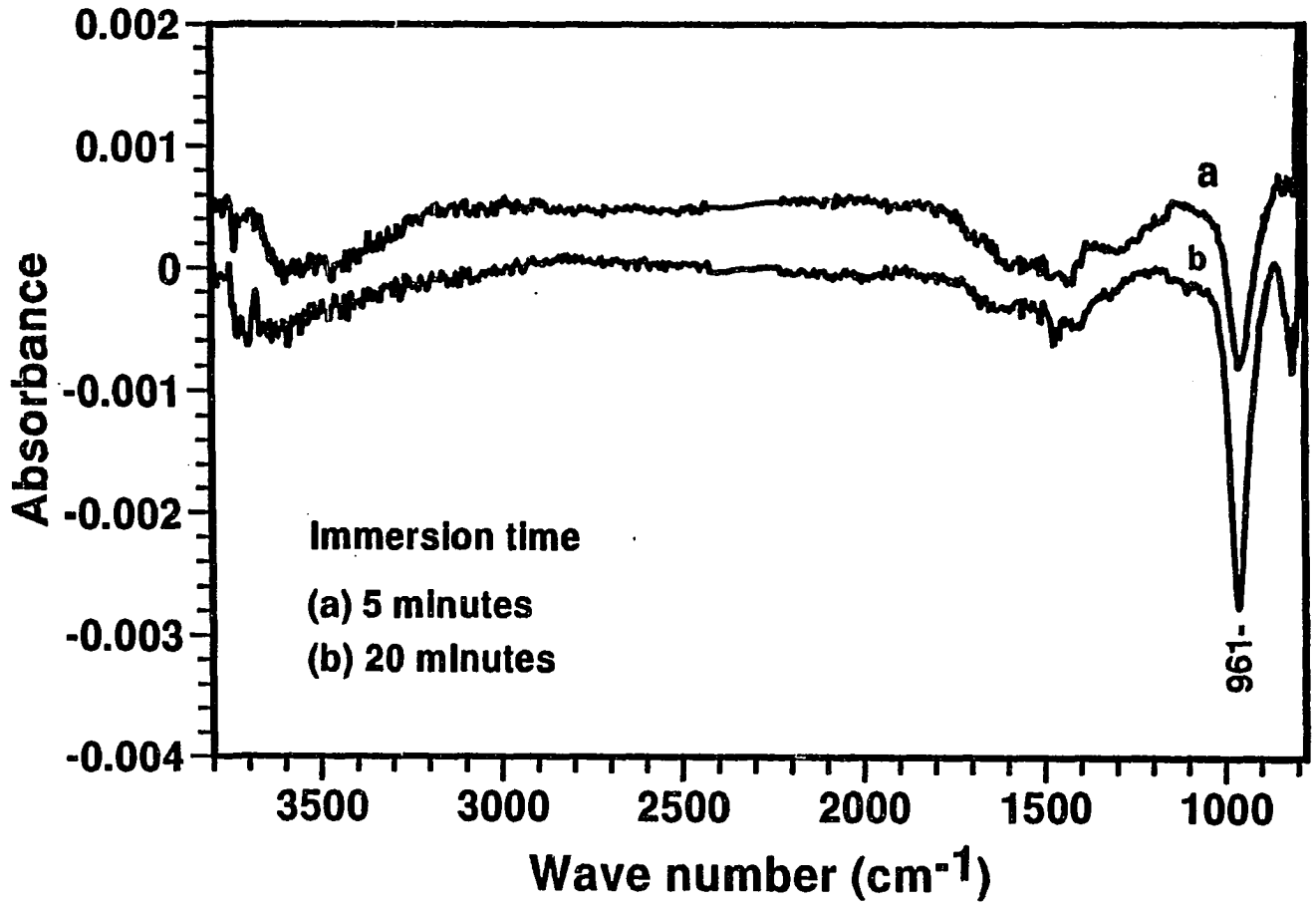

Figure 3. Differences of infrared external reflection spectra for Al films before and after immersion in 0.1M HCl at room temperature. Immersion time (a) 5 min; (b) 20 min.

Infrared spectra of oxide films formed during cathodic charging.- Infrared reflectance spectra for aluminum evaporated films, after cathodic charging in 0.1M HCl at ambient temperature, are shown in Fig. 4. The spectra in Fig. 4 are difference spectra referenced to the spectrum of the film after 0.1M HCl pretreatment. No increase in absorbance of the spectrum was noted for the film with 4.7 mC/cm^2 cathodic charge applied. For charges above 10.7 mC/cm^2, the intensities for the peaks in the spectra increased continuously. A peak which was not present in the spectrum of the native oxide film before pretreatment, centered at 905 cm^{-1} with a shoulder at around 1050 cm^{-1}, became apparent and increased significantly with cathodic charge (see Fig. 4b). The band at 1644 cm^{-1}, also grew with cathodic charge. The maximum of the broad band at high frequency shifted gradually from 3389 cm^{-1} for the bare film toward a higher frequency of 3459 cm^{-1} for the cathodically charged films. It should be noted here that the spectra do not indicate composition of film immediately after cathodic charging, because of open circuit oxidation, observed with the quartz crystal microbalance, after cathodic polarization was interrupted (6).

Figure 4 shows that the critical charge for the products of cathodic polarization to be detected by *ex-situ* infrared spectroscopy is between 4.7-10.7 mC/cm^2. This charge approximately agrees with the critical charge (7.2 mC/cm^2) for mass increase of the electrode in the quartz crystal microbalance experiments (see Fig. 6). The areas for the three major bands, which were integrated from the spectra shown in Fig. 4, increased linearly with cathodic charge as can be seen from Fig. 5. Thus, the

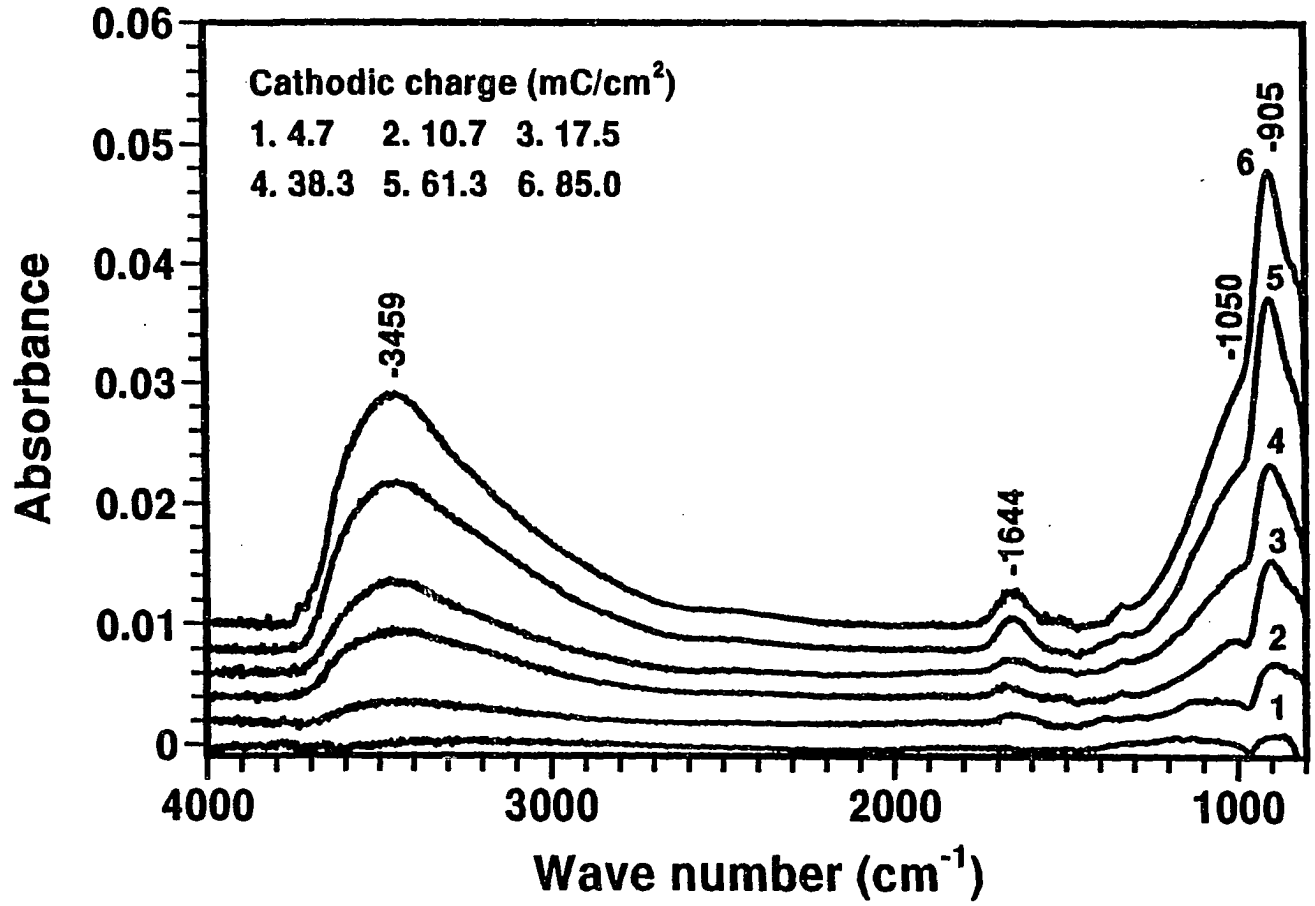

Figure 4. Effect of cathodic charging on infrared external reflection spectra of Al films. The spectra are difference spectra referenced to the spectrum of the film after 0.1M HCl pretreatment for 5 minutes. Cathodic potential -2.0V. Cathodic charges as indicated.

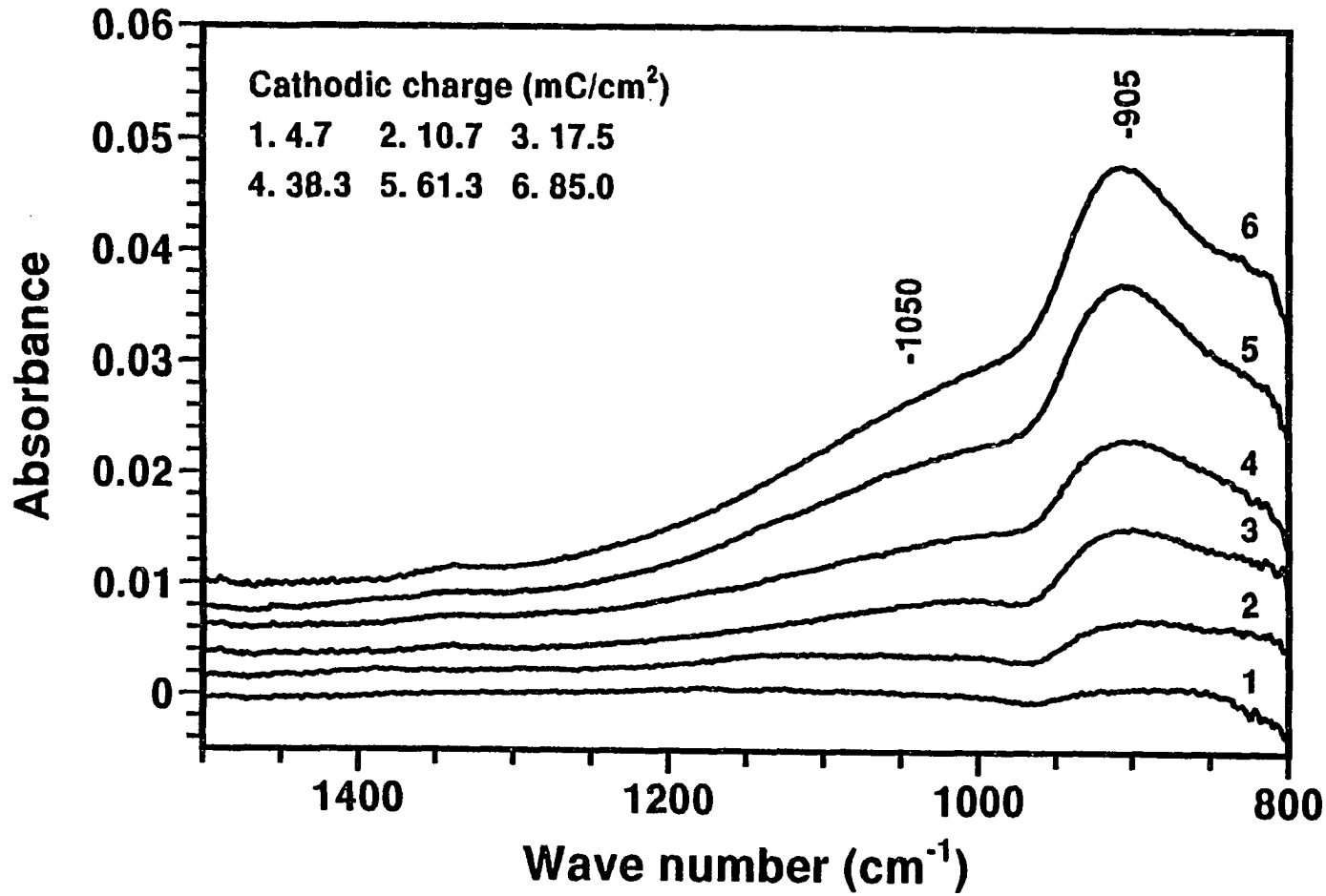

Figure 4b. Effect of cathodic charging on infrared external reflection spectra of Al films. The spectra are difference spectra referenced to the spectrum of the film after 0.1M HCl pretreatment for 5 minutes. Cathodic potential -2.0V. Cathodic charges as indicated. Expanded spectra for the 1500-800 cm^{-1} region in Fig. 4.

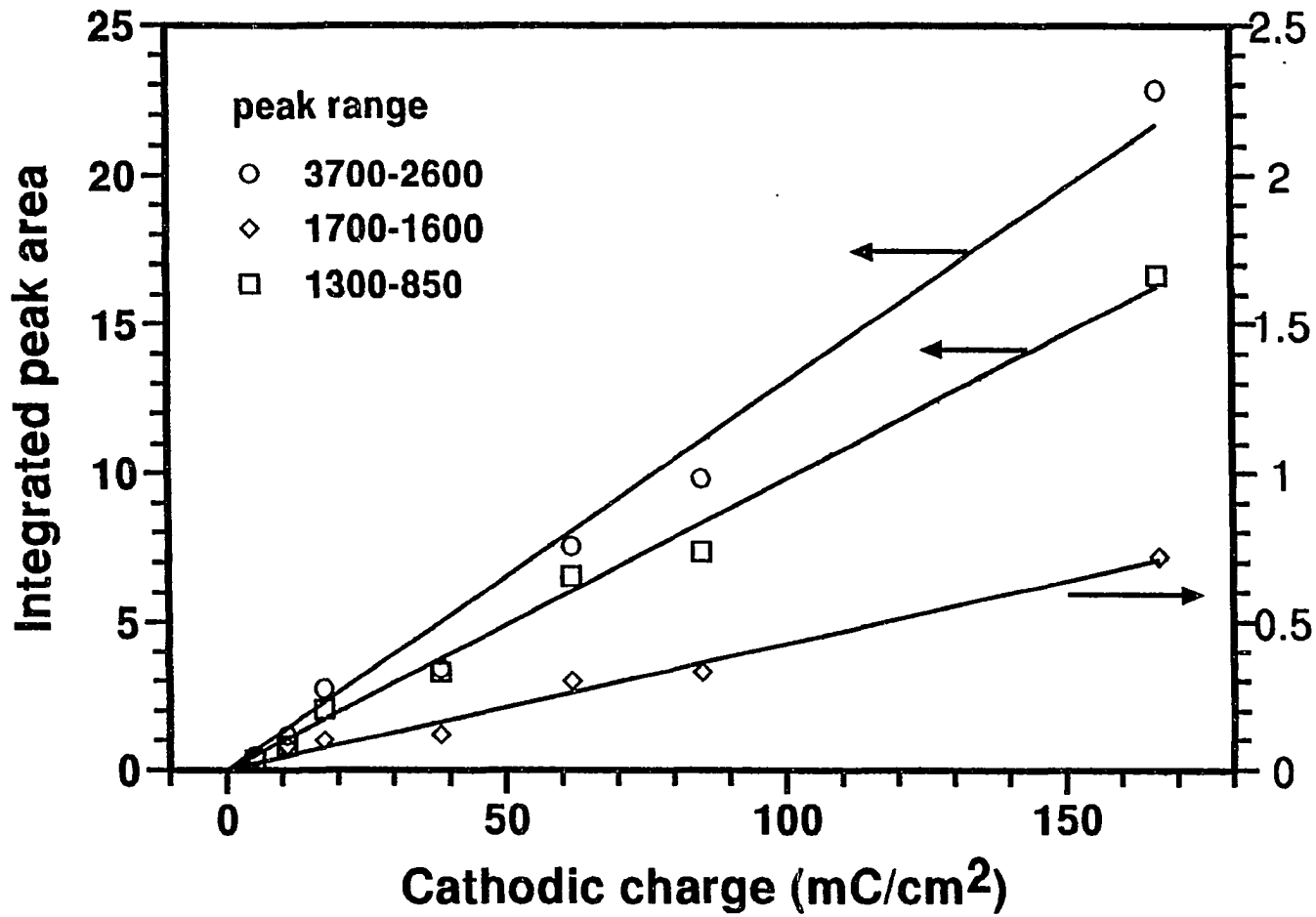

Figure 5. Integrated peak areas for the bands of the infrared spectra shown in Figure 4.

film maintains an approximately uniform composition as it becomes thicker. Peak areas were compared to the mass increases measured *in-situ* with the quartz crystal microbalance as shown in Fig. 6 (6). Figure 7 shows that both measurements have linear dependence on cathodic charge, suggesting that the films studied with infrared spectroscopy are the same as those whose growth was measured with QCM. Deuterium exchange and dehydration experiments were carried out to assist in the assignment of bands in the infrared spectra.

Deuterium exchange and dehydration studies.- Shown in Fig. 8 are the infrared reflectance spectra for aluminum film with 250 mC/cm^2 cathodic charge applied (a), and with 3 hours immersion in 99.8% D_2O after the cathodic charging (b). Deuterium exchange caused the 3462 cm^{-1} and the 1644 cm^{-1} bands to shift to 2543 cm^{-1} (O-D stretch) and 1501 cm^{-1}(D-O-D bend) (9) respectively. The shoulder at around 1050 cm^{-1} disappeared. The intensity for the band at 905 cm^{-1} increased, and the position for the peak shifted slightly to 890 cm^{-1}. It is possible that the 1050 cm^{-1} shoulder and the 905 cm-1 band collapsed into one band. The peak positions and intensities returned to their original values when the deuterated samples were immersed in H_2O for another 3 hours. Also, the spectra only changed slightly if the films were allowed to dry in the spin coater which exposed to atmosphere, after removal from liquid D_2O. These observations indicate that the exchange process is reversible.

Fig. 9 compares the infrared spectrum for cathodically charged aluminum and the spectrum for the same sample which had received subsequent heat treatment at

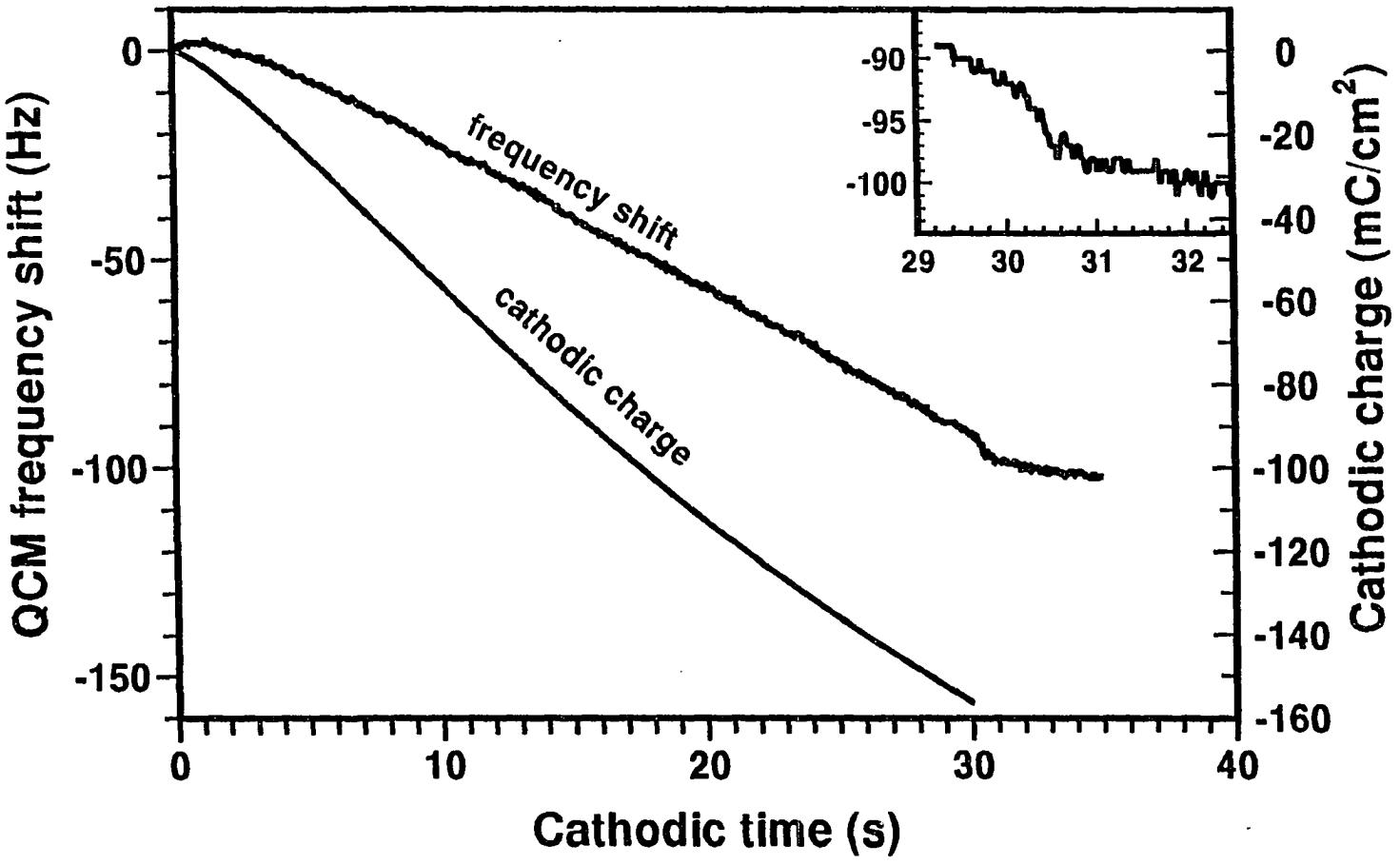

Figure 6. Quartz crystal frequency shift and accumulated cathodic charge obtained during cathodic polarization of Al in 0.1M HCl at room temperature. Cathodic potential -2.0 V.

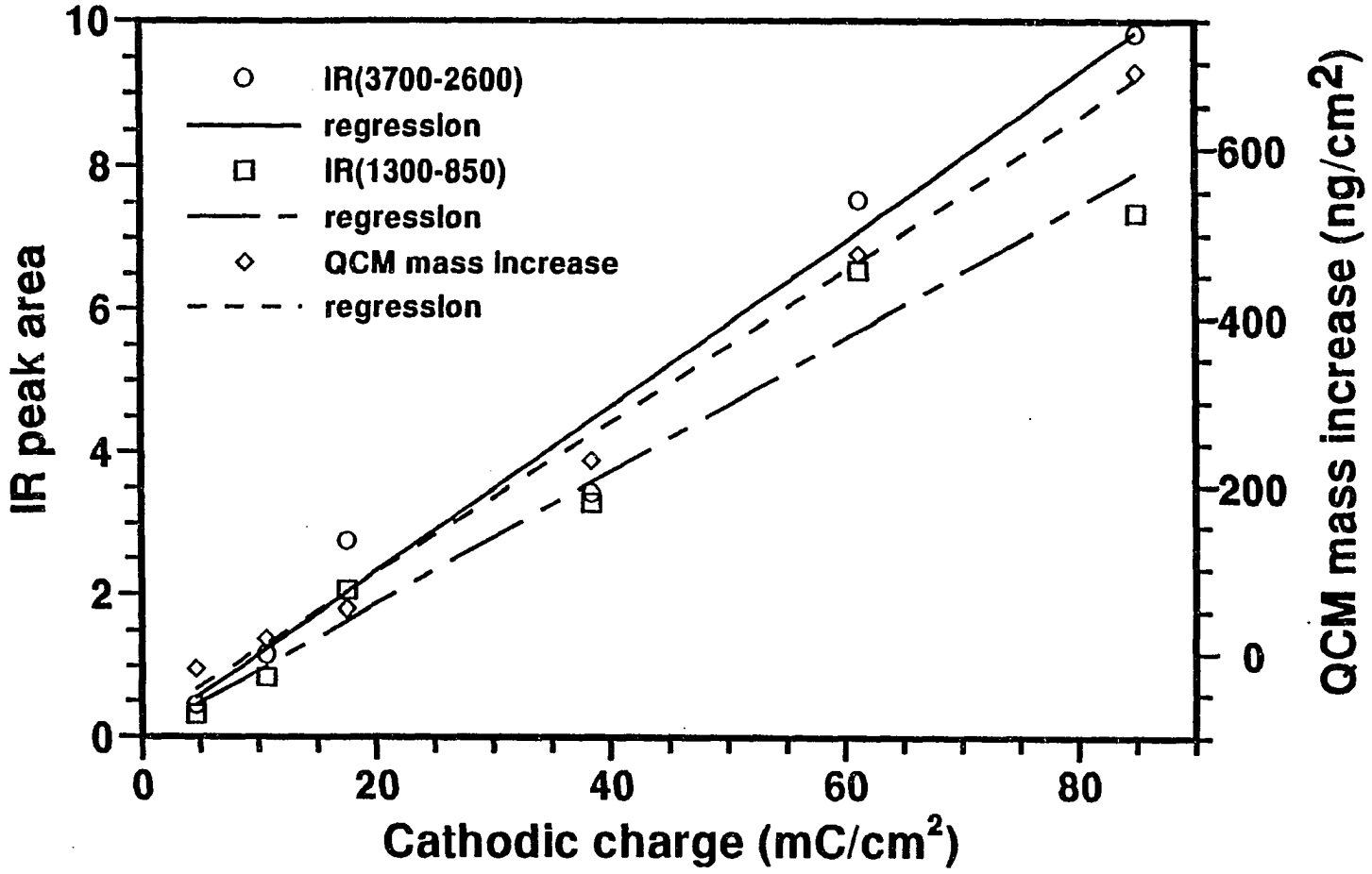

Figure 7. Infrared peak area and QCM mass increase as functions of applied cathodic charge. QCM mass increases were calculated from the frequency shift in Fig. 6 at charges corresponding to the charges applied in infrared experiments.

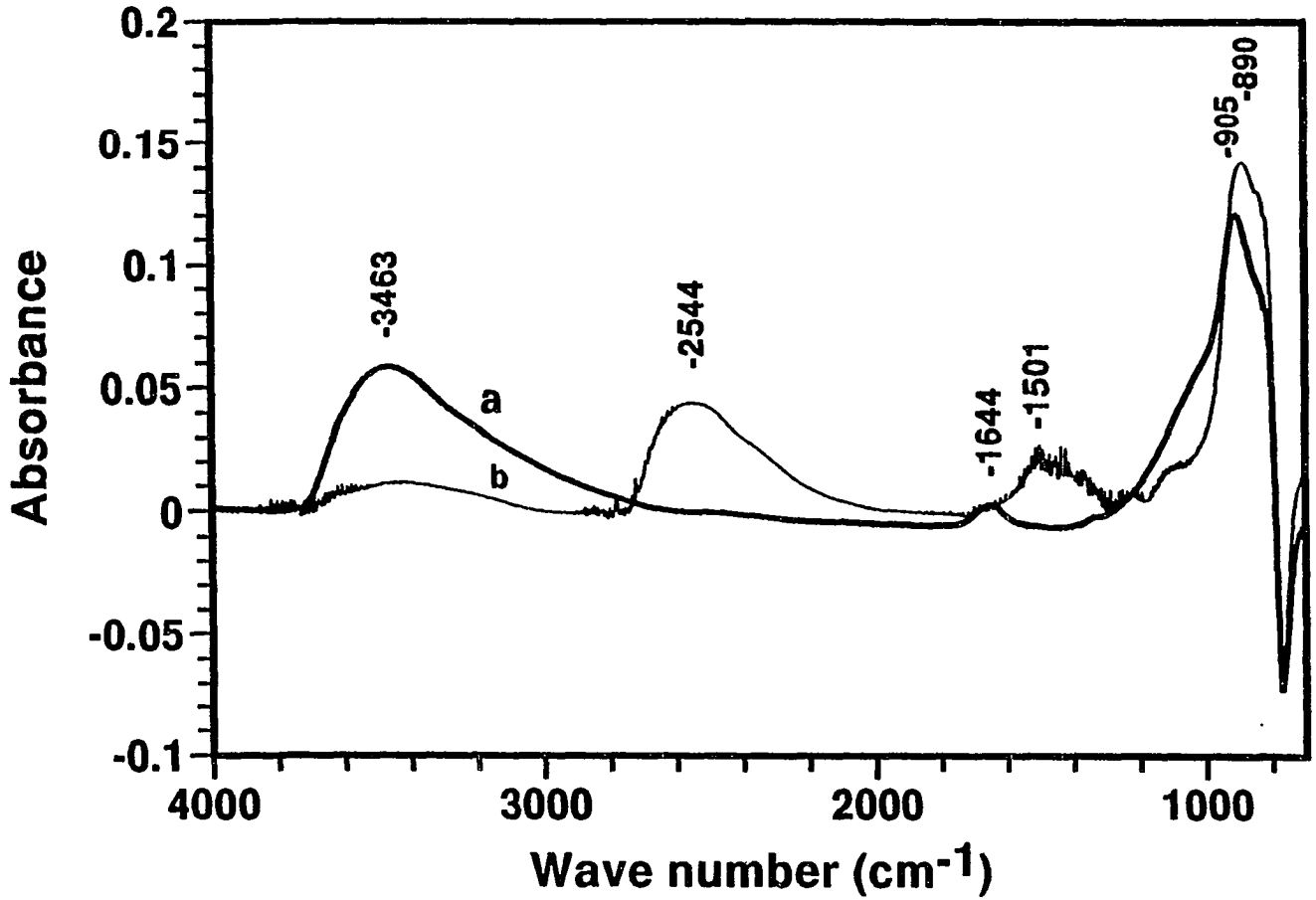

Figure 8. Effect of deuterium exchange on the infrared external reflection spectra of cathodic charged Al film. (a) After applied 250 mC/cm^2 cathodic charge; (b) after (a) and then immersion in 99.9% D_2O for three hours.

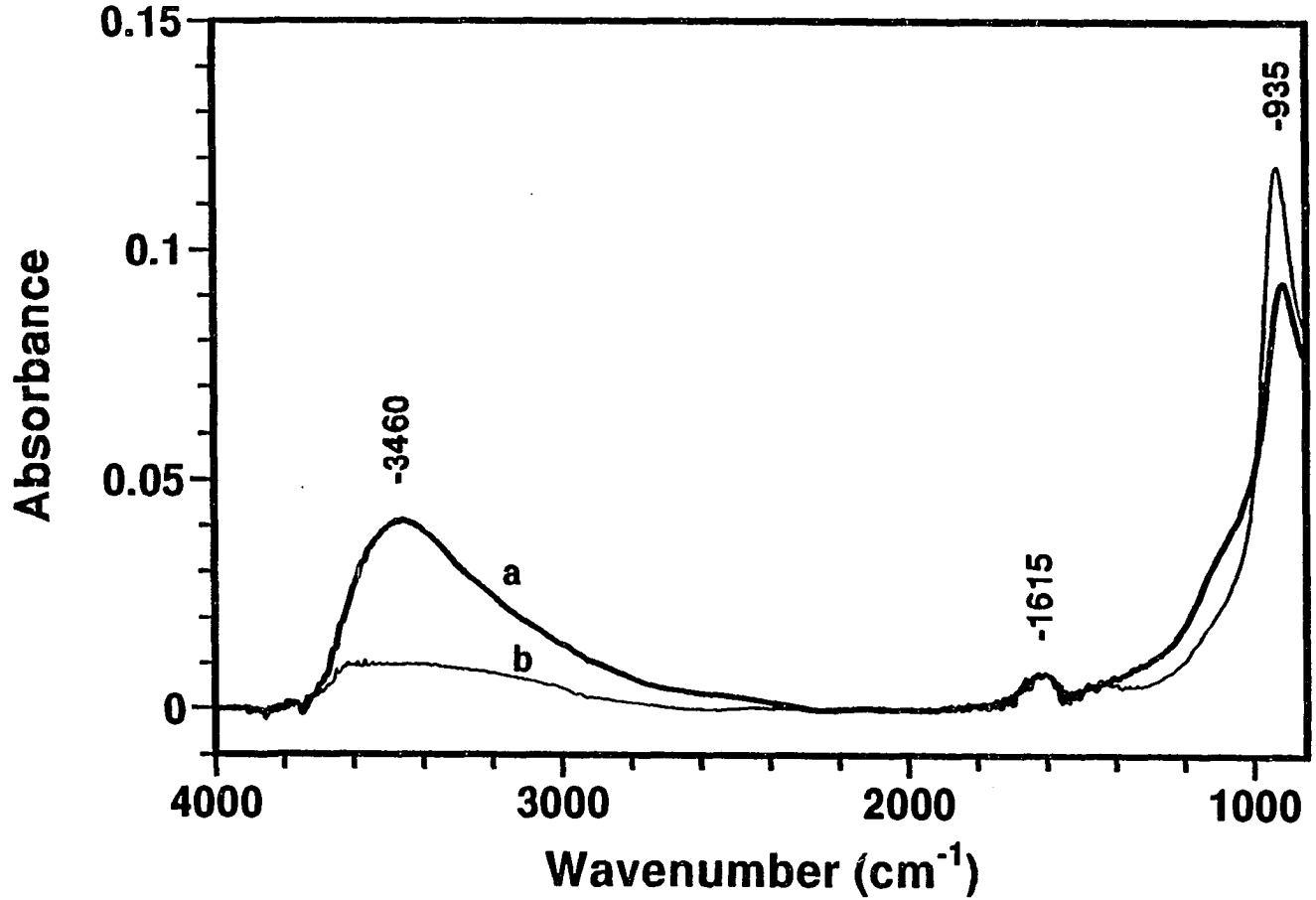

Figure 9. Effect of dehydration on the infrared external reflection spectra of cathodic charged Al film. (a) After applied 167 mC/cm^2 cathodic charge; (b) after (a) and then heated in furnace for 3 hours at 235^{o}C.

235°C for 3 hours. Similarly to deuterium exchange, dehydration causes the band at 3460 cm^{-1} and the shoulder at 1050 cm^{-1} to drop out. However, the intensity for the band at 905 cm^{-1} increased and the peak position shifted to 935 cm^{-1}, which is close to the position of the Al-O band for anhydrous Al_2O_3. The increase of peak intensity of the Al-O band may be caused by thermal oxidation. The dehydration experiment shows that the 905 cm^{-1} band is an Al-O vibration, whose wavenumber is different in the (anhydrous) thermally oxidized film, as opposed to the (hydrous) film produced by cathodic charging.

The band assignments can be given, based on deuterium exchange and dehydration experiments, and previously published peak assignments. The 3459 cm^{-1} band is an O-H stretching vibration (7,9-11,14). The shift of the 1050 cm^{-1} band upon deuteration shows that the 1050 cm^{-1} vibration is coupled to hydrogen. This shoulder also dropped out after dehydration. Therefore, the 1050 cm^{-1} shoulder is assigned to an Al-O-H bending vibration, in agreement with previous infrared investigations of bulk aluminum hydroxides and oxyhydroxides (7). The 905 cm^{-1} band is considered to be associated with an aluminum-oxygen bond in a hydrogen-bonded environment. When the coupling of Al-O to hydrogen is removed by dehydration, this band shifts to higher wavenumbers. The slight negative shift in this band after deuterium exchange may be the result of Al-O coupling to the more massive deuterium, as opposed to hydrogen.

DISCUSSION AND CONCLUSIONS

The cathodic product detected by infrared spectroscopy is an aluminum oxide or hydroxide which contains water. Of the various aluminum oxides whose spectra have been published, the spectra in Fig. 4 compare most favorably to that of the porous, amorphous oxide films formed by anodizing in acid solutions (9-11).

Previous work has shown that the resistance of the surface oxide layer on aluminum is reduced dramatically by cathodic charging, at potentials below a critical potential of about -1.65V *vs.* Ag/AgCl/4M KCl reference electrode (6). The reduction in film resistance facilitates transport of hydrogen ions as well as aluminum and oxygen ions in the film, permitting film growth. When the electrode potential was stepped from the cathodic potential to a potential near the open circuit potential, an anodic current decay accompanied by a mass increase was observed. This anodic current decay was attributed to a chemical change, which restores the resistance (20). Thus, the film observed with the infrared spectroscopy may not be the same composition as during cathodic charging.

The areas for the three bands increase linearly with cathodic charge suggesting that the composition of the cathodic produced film is uniform. The H-O-H bend band indicates the presence of water absorbed in the film. O'Sullivan *et al.* (9) found that porous anodic films formed in acid solutions exchanged completely with deuterium, but that when the pores in these films were "sealed" by immersion in boiling water, the

exchange was not complete. Thus, the ability to exchange deuterium is a reflection of the porosity or "openness" of the film structure. The anodic films formed in acid solutions are considered to consist of small amorphous alumina particles in an aqueous matrix. Based on their ability to exchange deuterium reversibly, the films produced by cathodic charging can be inferred to posses a similar structure. Also, in Ref. (6), it was observed that the cathodic films are ohmic proton conductors, with the conductivity on the same order of magnitude as precipitated aluminum hydroxide (21). The proton conductive properties of aluminum hydroxide were attributed to their "particle hydrous" structure (i.e., solid crystallites in an aqueous matrix), which is similar to the structure described above for anodic alumina films. The complex band structure around 900-1100 cm^{-1} indicates a high degree of coordination of Al^{+3} to OH or H_2O in final film. The OH groups or H_2O molecules are readily accessible to exchange by D_2O.

ACKNOWLEDGMENTS

Financial support for this work was provided by KDK Corporation (Takahagi, Japan) through a fellowship to Mr. Lin. The authors thank C. C. Wu for assisting in FTIR measurement.

REFERENCES

1. H. Kaesche, in "Localized Corrosion," R. W. Staehle *et al.* Editors, p. 516, NACE, Houston (1974).

2. E.P.G.T. ven de Ven and H. Koelmans, *J. Electrochem. Soc.*, **123**, 143 (1976).

3. W. Vedder and D. A. Vermilyea, *Trans. Faraday Soc.*, **65**, 561 (1969).

4. J. Radoševič, M. Kliškič, P. Dabič, R. Stevanovič and A. Despič, *J. Electroanal. Chem.*, **277**, 105 (1990).

5. C.-F. Lin and K. R. Hebert, *J. Electrochem. Soc.*, **137**, 3723 (1990).

6. C.-F. Lin and K. R. Hebert, to be submitted.

7. R. S. Alwitt, in "Oxides and Oxide Films," J. W. Diggle and A. K. Vijh, Editors, Vol. 4, p. 183, New York (1976).

8. S. M. Stole and M. D. Porter, *App. Spectrosc.*, **49**, 1418 (1990).

9. J. P. O'Sullivan, J. A. Hockey, and G. C. Wood, *Trans. Faraday Soc.*, **65**, 535 (1969).

10. G. A. Dorsey, Jr., *J. Electrochem. Soc.*, **113**, 169 (1966).

11. A. B. Kiss and E. Szontágh, *Acta Chim. (Budapest)*, **92**, 129 (1977).

12. A. J. Maeland, R. Rittenhouse, W. Lahar and P. V. Romano, *Thin Solid Films*, **21**, 67 (1974).

13. T. Takamura, H. Kihara-Morishita and U. Moriyama, *Thin Solid Films*, **6**, R17 (1970).

14. R. W. Hannah, *Appl. Spectrosc.*, **17**, 23 (1963).

15. R. K. Hart, *Trans. Faraday Soc.*, **50**, 269 (1950).

16. R. K. Hart, *Proc., Royal Soc.*, **A236**, 68 (1958).

17. Z. Szklarska-Smialowska, "Pitting Corrosion of Metals," p. 8, NACE, Houston, Texas (1986).

18. P. B. Barna, Z. Bodó and G. Gergely, *Thin Solid Films*, **120**, 249 (1984).

19. K. A. Wickersheim and G. K. Korpi, *J. Chem. Phys.*, **42**, 579 (1965).

20. C.-F. Lin and K. R. Hebert, to be submitted.

21. D. J. Dzimitrowicz, J. B. Goodenough, and P. J. Wiseman, *Mat. Res. Bull.*, **17**, 971 (1982).

PAPER III.

STUDY OF CATHODICALLY-INDUCED OXIDATION REACTIONS ON ALUMINUM IN ACID SOLUTIONS

Study of Cathodically-induced Oxidation Reactions on Aluminum in Acid Solutions

Ching-Feng Lin and Kurt R. Hebert

Department of Chemical Engineering

Iowa State University
Ames, IA 50011

ABSTRACT

The effect of prior cathodic polarization on anodic oxidation processes on aluminum was investigated using the quartz crystal microbalance technique. Cathodic charging of aluminum in acid solution induced an anodic current transient in the passive potential region, accompanied by electrode mass increase, which was primarily due to water absorption into the film. The anodic current decay, by three orders of magnitude, was due to an increase of the film resistance. The reaction with the metal surface of water which had been stored in the film during cathodic charging, to form aluminum oxide, was considered to be responsible for the increase of resistance.

INTRODUCTION

Cathodic polarization of natural oxide covered aluminum in aqueous acid solution results in dramatic change in hydrogen evolution kinetics (1). Cathodic charging "activates" the aluminum surface at potentials around -1.65V *vs.* Ag/AgCl//4M KCl, where the hydrogen evolution reaction follows Tafel kinetics. The effect of cathodic charging is to reduce the oxide film resistance for ion transport, through change of film composition from oxide to hydroxide. At the potential where the hydrogen evolution kinetics changed, formation of surface oxide film was also found by *in-situ* quartz crystal microbalance measurement. Proton conduction in the film was found to follow Ohm's law, and the conductivity of the film has the same order of magnitude as precipitated aluminum hydroxide. The film, which was shown from infrared spectroscopy to posses an "open" structure (2), contains appreciable amounts of water, which was considered to be responsible for the increase of film conductivity.

In Ref. (1), after the potential was stepped from a cathodic potential to a potential between the open circuit potential and the pitting potential, an anodic current transient accompanied by a mass increase was observed. The mass increase may be associated with an anodic oxidation reaction. Similar anodic current transients induced by prior cathodic charging were observed by Radoševiĉ *et al.* (3). These authors concluded that they represent oxidation of various substances which were generated by the cathodic reaction, and which did not diffuse away into the solution.

The goal of the present work is to investigate the cathodically-induced oxidation reaction and mass increase as part of an effort to determine the relation between the electrochemistry of aluminum, the composition of the surface film, and the corrosion resistance of the metal. Quantitative analysis of the dependence of anodic charge and mass increase were carried out using electrochemical methods and the quartz crystal microbalance technique.

EXPERIMENTAL

Al film samples used in this study were approximately 0.25 μm thick evaporated from a pure source (99.99% Al foil, provided by KDK corporation, Japan) onto quartz disks. The pressure in a cryopumped coating system (E360A, Edwards, West Sussex, England) was < $1x10^{-6}$ torr and the base pressure was < $4x10^{-7}$ torr. The detailed procedures for deposition of Al films have been described in a previous paper (1). The evaporated aluminum films were exposed in laboratory ambient for 24 hours. The electrochemical quartz crystal microbalance (QCM) system utilized for *in-situ* weight change measurement was the same as that employed in previous studies (4-6). Potentiostatic control and current measurement were accomplished by interfacing the QCM to a personal computer using a Lab-PC data acquisition board (National Instruments). The frequency was measured with a frequency counter (Hewlett Packard 5334b) interfaced with a GPIB-PCII board. A QuickBasic (Microsoft) program was developed to drive the two boards simultaneously. The frequency was measured at the rate of 18 ms per reading.

Aluminum film samples were evaporated onto both sides of planar (1 inch diam), overtone-polished, AT-cut quartz crystal (Valpey-Fisher). In some experiments, 5 MHz, BT-cut crystals were used. The films, which were deposited using a standard keyhole design (7), were ca. 0.25 μm thick and 0.34 cm^2 electrode area. The crystals were operated at the fundamental frequency of 5 MHz with the mass sensitivity of 17.67

$ngHz^{-1}cm^{-2}$, according to Sauerbrey relationship (7,8). The crystal was mounted in the wall of the electrochemical cell using an O-ring joint and two O-rings. Prior to a polarization experiment, the Al film was allowed to contact the electrolyte for 5 minutes at open circuit.

The reference electrode was a commercial Ag/AgCl/4M KCl electrode (Fisher). All reported potential values were referred to this reference electrode. The counter electrode was a Pt wire inserted into the cell. Cathodic polarization was at constant potential of -2.0V; the cathodic time was an experimental variable. Anodic potentials varied from -0.9V to 0.0V. In all experiments the electrolyte solutions were 25 ml aqueous 0.1M HCl or 0.1M H_2SO_4 solutions and the temperature was ambient (25^oC).

For the study of early anodic current transients, a potentiostat/galvanostat (PAR 273) was used for potential control. Al samples were used which had been deposited onto microscope slides with exposed area of 0.34 cm^2. A personal computer along with a GPIB interface were employed to execute the etching experiments and to retrieve the potential and current values from the potentiostat's memory. The very early stage anodic currents were measured simultaneously through a high speed voltmeter (Keithley K194A) at the rate of 10 μs.

RESULTS

Mass and charge transients.- Quantitative investigation of the cathodically-induced mass changes accompanying anodic current transients was conducted through *in-situ* QCM measurement. The vibration frequency of the electrode as well as the anodic charge applied were measured simultaneously. Figure 1 shows the QCM frequency transient during cathodic charging at -2.0V (first 30s), followed by anodic polarization at -0.9V (after 30s). Both the frequency shift (mass increase) and cathodic charge changed linearly with time. Since the mass increase was due to surface film formation (1), it is apparent that the amount of surface hydroxide film is a linear function of cathodic charge. The inset in Fig. 1 shows the frequency transient after stepping to -0.9V. Figure 2 shows another example of a frequency transient at -0.9V, after cathodic charging for 10s at -2.0V. The anodic charge transient is also shown in the figure. Figure 2 shows that both mass and charge transients have the same time dependence. The frequency and the anodic charge approached a steady value at about 3s. The same time dependence for both transients suggests that uniform anodic oxidation accompanies mass increase on the electrode surface.

When the potential was stepped to -0.9V, the initial currents were larger then 10 mA/cm^2. The final steady state currents after the anodic transients were lower by approximately three orders of magnitude, about 10 $\mu A/cm^2$. The details of current transients will be discussed further below.

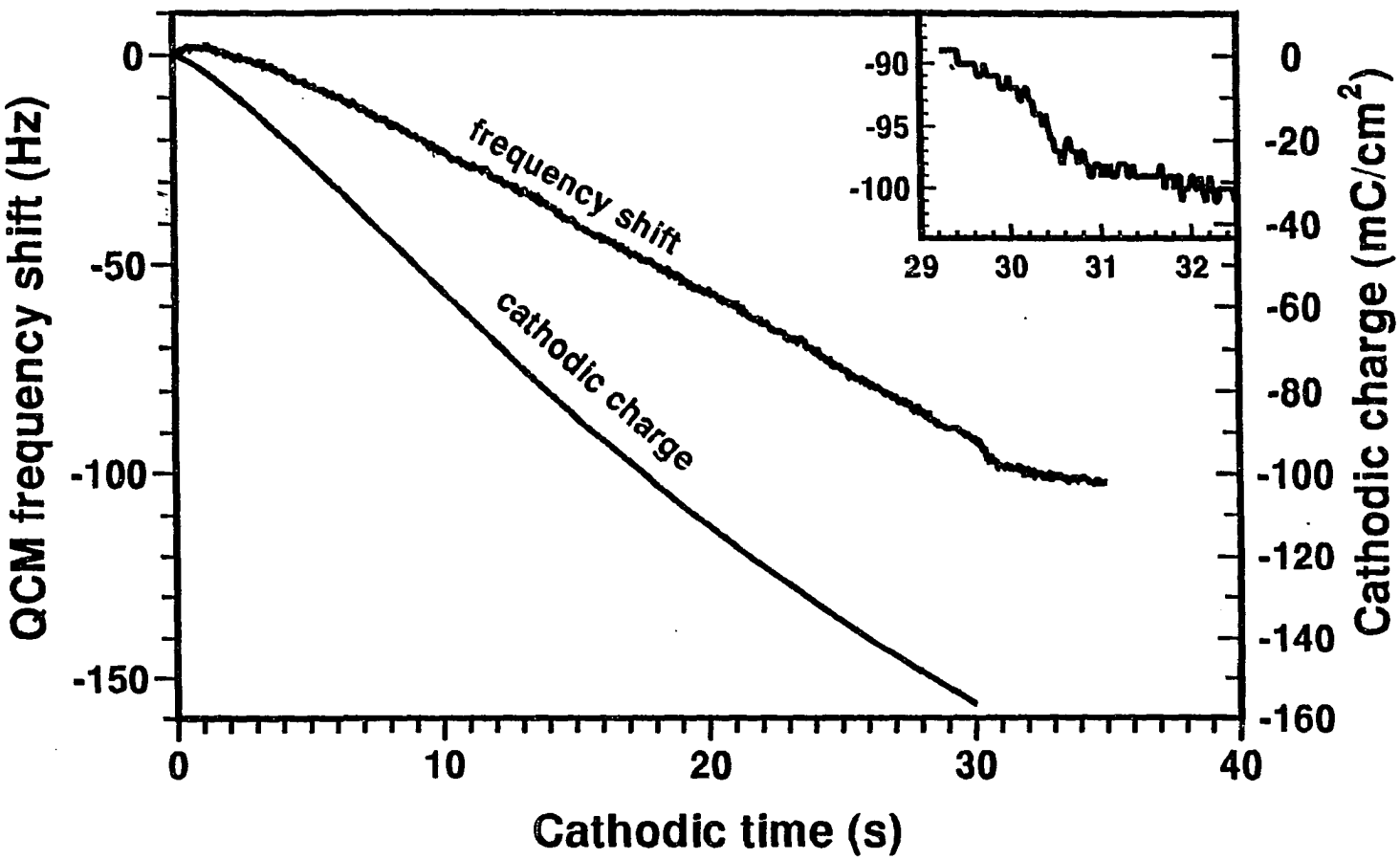

Figure 1. Quartz crystal frequency shift and accumulated cathodic charge obtained during cathodic polarization of Al in 0.1M HCl at room temperature. Cathodic potential -2.0V.

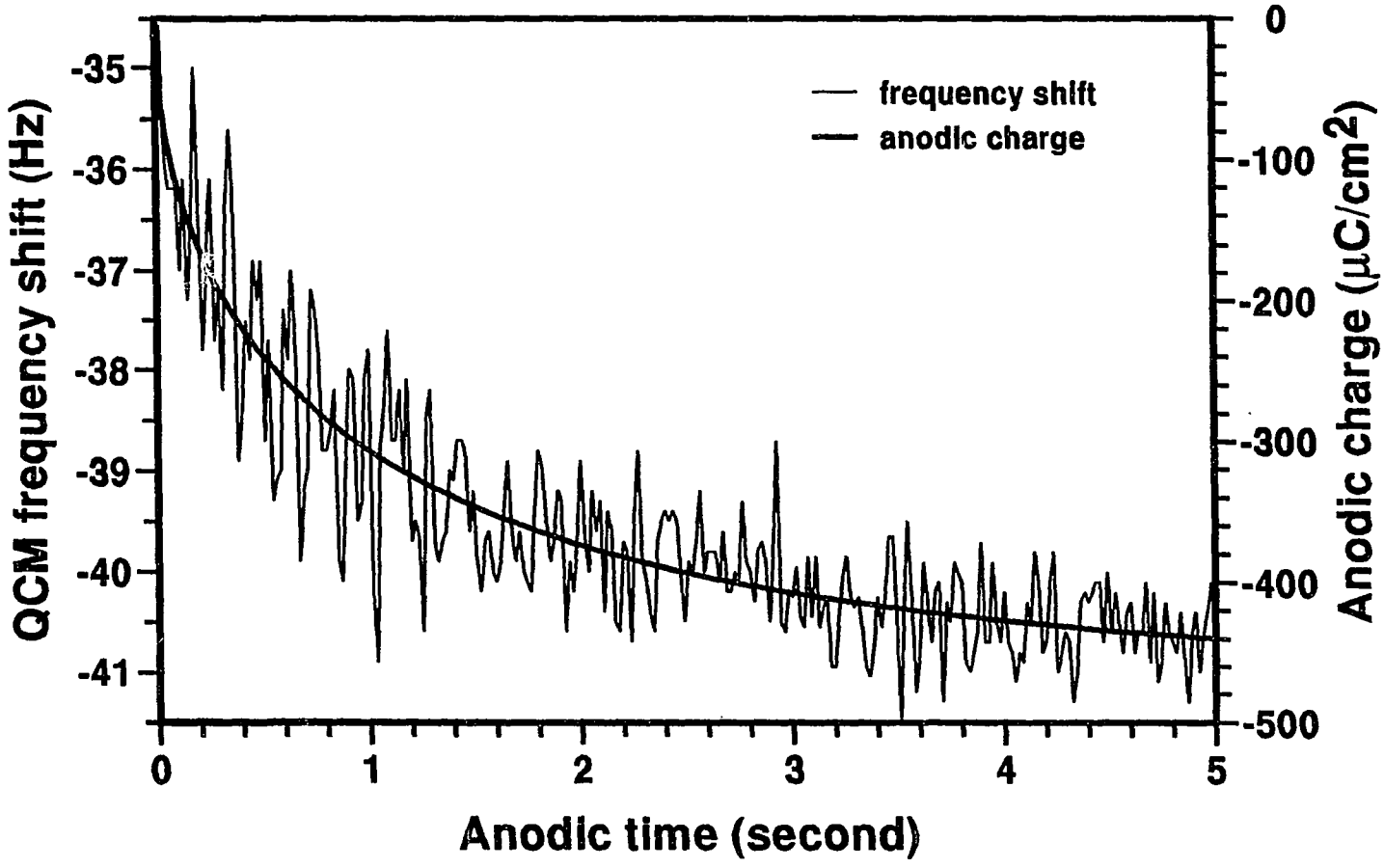

Figure 2. Transients of quartz crystal frequency shift and anodic charge obtained when the potential was stepped from anodic to -0.9V; 0.1M HCl solution, room temperature. Prior cathodic conditions: -2.0V, 10s.

Changes of stress of aluminum films can contribute to the frequency shift (7,9). Experiments were also carried out on aluminum samples which had been evaporated onto BT-cut quartz crystals to determine any stress effect on the frequency transient, at the potential of -0.9V. AT-cut and BT-cut quartz crystals have the same mass coefficient of frequency but stress coefficients which are opposite in sign (10,11), and have been employed to study the effect of stress change in metallic films on frequency shift (10). Figure 3 shows corresponding frequency transients for 5M Hz AT-cut and BT-cut crystals. For the BT-cut crystal, there was no frequency decrease as the electrode potential was stepped from -2.0V to -0.9V. In fact, no anodic frequency decrease was ever measured with BT-cut quartz, for any combination of solution, cathodic charge, and anodic potential below the pitting potential. Thus, stress changes accompany oxidation reactions. The mass and stress components of the frequency shifts at -0.9V in Fig. 3 were calculated according to the method of EerNisse (10,12). The integrated stress change at 3s of the anodic time is -7.3×10^3 dyne/cm, the negative sign indicating the stress in the aluminum film is compressive in nature (10). Compressive stress was also observed during growth of oxide film on iron by Heusler *et al.* (13), and was attributed to inward migration of oxygen-containing species during film growth. Tensile stress in aluminum film accompanying mass increase, on the other hand, was found at potentials above the pitting potential, after cathodic charging (9).

Figure 4 shows that the anodic mass increase is proportional to the prior cathodic mass increase. The anodic mass changes shown in Fig. 4 were calculated from the

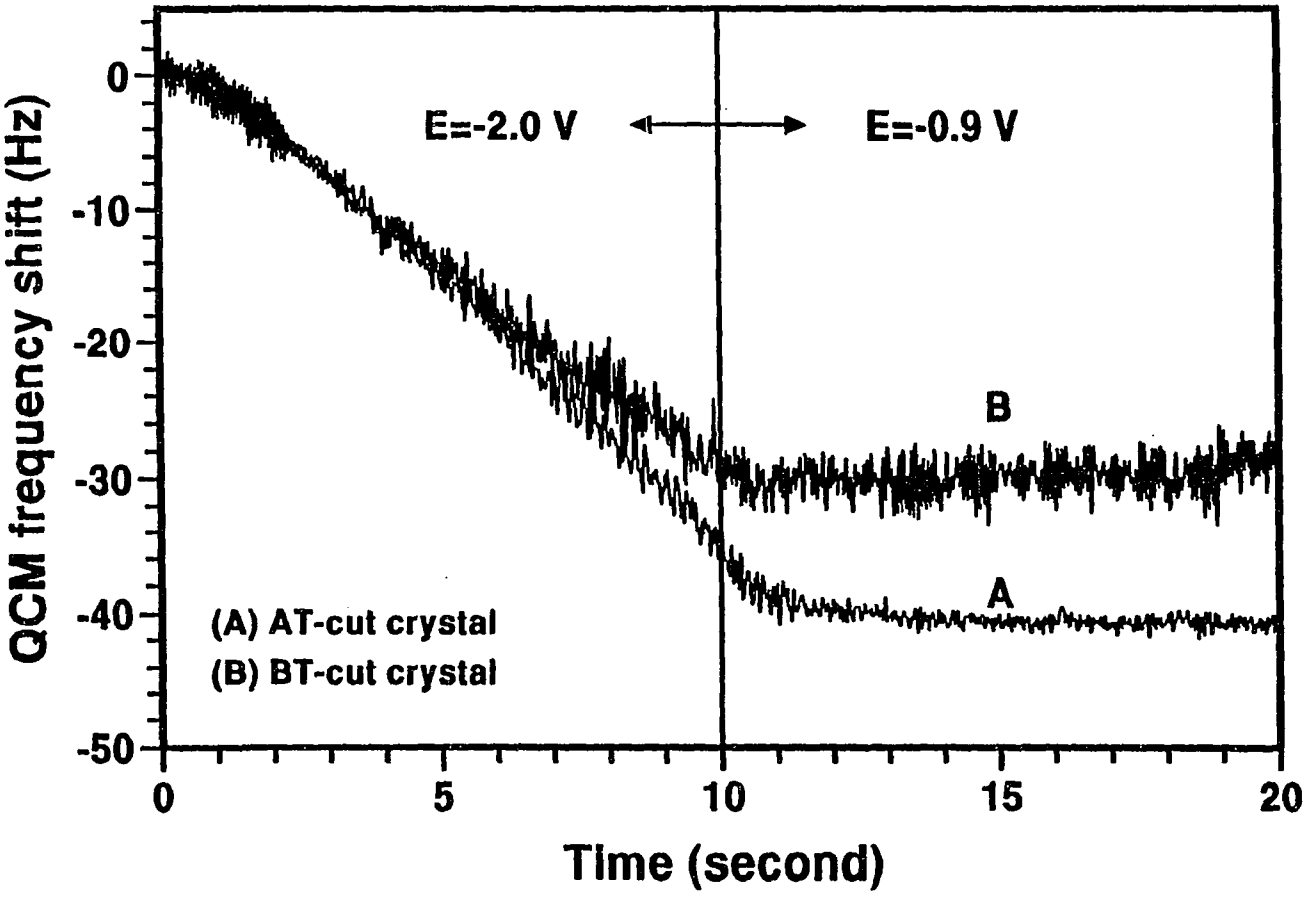

Figure 3. Effect of AT-cut and BT-cut quartz crystals on frequency transient at the potential of -0.9V; 0.1M HCl solution, room temperature. Prior cathodic conditions: -2.0V, 10s.

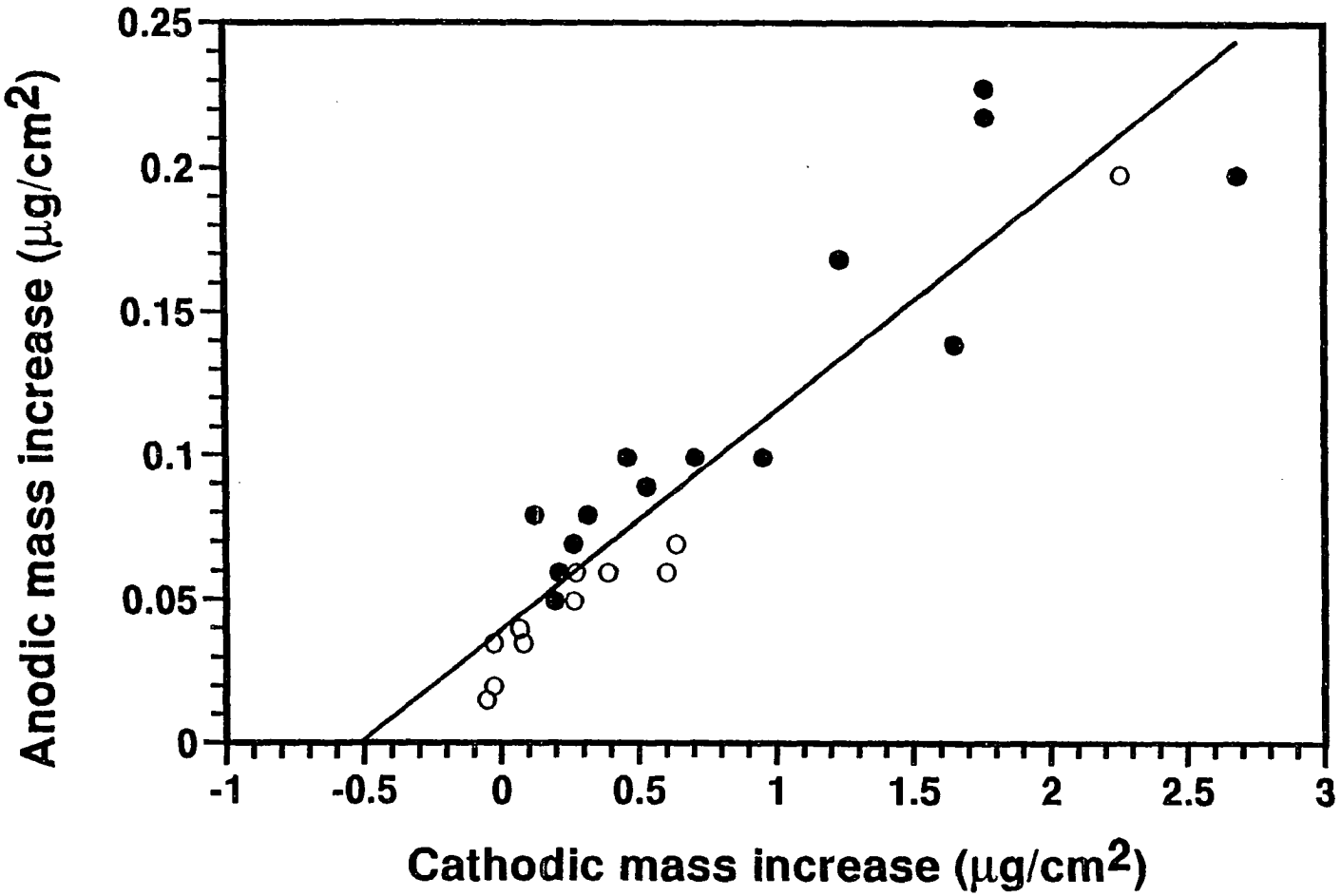

Figure 4. Effect of prior cathodic mass increase on anodic mass increase. Electrolyte solutions: open markers 0.1M HCl; closed markers 0.1M H_2SO_4. Cathodic potential -2.0V. Anodic potentials: 0.1M HCl solution -0.9, -0.7,and -0.65V; 0.1M H_2SO_4 solution -0.9, -0.6, -0.5, -0.3, -0.2, and 0.0V.

anodic frequency shifts for experiments carried out on AT-cut crystals, with the knowledge that the anodic frequency changes for BT-cut crystals are zero. Figure 4 shows that the anodic mass increase was independent of electrolyte solution used. This result indicates that the anion of the electrolyte is not involved in the oxidation reaction. The anodic potentials in Fig. 4 varied from -0.9V to 0.0V for the experiments carried out in H_2SO_4 solution. Apparently, the anodic mass increase is much more dependent on cathodic mass increase than on potential. As mentioned above, cathodic frequency decreases have been shown to be caused by the growth of surface hydroxide film on aluminum. Thus, Fig. 4 indicates that anodic mass change increased linearly with film thickness. The x-axis intercept at zero anodic mass increase is -0.514 $\mu g/cm^2$. The absolute value of this intercept corresponds to the mass of original oxide film prior to cathodic charging.

The charges passed during anodic current decays were also examined. The charges were integrated from time zero to the time when anodic current decayed to zero, and are show in Fig 5. Anodic charges obtained from experiments carried out in both HCl and H_2SO_4 solutions at different anodic potentials are included in the figure. Two general trends are observed from Fig. 5. First, the anodic charges increase with cathodic mass increase, at the same anodic potential. Second, the charges increase with anodic potential, at constant cathodic mass increase.

The times for the anodic charges to increase to steady-state values are shown in Fig. 6. The cathodic time was 10 s and the cathodic mass increases varied from

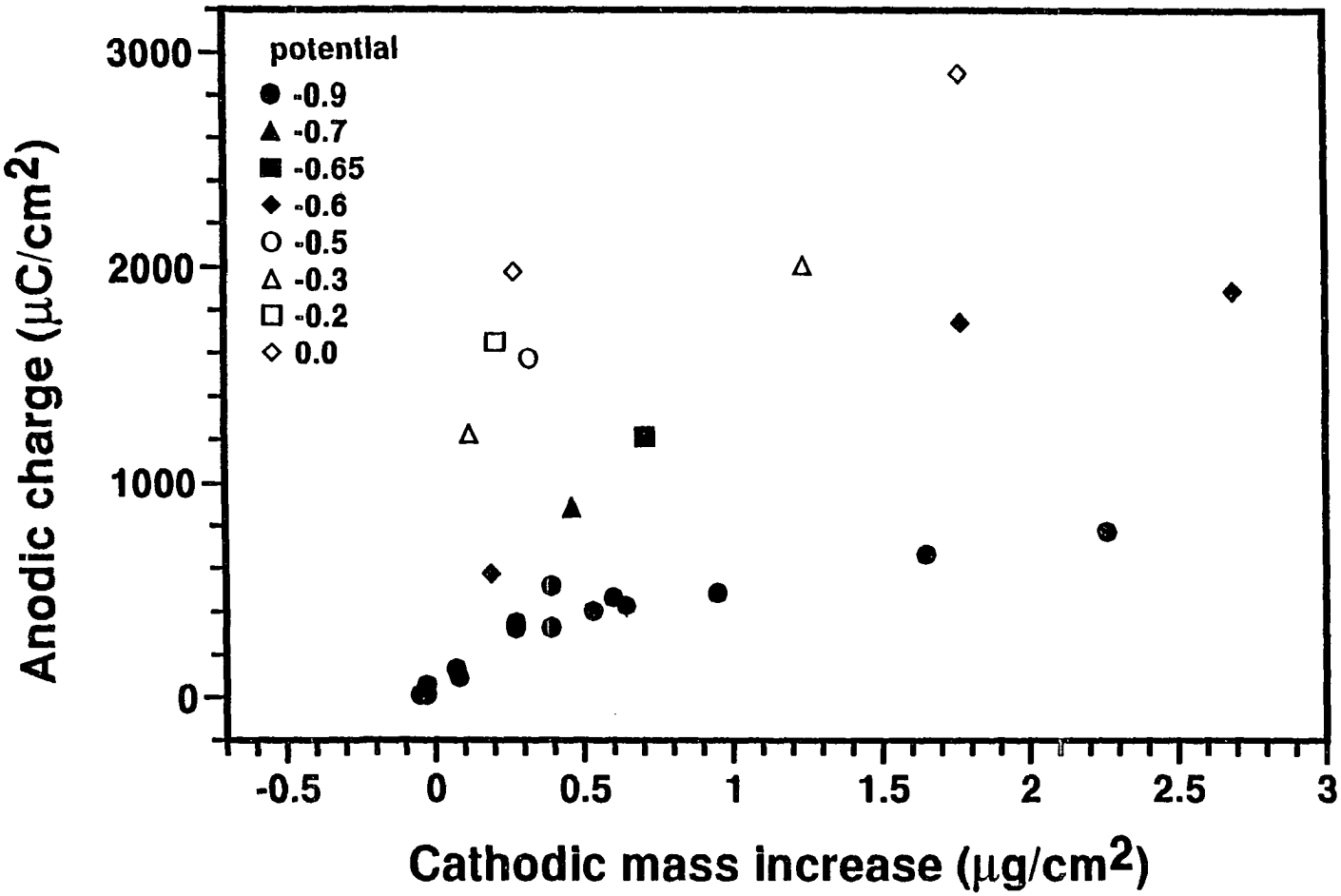

Figure 5. Effect of cathodic mass increase on anodic charge; 0.1M HCl or 0.1M H_2SO_4 solution. Cathodic potential -2.0V; anodic potentials as indicated.

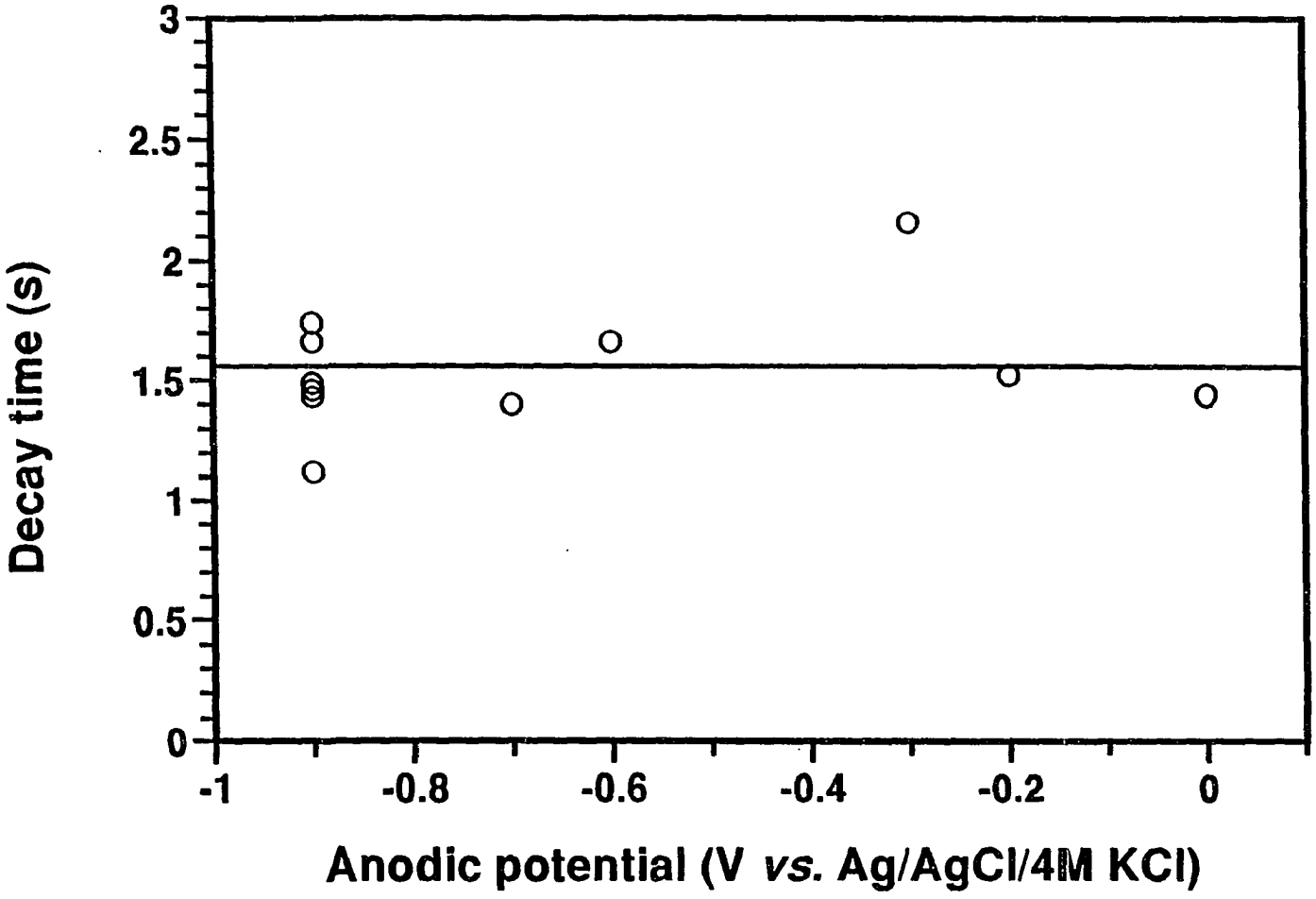

Figure 6. Plot of decay time for anodic charge *vs.* anodic potential; 0.1M HCl or 0.1M H_2SO_4 solution. Cathodic potential -2.0V; cathodic time 10s.

0.12-0.64 $\mu g/cm^2$. The decay time in Fig. 6 is defined as the time for the anodic charge to approach to 85% of its steady-state value. Figure 6 indicates that the time for the anodic current to decay is independent of electrode potential.

The anodic mass changes were considered to be due to electrochemical processes at the film/solution interface, and absorption of water into the film. During the growth of oxide film the anodic current at the film/solution interface results from the incorporation of oxygen into the film (i_l),

$$H2O_{(aq.)} \rightleftharpoons O^{=}_{(oxide)} + 2H^{-}_{(aq.)} \qquad [1]$$

and from loss of aluminum by dissolution into the electrolyte (i_c)

$$Al^{+3}_{(oxide)} \rightarrow Al^{+3}_{(aq.)} \qquad [2]$$

Vetter and Gorn (14) found that in the case of iron, transfer of ions through the film/solution interface was the rate determining step for reactions [1] and [2], yielding

$$i_c = i_{co} \exp\left(\frac{\alpha_c^{+} F}{RT}\eta_O^{23}\right) \qquad [3]$$

and

$$i_l = i_{lo}\left[\exp\left(\frac{\alpha_l^{+} F}{RT}\eta_O^{23}\right) - \exp\left(-\frac{\alpha_l^{-} F}{RT}\eta_O^{23}\right)\right] \qquad [4]$$

The measured current i is

$$i = i_c + i_l \qquad [5]$$

and η_O[23] is the overpotential for film formation/dissolution at the film/solution interface. Eq. [5] neglects current flow due to proton transport. The film formation current and Al^{+3} dissolution current were calculated from the measured current and Eq. [5]. The kinetic parameters used in Eqs. [3-4] were obtained from Våland and Heusler's results at the experimental pH of 1.55 (15). These parameters are $i_{o,Al}$= 3.6x10^{-6} A/cm^2; $i_{o,l}$=2.6x10^{-6} A/cm^2; $\alpha_{Al}{}^{+}$=1.11; $\alpha_l{}^{+}$=1.76; $\alpha_l{}^{-}$=0.24. The amount of water absorbed was then calculated by subtracting the net mass change due to reactions [2] and [3] from the measured mass changes.

The calculated mass increases due to water absorption are plotted *vs.* anodic potentials in Fig. 7. The y-axis in Fig. 7 has been normalized by dividing the mass increases due to H_2O by the sum of the cathodic mass change and the zero anodic mass increase intercept in Fig. 4. This later quantity is proportional to the film mass including both the original film and the film grown during cathodic charging. Figure 7 shows that the ratio of water mass increase to film mass was approximately constant for all the anodic potentials. This result would be expected, since incorporation of water during anodic oxidation would be by absorption, and would not be directly associated with electrochemical reactions. The assignment of the mass increase to water absorption also explains the independence of the transient decay time on potential, shown in Fig. 6. The potential dependence of the anodic charge in Fig. 5 is due to the potential driving force for reactions [1] and [2].

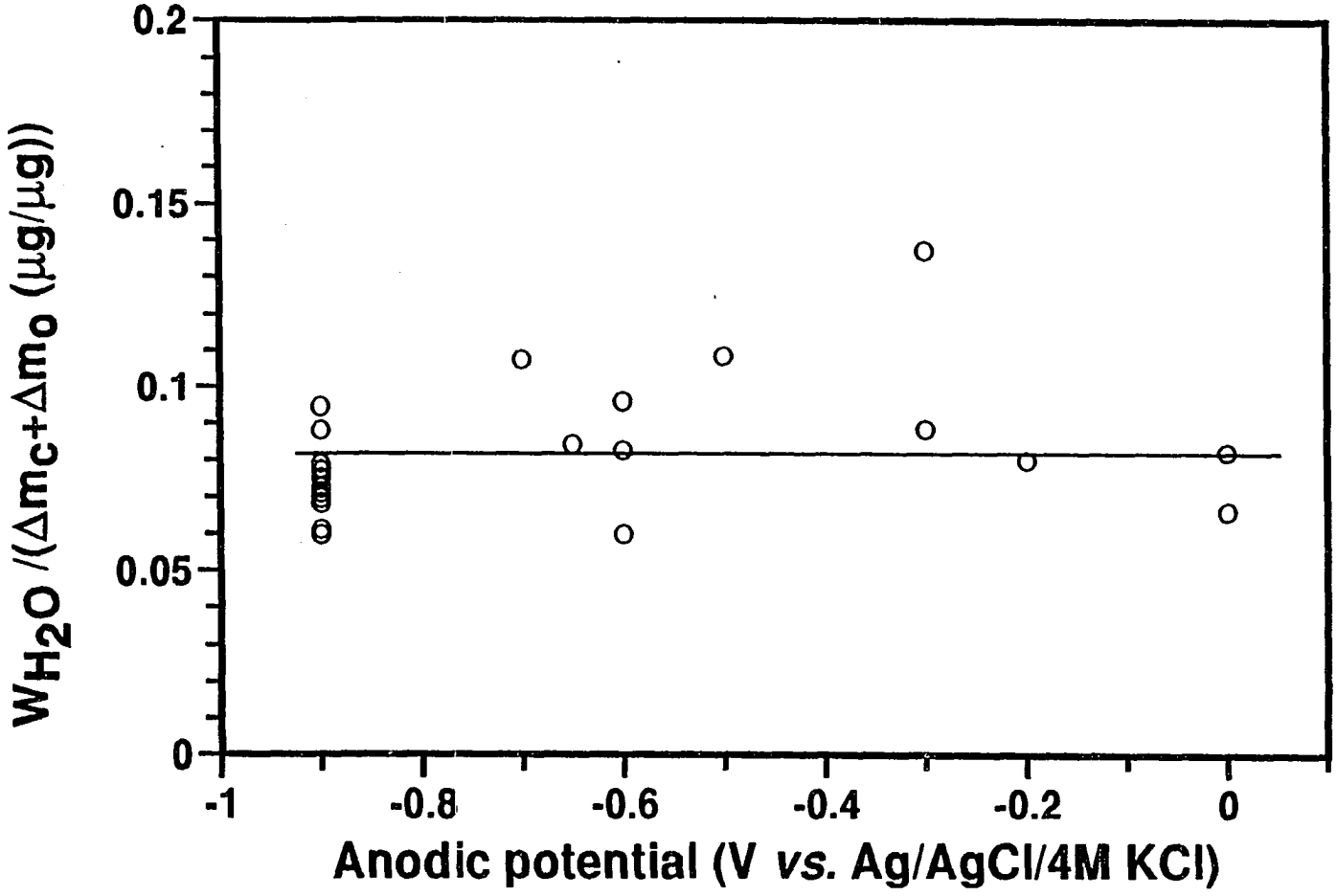

Figure 7. Effect of anodic potentials on amount of water absorbed during anodic polarization; 0.1M HCl or 0.1M H2SO4 solution. Cathodic potential -2.0V. Δm_c cathodic mass increase; Δm_o zero anodic mass increase intercept in Fig. 4.

Study of cathodically-induced oxidation reactions.- The early-time behavior of anodic current transients was examined using a high speed voltmeter sampling the current at 10 μs intervals and a potentiostat sampling at the rate of 1 ms. Fig. 8 shows an anodic current transient from such an experiment. Similar anodic current transients were reported by Radoševič *et al.* (3), following cathodic charging of aluminum in neutral chloride solutions. As in Ref. (3), the current transients were considered to be additive combinations of exponential functions. Component exponential decays with time constants of 0.2 ms and 118 ms are evident in Fig. 8. These two component transients were subtracted from the original current, and the procedure was repeated until the original current transient had been decomposed into a sum of exponential functions. This representation of the current transient was sufficiently accurate so that it could not be distinguished from the original on a plot like that in Fig. 8. The time constants for the component transients are shown in Table I. The anodic charge for each component transient, which is also shown in Table I, was obtained by integration of that component exponential function from time zero to infinity. The component current decays are referred to as A_0, A_1, etc., and the time constants and charges in Table I are labelled accordingly. The A_0, A_1 and A_2 component transients were measured with the high speed voltmeter and the A_3 component through the potentiostat.

The exponential decay with the smallest time constant was considered to represent capacitive charging current. The equivalent circuit of the cell at small anodic

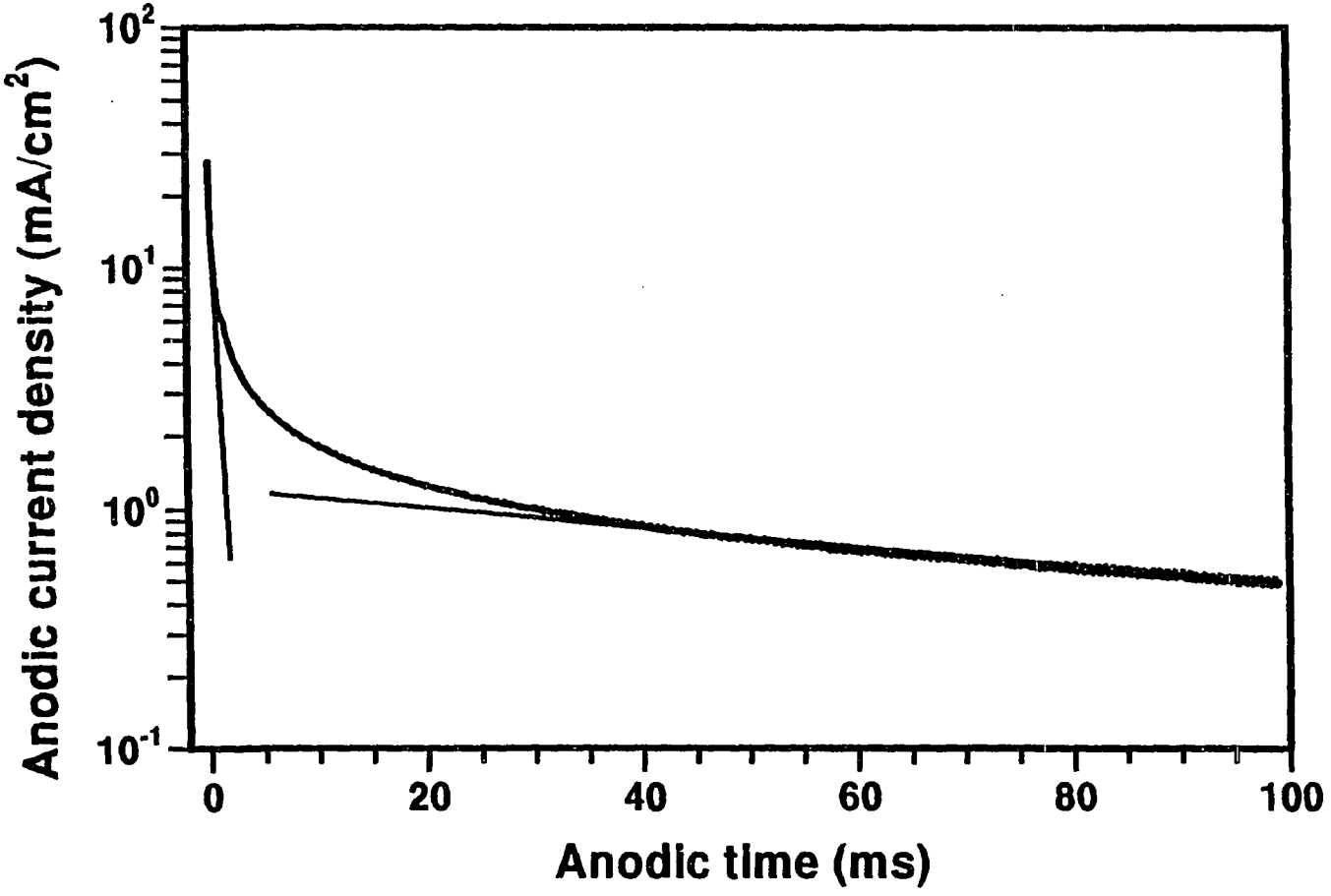

Figure 8. Anodic current transient following cathodic charging of Al in 0.1M HCl. Anodic potential -0.9V, cathodic potential -2.0V, cathodic time 3s, cathodic charge 11.2 mC/cm^2.

Table I. Summary of applied cathodic charges, integrated anodic charges, time constants, and capacitances for anodic current transients at -0.9V.

$Q_{cathodic}$ mC/cm^2	τ_o ms	Q_o $\mu C/cm^2$	$C=Q_o/\Delta E$ $\mu F/cm^2$	$C=\tau_o/AR_\Omega$ $\mu F/cm^2$	τ_1 ms	Q_1 $\mu C/cm^2$	τ_2 ms	Q_2 $\mu C/cm^2$	τ_3 sec	Q_3 $\mu C/cm^2$
.002	0.25	8.20	7.46	6.70	0.55	1.37	1.90	1.23		
.014	0.25	8.68	7.89	6.77	0.69	2.83	3.88	1.47		
.065	0.24	8.96	8.14	6.42	0.56	3.59	1.90	2.18		
0.65	0.21	7.79	7.08	5.66	0.76	4.76	3.44	3.15		
2.59	0.22	7.54	6.86	5.82	0.92	5.03	4.90	12.6	0.45	57.4
11.3	0.19	6.02	5.48	5.07	0.97	5.46	6.64	22.4	0.60	147
18.0	0.19	5.83	5.30	5.06	0.90	5.78	6.00	22.7	0.63	159
36.1	0.18	5.72	5.20	4.91	1.49	8.11	8.83	29.6	0.70	253
45.8	0.17	5.07	4.61	4.67	1.67	8.51	9.73	37.4	0.84	303
60.2	0.14	4.70	4.27	3.74	1.98	11.2	10.8	39.8	0.91	287

times was taken to be a series combination of a resistance R_Ω, representing ohmic conduction in the electrolyte solution, and a differential capacitance C_d for the surface oxide film,

$$i = \left(\frac{\Delta E}{AR_\Omega}\right)\exp\left(\frac{-t}{AR_\Omega C_d}\right) = i_o \exp\left(\frac{-t}{\tau_o}\right) \qquad [6]$$

Where R_Ω is the cell resistance, A is the electrode area, i is the current density and C_d is the capacitance per unit area. According to Eq. [6], the charging current for a potential step experiment should follow an exponential decay with a time constant $AR_\Omega C_d$; the charge associated with the capacitive process should be $C_d\Delta E$, where ΔE is the potential step. AR_Ω was determined to be 37 Ω-cm^2 from the measured slope of the steady state current-potential curve above the pitting potential; it had previously been shown that the steady state pitting current is controlled by the cell ohmic resistance (16). Table I shows values of the capacitance calculated from the time constant, as well as from the charge. Theses two independently determined capacitances are in good agreement, and for small cathodic charges, the capacitances agree with results from the literature for native oxide films on aluminum (17). This agreement confirms the assignment of the most rapidly decaying component exponential to capacitive current. For cathodic charge above 0.65 mC/cm^2, Table I shows that the capacitance decreases with increasing cathodic charge. Formation of surface oxide film during cathodic charging had been noted in previous studies (see Fig 1) (1).

Figures 9 and 10 show that all the time constants for the faradaic current component decays are linear functions of the cathodic charge. The linear dependence of the cathodic mass increase on cathodic charge (Fig. 1) further indicates that the time constants are linear functions of the film mass. Since the anodic current is a measurement of film "conductivity", the current decay indicates that the film resistance increases. The dependence of time constants on film mass would be expected from a "thin-layer cell" model of the oxide film, in which chemical reaction proceeds with first-order kinetics, and the reactant is distributed uniformly throughout the film. The film resistance is then increased as a consequence of the reaction. According to this model, the reactant concentration in the film would be determined by the mass balance differential equation,

$$\delta \frac{dC_o}{dt} = -k C_o \qquad [7]$$

in which δ is the film thickness, k the reaction rate constant, and C_o the concentration of reactant. The reactant concentration, obtained by integrating this equation, is $C_o=C_{oi}e^{-kt/\delta}$, where C_{oi} is the initial reactant concentration. The time constant in the thin-layer cell model is thus δ/k which is a linear function of the film thickness. The agreement of this prediction with Fig. 9 and Fig. 10 therefore indicates that the current transients at -0.9V were controlled by reactions of cathodic products which had been stored in the oxide film. Figure 4 shows that the anodic mass increase, which is primarily due to physical absorption of water, is a linear function of cathodic film mass

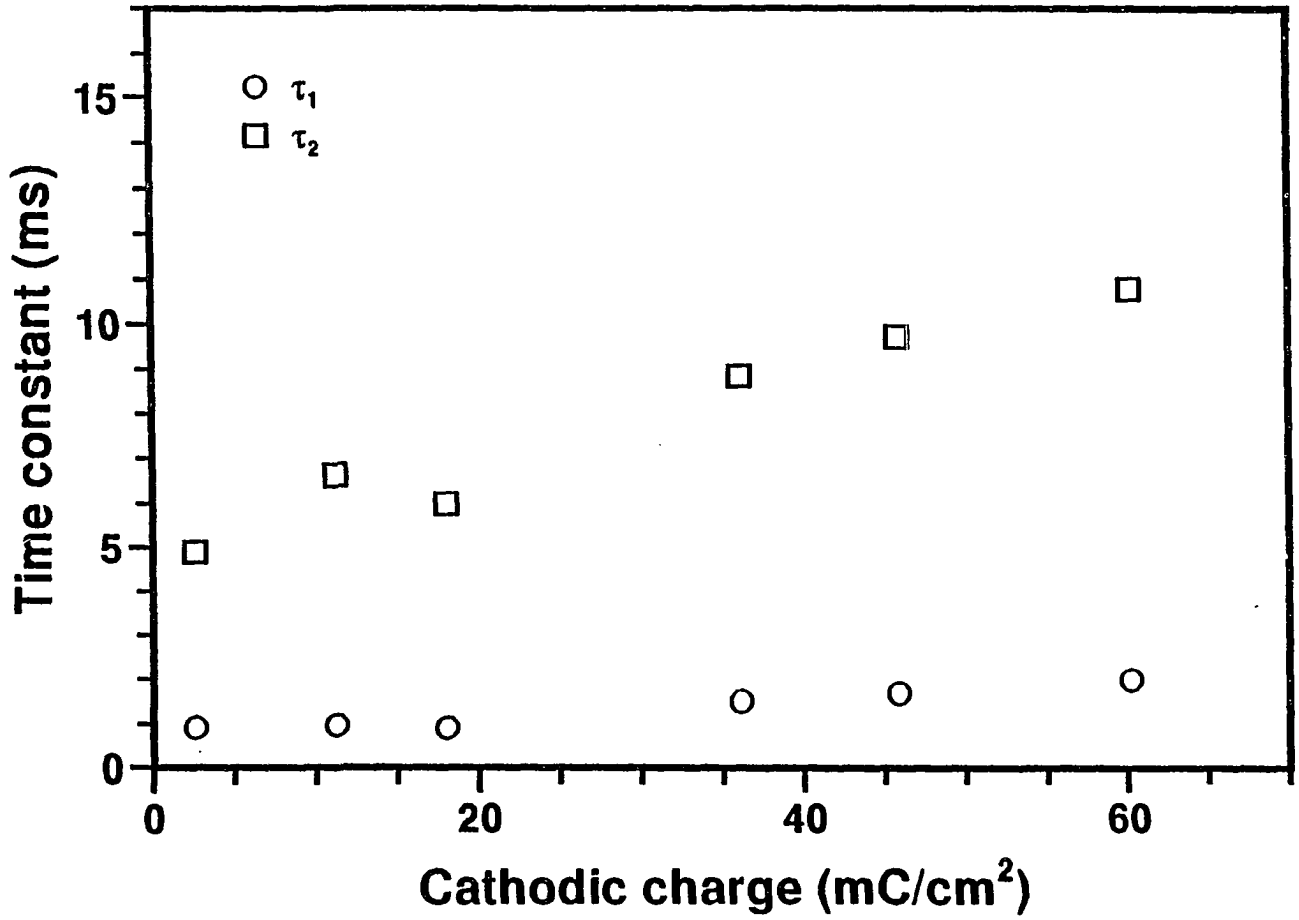

Figure 9. Dependence of time constants for initial anodic current decay on applied cathodic charges. (see Table I).

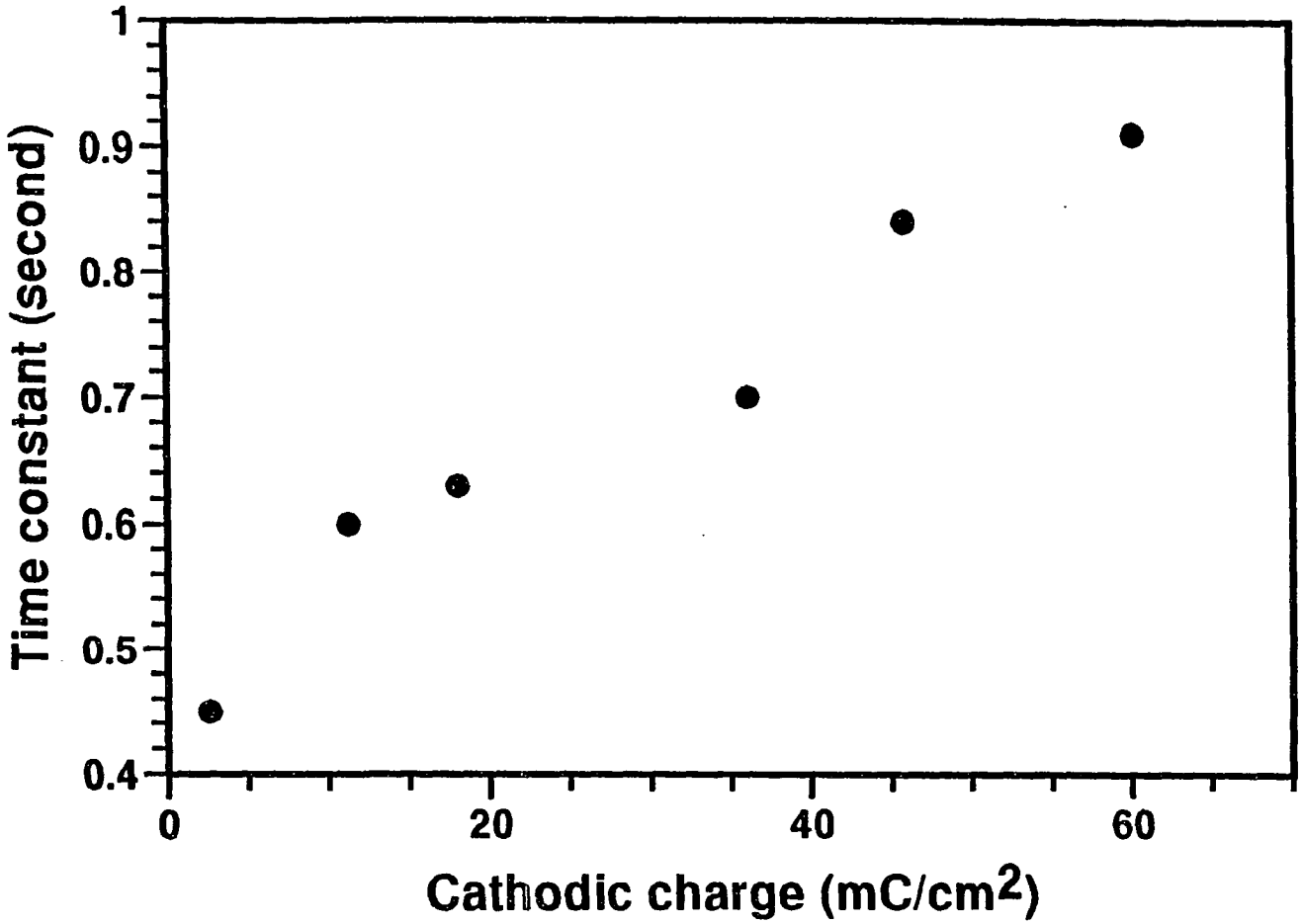

Figure 10. Dependence of time constant for anodic current decay at longer time on applied cathodic charges. (see Table I).

increase. The water absorption has been shown above to be independent of electrochemical reaction, so it must be related to the chemical reaction which occurs in the film. Since the chemical reaction depends on film mass, the amount of water incorporated is also a function of film mass.

The cathodic proton conduction rate in the film has been shown to follow Ohm's law (1). If Ohm's law applies to the conduction of all ionic species in the film, the initial anodic currents, i.e., the anodic currents at the film composition which have not been modified by oxidation reactions, should be a linear function of potential drop across the film ($\eta_{Al}{}^2$),

$$i = \frac{\kappa}{\delta} \eta_{Al}^2 \qquad [8]$$

where κ is the film conductivity and δ is the film thickness. $\eta_{Al}{}^2$ is a function of applied potential (Appendix),

$$\eta_{Al}^2 = V - \frac{1}{2F}(\mu_{Al_2O_3}^{23} - \mu_{H_2O}^{3}) - \eta_{Al}^{12} - \eta_O^{23} - \eta_\Omega \qquad [9]$$

The film composition is assumed to be not changed at the beginning of the anodic reaction; therefore, the chemical potential term in Eq. [9] is constant. The potential drop at the metal/film interface ($\eta_{Al}{}^{12}$) was assumed to be relatively small and can be neglected. The last two terms in Eq. [9] can be calculated from the measured anodic current, from Eq. [5] and from the known cell ohmic resistance, respectively. Figure 11 is the plot of anodic current density times film mass *vs.* anodic potential. The applied

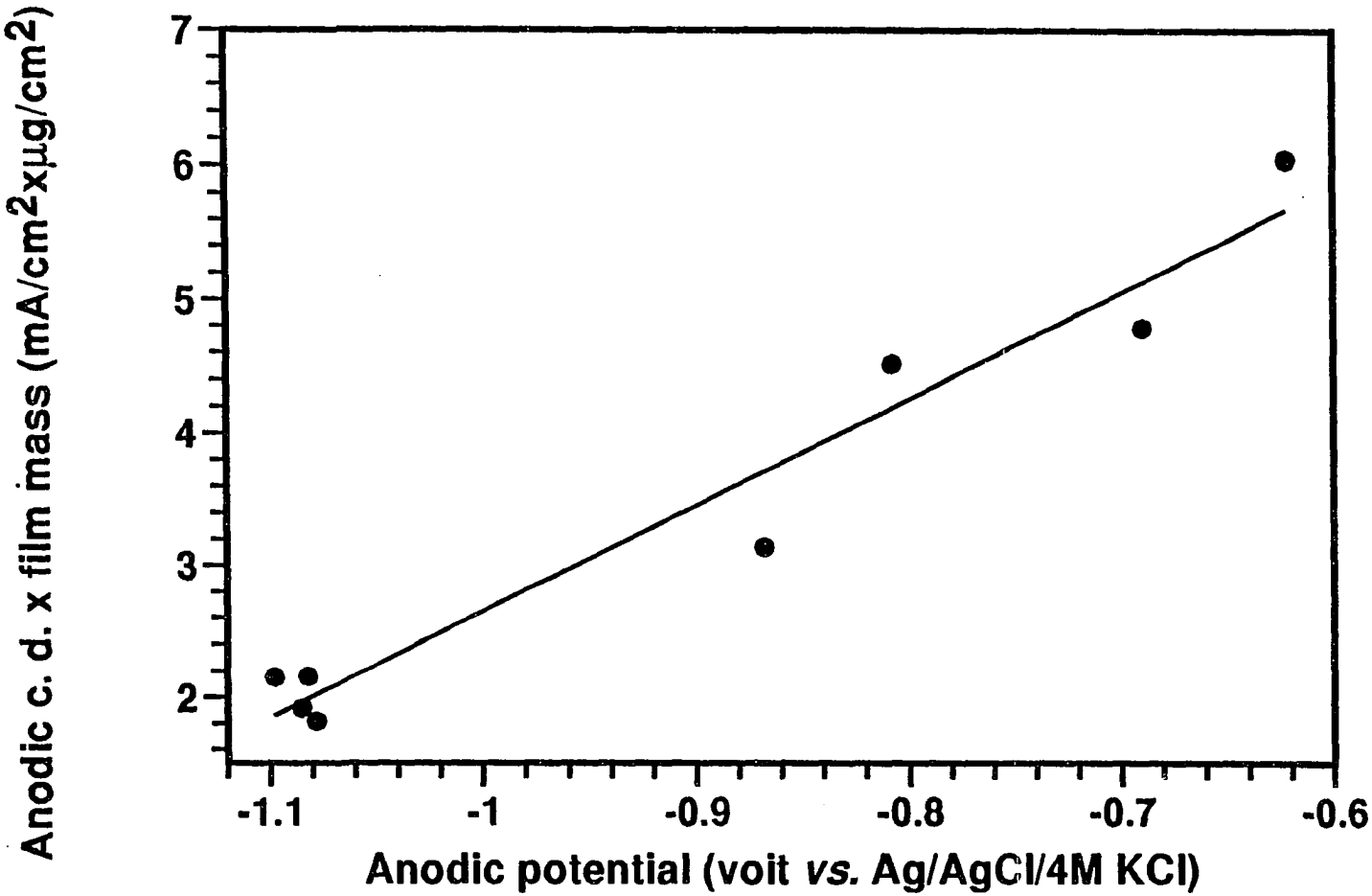

Figure 11. Dependence of initial anodic current density on anodic potential; 0.1M H_2SO_4 solution. Cathodic potential -2.0V, cathodic time 10s. Anodic potentials had been corrected with $\eta_O 23$ and ohmic resistance (see text). Film mass is the sum of cathodic mass increase and zero anodic mass increase intercept in Fig. 4.

potentials had been corrected with η_O^{23} and ohmic resistance, as indicated in Eq. [9], so that they are η_{Al}^{2} together with an addition constant. The anodic currents in Fig. 11 were obtained from experiments conducted in H_2SO_4 solution. The anodic time was 4 ms, which was selected because it was the earliest data point which would not include capacitive charging current. Figure 11 shows that the product of initial anodic current and film mass is a linear function of potential up to the potential of -0.62V (applied potential -0.2V), as expected from Eq. [8]. The linear dependence of initial anodic currents on potential indicates transport of aluminum ions and oxygen ions in the film followed Ohm's law and that η_{Al}^{12} is negligible. The film conductivity calculated from the slope in Fig. 11, assuming that the density of the film is 2.4 g/cm^3, is $0.33 \times 10^{-8}\ \Omega^{-1}\ cm^{-1}$, which is on the same order of magnitude as the film conductivity of $1.1 \times 10^{-8}\ \Omega^{-1} cm^{-1}$ for proton conduction (1). The small film resistance resulted in high initial anodic current when the potential was stepped from the cathodic potential to near open circuit.

DISCUSSION AND CONCLUSIONS

Results from mass transient studies show that cathodically-induced oxidation accompanies absorption of water into the film. Figure 7 shows that the amount of water absorbed is independent of anodic potential, which suggests that incorporation of water during anodic oxidation is not directly associated with electrochemical reactions. Alternatively, water absorption may be related to reactions in the film resulting from cathodic charging. Possible reactions in the film when the potential stepped from cathodic to anodic values will be discussed below.

The cell potential can be decomposed into a series of overpotentials for hydrogen evolution,

$$V = \eta_H^{12} + \eta_H^{2} + \eta_H^{23} + \eta_H^{3} \qquad [10]$$

where V is the potential measured with a hydrogen electrode in equilibrium with the bulk solution, $\eta_H{}^{12}$ is the overpotential at m/f interface, $\eta_H{}^{2}$ is the potential drop across the film, and $\eta_H{}^{3}$ is the ohmic drop in the solution. $\eta_H{}^{23}$, the potential drop at the f/s interface, is assumed to be relatively small and negligible (Appendix). During cathodic charging, V is -1.73V (or -2.0V *vs.* Ag/AgCl/4M KCl) and $\eta_H{}^{12}$ was found to be around -1.53V (1). According the relationship between overpotentials (Appendix),

$$\eta_H^{12} = \eta_{Al}^{12} + \frac{1}{3F}\left(\mu_{Al_2O_3}^{12} - \mu_{Al(OH)_3}^{12}\right) \qquad [11]$$

$\eta_H{}^{12}$ is dependent on $\eta_{Al}{}^{12}$ and the film composition. Immediately after the potential

step to V=-0.63V (or -0.9V *vs.* Ag/AgCl/4M KCl), $\eta_{Al}{}^{12}$ and the film composition is unchanged, since there has been no time for reactions to take place. Also, Fig 11 indicates that $\eta_{Al}{}^{12}$ is negligible; therefore, $\eta_{H}{}^{12}$ remains unchanged and is still -1.53V. $\eta_{H}{}^{3}$ is 0.092V at the initial anodic current of 2.48 mA/cm^2. The potential drop in the film ($\eta_{H}{}^{2}$) calculated from Eq. [10] is 0.81V. Accordingly, at the beginning of anodic polarization, the overpotential for hydrogen evolution at the m/f interface is cathodic while the overpotential for proton transport in the film is anodic. Anodic $\eta_{H}{}^{2}$ suggests transport of H^+ from the film outward to the solution. Further, since $\eta_{H}{}^{12}$ is negative, hydrogen evolution reaction at the m/f interface occurs at the beginning of anodic polarization. The sources for H^+ would be hydroxide or water in the film. Therefore, the water and hydroxide in the film would be reduced by both reaction and transport to oxide as anodic polarization proceeds.

Since the overall current is anodic, the cathodic hydrogen evolution reaction at the m/f interface must be accompanied by aluminum oxidation. Therefore, the overall reaction at the m/f interface would be equivalent to the chemical oxidation of Al by water, coupled with anodic aluminum oxidation. It is suggested that the aluminum ions in the aluminum oxide produced by chemical reaction require additional water molecules for coordination, so that water is imported from solution by physical absorption.

According to Eq. [11] $\eta_{H}{}^{12}$ is governed by the film composition because $\eta_{Al}{}^{12}$ is small during the oxidation period (Fig. 11). As mentioned above, the film would be converted from hydroxide to oxide as a consequence of H^+ transport from the film to

the solution, and H^+ reduction at the m/f interface. According to Eq. [11], η_H[12] would become less negative and the rate of hydrogen evolution reaction would decrease. Simultaneously, the rate of Al oxidation would decreases as the film resistance increases. Decay of the rate of chemical reaction at the m/f interface will decrease the rate of water absorption; therefore, absorption of water during anodic polarization is transient, as observed experimentally.

According to the above reaction scheme, the dramatic current decay of three orders of magnitude at -0.9V is due to an increase in film resistance. The resistance increase is brought about by the chemical reaction of excess water in the film with aluminum metal forming aluminum oxide. The linear dependence of the current decay time constants on film thickness indicates that the controlling reaction (probably water) is uniformly distributed in the film and that its transport to metal surface is rapid. The results of this paper demonstrate the close relationship between the chemical composition of a surface film and the corrosion resistance which it provides.

ACKNOWLEDGMENTS

Financial support for this work was provided by KDK corporation (Takahagi, Japan) through a fellowship to Mr. Lin. The authors thank M. D. Porter for supplying the Edwards coating system.

REFERENCES

1. C.-F. Lin and K. R. Hebert, to be submitted.

2. C.-F. Lin and K. R. Hebert, and M. D. Porter, to be submitted.

3. J. Radoševič, M. Kliškič, P. Dabič, R. Stevanovič and A.Despič, *J. Electroanal. Chem.*, **277**, 105 (1990).

4. O. Melroy, K. Kanazawa, J. G. Gordon II, and D. A. Buttry, *Langmuir*, **2**, 697 (1986).

5. G. S. Ostrom and D. A. Buttry, *J. Electroanal. Chem.*, **256**, 411 (1988).

6. L. A. Larew, J. S. Gordon, Y.-L. Hsiao, D. C. Johnson, and D. A. Buttry, *J. Electrochem. Soc.*, **137**, 3071 (1990).

7. S. Bruckenstein and M. Shay, *Electrochim. Acta.*, **30**, 1295 (1985).

8. G. Sauerbrey, *Z. Phys.*, **155**, 206 (1959).

9. C.-F. Lin and K. R. Hebert, to be submitted.

10. G. T. Cheek and W. E. O'Grady, *J. Electroanal. Chem.*, **277**, 341 (1990).

11. E.P. EerNisse, *J. Appl. Phy.*, **44**, 4482 (1973).

12. E.P. EerNisse, *J. Appl. Phy.*, **43**, 1330 (1972).

13. K. E. Heusler, A. Grzegorzewski, L. Jäckel, and J. Pietrucha, *Ber. Bunsenges. Phys. Chem.*, **92**, 1218 (1988).

14. K. J. Vetter and F. Gorn, *Electrochim. Acta*, **18** 321 (1973).

15. T. Våland and K. E. Heusler, *J. Electroanal. Chem.*, **149**, 71 (1983).

16. C.-F. Lin and K. R. Hebert, *J. Electrochem. Soc.*, **137**, 3723 (1990).

17. W. Wilhelmsen and T. Hurlen, *Electrochim. Acta*, **32**, 95 (1987).

PAPER IV.

THE EFFECT OF CATHODIC CHARGING ON PITTING CORROSION RESISTANCE OF ALUMINUM IN ACID SOLUTION

The Effect of Cathodic Charging on Pitting Corrosion Resistance of Aluminum in Acid Solution

Ching-Feng Lin and Kurt R. Hebert

Department of Chemical Engineering

Iowa State University
Ames, IA 50011

ABSTRACT

The effect of cathodic charging on pitting corrosion resistance of aluminum films in acid aqueous solution was studied using electrochemical methods and scanning electronic microscopy. Prior cathodic polarization induced rapid oxidation reactions during the first 20 ms of anodic polarization at -0.4V, above the pitting potential. The rates of pit initiation and pit growth were also enhanced by cathodic charging during the first 30 ms. The effect of cathodic charging was to reduce film resistance for ion transport, which was considered to be responsible for the increased rates of pit initiation and pit growth. Pits initiate over a longer period of time with greater oxide film mass. The pitting current diminished if oxidation reaction was allowed to take place more than 20 ms at -0.9V before the potential was stepped to -0.4V. The film resistance increased three order of magnitude after 1s oxidation at -0.9V, below the pitting potential. Increase of film resistance was responsible for the decrease of rates of pit initiation and pit growth.

INTRODUCTION

Alternating current etching of aluminum in acid chloride solutions promotes extremely high pit densities. For this reason, it is applied in the manufacture of aluminum foil for electrolytic capacitors. The pitting behavior of aluminum in hydrochloric acid under applied alternating voltage has been examined by Thompson and Wood (1). A large population of pits is produced rapidly and a thin hydrated aluminum oxide film is present on the substrate surface. Dyer and Alwitt (2) have studied the surface changes during AC etching of aluminum and found that the frequency of an alternating current has a great effect on the size of cubic etch pits. These observations indicate that AC etching is relevant to the initiation and early growth of pits.

Previously, in order to understand the role of prior cathodic polarization on the subsequent anodic pitting, aluminum foils in 1M HCl solution were subjected to single cycles of cathodic followed by anodic polarization (3). The cathodic potential was in the potential region of significant cathodic currents (E < -1.7V *vs.* Ag/AgCl/4M KCl), while the anodic potential was -0.4V *vs.* Ag/AgCl/4M KCl, above the pitting potential. It was observed that, with a 100 ms of prior cathodic polarization at -2.0V, the pit densities on aluminum surface during the first 20 ms of anodic etching were as high as $10^7/cm^2$. Also the pit growth rate was enhanced during the first 20 ms of the anodic period. Apparently, cathodic charging of aluminum modifies the metal surface in a way which greatly increases the susceptibility of the metal to pitting.

In a previous study, the film resistance for hydrogen evolution reaction was found to decrease dramatically when aluminum samples were subjected to cathodic polarization at potentials below -1.65V *vs.* Ag/AgCl/4M KCl (4). The effect of cathodic charging is to reduce the surface film resistance for ion transport, through change of film composition from oxide to hydroxide. At potentials where the hydrogen evolution kinetics changed, formation of surface film was also found by *in-situ* quartz crystal microbalance measurement. The film, which was shown from infrared spectroscopy to possess an "open" structure (5), contains appreciable amounts of water, which was attributed to be responsible for the increase of film conductivity.

In Ref. (6), after the potential was stepped from cathodic values to a potential between the open circuit potential and the pitting potential, an anodic current transient accompanied by a mass increase was observed. The decrease of current during this transient by three orders of magnitude was due to an increase of the film resistance. The mass increase is primarily due to water absorption into film when aluminum oxide is produced through chemical reaction. Film resistance increase due to chemical reaction results in the decrease of anodic current as well as the rate of water absorption. In the present work the effect of surface modification due to cathodic charging on pitting corrosion resistance of aluminum at potentials above the pitting potential was investigated.

EXPERIMENTAL

Al film samples used in cathodic-anodic polarization experiments were approximately 0.25 μm thick evaporated from a pure source (99.99% Al foil, provided by KDK corporation, Japan) onto microscope glass slides with an exposed area of 0.34 cm^2. The pressure in a cryopumped coating system (E360A, Edwards, West Sussex, England) was < $1x10^{-6}$ torr and the base pressure was < $4x10^{-7}$ torr. The detailed procedures for deposition of Al films have been described in a previous paper (4). The evaporated aluminum films were exposed in laboratory ambient for 24 hours.

For the study of pit initiation and growth, many cycles of cathodic-anodic polarization (AC etching) were employed to increase the pit number density to statistically significant levels. For this purpose, square potential wave forms were used. Potential control and current measurement were accomplished by interfacing the potentiostat to a personal computer using a Lab-PC data acquisition board (National Instrument). A QuickBasic (Microsoft) program was developed to drive the potentiostat and to measure potential and current.

The evaporated Al films were mounted in the wall of the electrochemical cell using an O-ring joint. The reference electrode was a commercial Ag/AgCl/4M KCl electrode (Fisher). All reported potential values were referred to this reference electrode. The counter electrode was A Pt wire insert into the cell. Cathodic polarization was at constant potential of -2.0V; the cathodic time was 1s. Anodic

polarization was at -0.4V for various times. In all experiments the electrolyte was 25 ml aqueous 0.1M HCl solution and the temperature was ambient (25°C). Prior to etching, the Al films were allowed to contact with the electrolyte for 5 minutes at open circuit.

A scanning electron microscope (JEOL-JSM 840) was used to study the morphology of the Al film surfaces. Pit size distributions and pit number densities were determined with the aid of photomicrographs at 10,000 X magnification. This magnification allowed one to view those pits with size greater than 0.05 μm. For size distributions, the dimensions of about 300-600 pits from 12 micrographs taken at random positions on the surface were measured. For the determination of pit number density, pits from a total number of about 80 SEM screens, uniformly and randomly chosen from the sample surface, were counted. For observations of the three-dimensional structures of pits, oxide replicas of the etched surfaces were formed at 60 V (7). The depth and width of pits were determined using the atomic force microscope (AFM)(Nanoscope III, Digital instruments).

For the study of effects of cathodic charging and potential interruption on the early anodic current transients, a PAR 273 potentiostat/galvanostat was used for potential control. A personal computer along with a GPIB interface were employed to execute the etching experiments and to retrieve the potential and current values from the potentiostat's memory. Cathodic polarization was at constant potential of -2.0V; cathodic time was an experimental variable. Anodic polarization was at -0.9V and/or

-0.4V for various times. The electrodes were evaporated Al films with exposed area of 0.28 cm^2. The electrochemical cell was the same as that used for pit initiation and growth study.

RESULTS

Pit initiation and growth.- Microscopic studies of the effect of cathodic charging on anodic pit initiation and pit growth were carried out on aluminum evaporated film samples in 0.1M HCl solution at ambient temperature. These experimental conditions were chosen so that results could be compared to previous studies on the electrochemical behavior of Al below the pitting potential (6). The pit number density for one cycle of cathodic-anodic polarization was found to relatively small. Since pit initiation rates, pit growth rates as well as pit volumes were to be determined through measurement of pit number densities and size distributions, many cycles of cathodic-anodic polarization (AC etching) were employed to increase the number pit density to statistically significant levels.

Figure 1 shows an example of anodic current transients at different stages of a 25 cycle AC etching experiment. The cathodic conditions were -2.0V, 1s; the anodic conditions were -0.4V, 20ms. The average charge passed during the 1s cathodic period was 9.92 mC/cm^2. The anodic current decreased initially for about 4 ms, and then rose rapidly to a plateau value. This is characteristic of the cathodically-enhanced pitting current transient. The current plateau has been identified previously with an ohmic limitation (3). The current transients in Fig. 1 indicate that pit initiation and pit growth occurred in each anodic half-cycle. The sample surface after 25 cycles etching was examined through SEM, and is shown in Fig. 2a. The micrograph shows that pits were

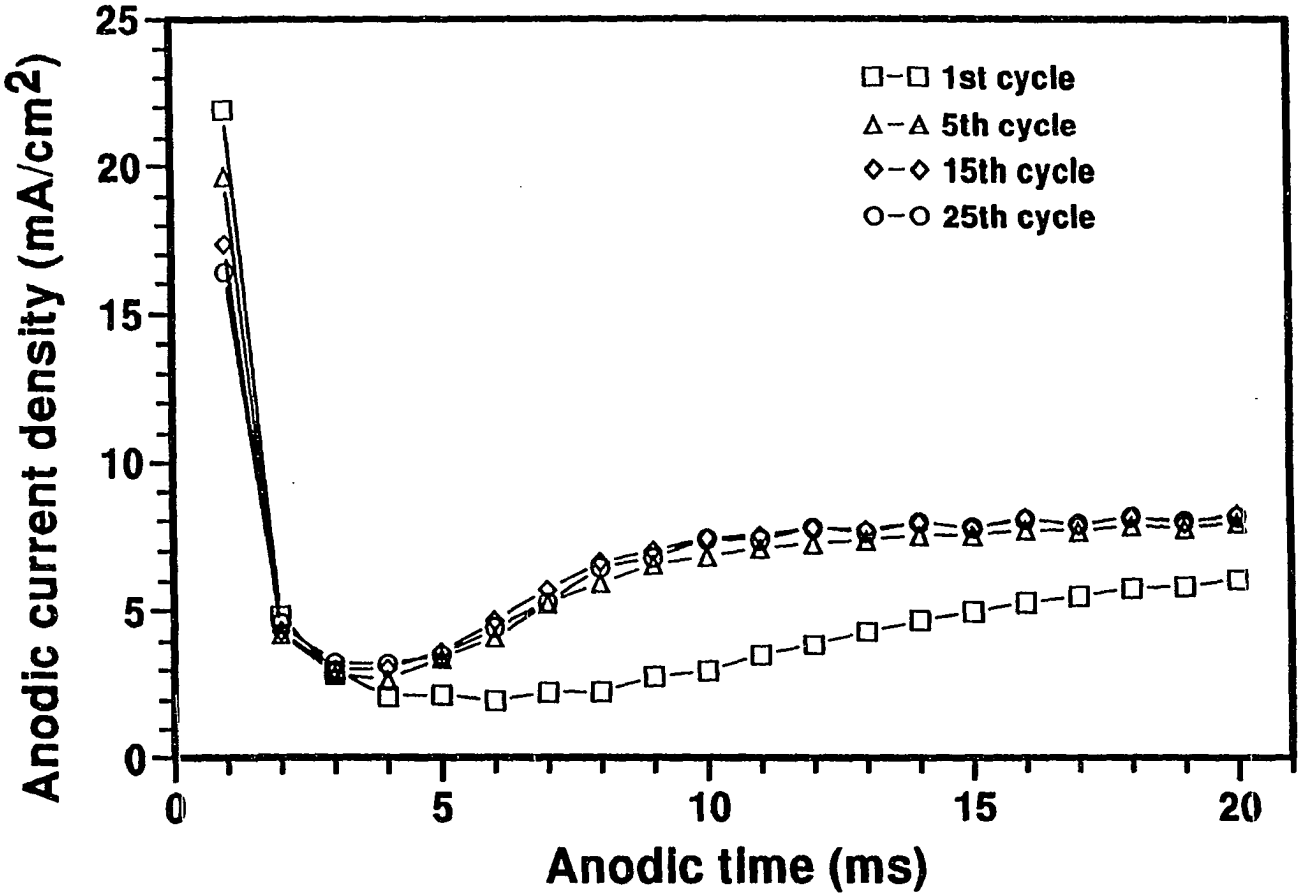

Figure 1. Representative anodic current transients during the anodic half-cycle of the alternating voltage etching of Al; 0.1M HCl, room temperature. Applied potential cycle: -2.0V cathodic 1s; -0.4V anodic, 20ms.

Figure 2. Scanning electron micrographs of pits formed during anodic polarization following cathodic polarization. (a) Applied potential cycle: -2.0V cathodic 1s; -0.4V anodic, 20 ms; 25 cycles. (b) Oxide replica of pits. Applied potential cycle: -2.0V cathodic 1s; -0.4V anodic, 30 ms; 25 cycles.

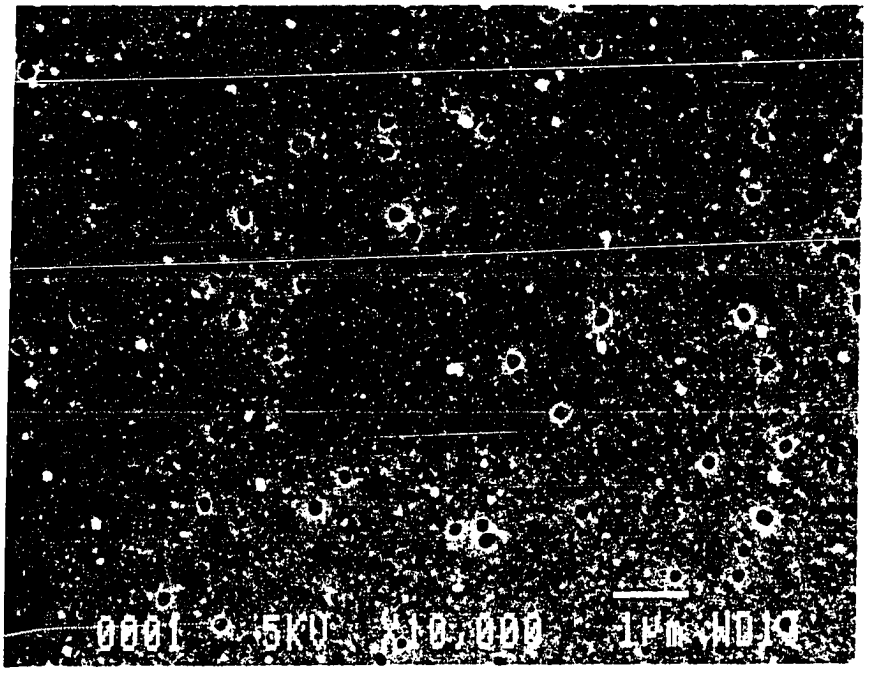
0001 5KV X10,000 1μm WD14

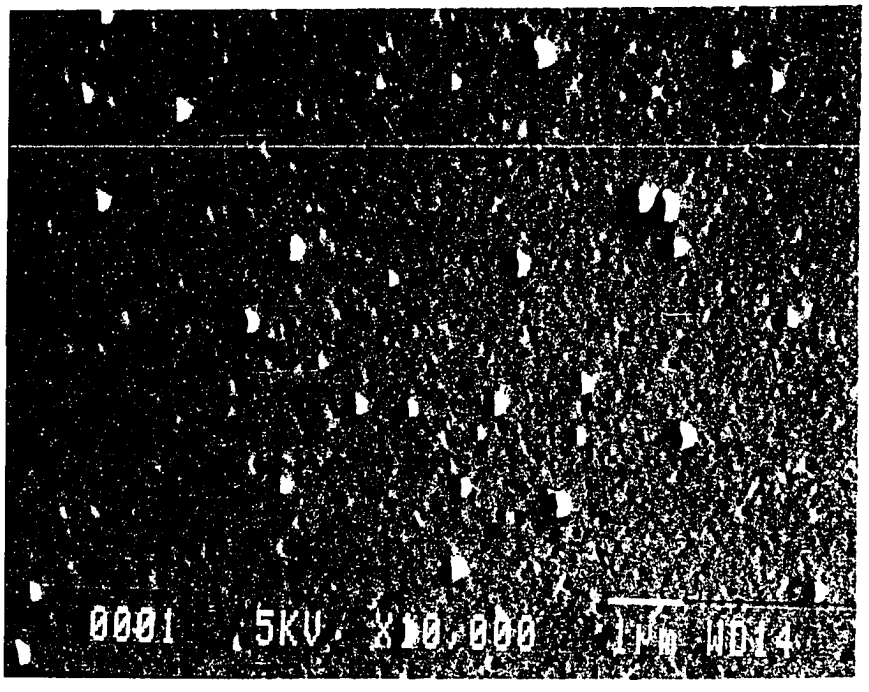
0001 5KV X10,000 1μm WD14

distributed uniformly over the sample surface. The shape of the pits is between round and square; their sizes ranged from 0.05 to 0.2 μm. Half cubic pits have been observed for aluminum foils after AC etching in HCl solution (3).

To confirm that pitting occurs independently in each anodic half-cycle, pit number densities and size distributions were measured by varying the number of AC cycles. Figure 3 shows that pit number densities increased linearly with the number of AC cycles, at least up to 50 cycles. In the last 30 cycles of the 100 cycle experiment, the time for the initial anodic current decay (see Fig 1.) increased, and eventually, no current rise was observed. Pit size distributions for all the cycles were similar as can be seen from Fig. 4. Average pit sizes from the distributions are 0.13, 0.12, 0.14 and 0.14 μm for samples etched with 10, 25, 50 and 100 cycles, respectively. It is concluded from anodic current transients, pit number densities as well as size distributions that pit initiation and growth are initiated and terminated in each anodic-half cycle, and that the pitting behavior is approximately reproducible in each cycle up to about 50 cycles. Therefore, pit number densities and pit sizes for one cycle can be determined from the average values of a number of cycles.

The period of anodic time during which pits initiated was studied by varying the anodic time, while keeping the number of AC cycles constant at 25. The cathodic time was 1s and the anodic times were varied from 2 ms to 50 ms. Pit number densities were measured through SEM. The minimum time for pits to be observed through SEM was 5 ms. Since this time corresponds to the time for initial anodic current decay

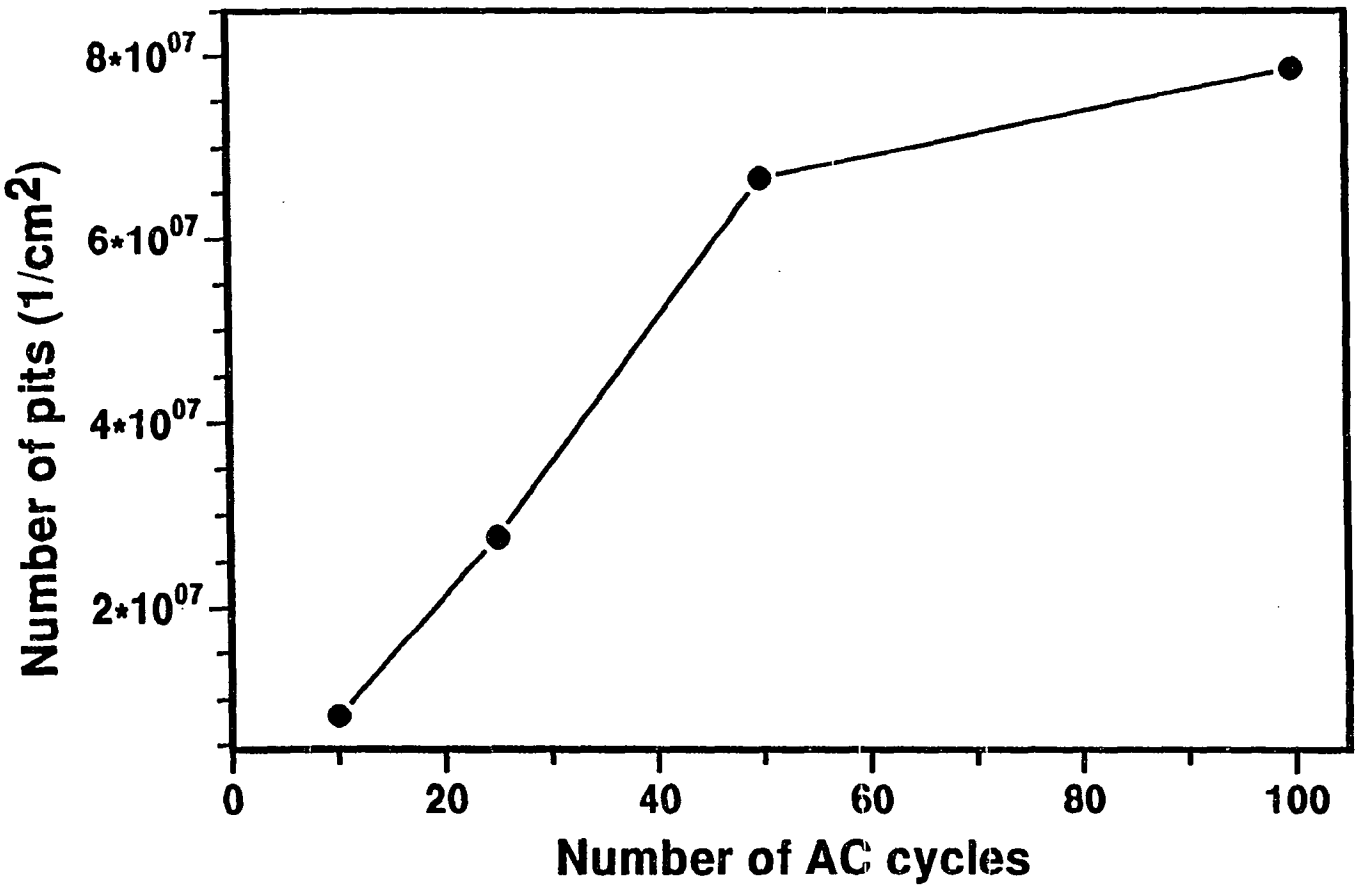

Figure 3. Pit number densities during anodic polarization following cathodic polarization as function of alternating voltage cycle; 0.1M HCl, room temperature. Applied potential cycle: -2.0V cathodic 1s; -0.4V anodic, 20ms.

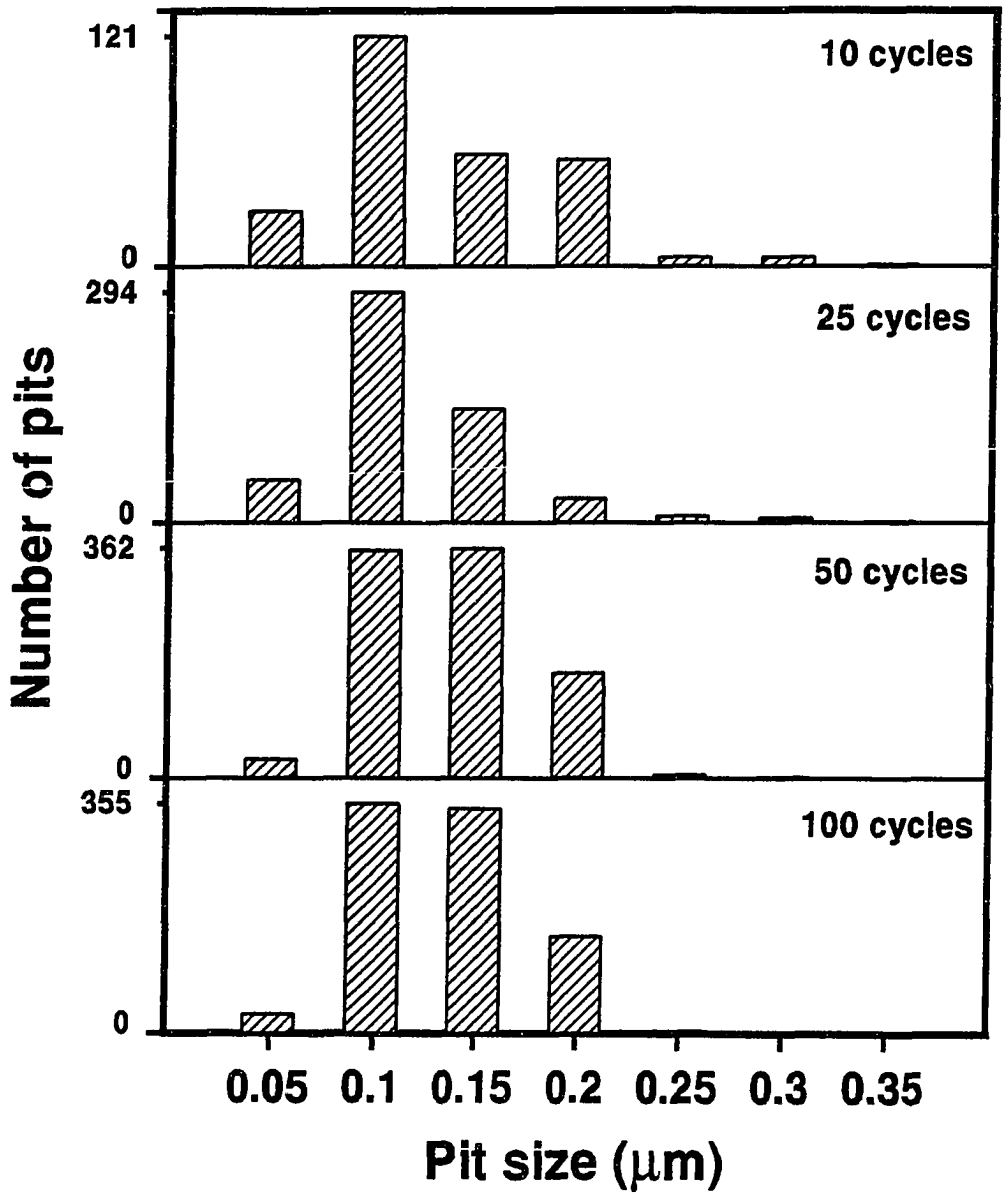

Figure 4. Pit size distributions during anodic polarization following cathodic polarization as function of alternating voltage cycle; 0.1M HCl, room temperature. Applied potential cycle: -2.0V cathodic 1s; -0.4V, 20ms.

(Fig. 1), it follows that no significant pits were nucleated during the initial anodic current decrease. The anodic current decay has been attributed due to an oxidation reaction induced by prior cathodic charging (6). Apparently, cathodically-induced oxidation reactions also occurred at potentials above the pitting potential. Figure 5 shows that the time period during which pits nucleated was about 30 ms, and the pits nucleated at approximately a constant rate prior to this time.

Pit size distributions were measured after each experiment, and the distributions at different anodic times are shown in Fig 6. The smallest pits which could be observed were about 0.05 μm in width. Figure 6 also shows that pit sizes spread over the histogram as anodic time increased. The spread of the peaks indicates that pits did not all grow at the same rate. By assuming that the leading peaks in each distribution were the pits first nucleated, representative pit growth rates were obtained from the time dependence of these leading peaks,

$$\frac{\Delta r}{\Delta t} = \frac{1}{2}\frac{\bar{s}_{i+1} - \bar{s}_i}{t_{i-1} - t_i} \qquad [1]$$

where s_i is the leading peak position at time t_i. Figure 7 shows that pit growth rates were high at early anodic times, but then decreased and approached a constant value of about 1.2 μm/s at 40-50 ms. In Ref. (3), high pit growth rate during the early stage of pitting corrosion were also observed after cathodic charging.

Comparison of pit volume with anodic charge.- In order to calculate pit volumes, the ratio of pit width to pit depth needed to be determined first. Three-dimensional

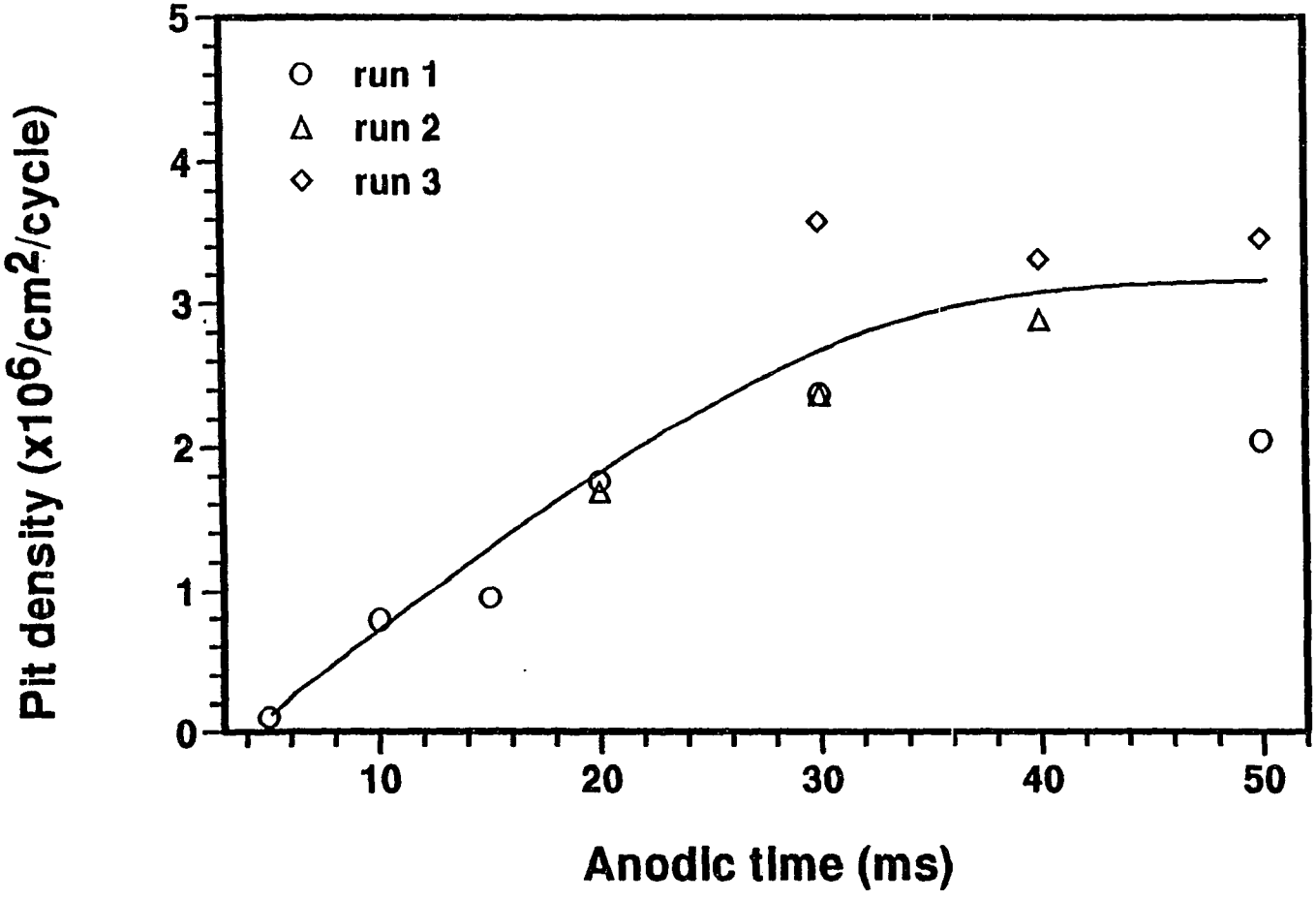

Figure 5. Average one cycle pit number densities during anodic polarization following cathodic polarization as function of anodic time; 0.1M HCl, room temperature. Applied potential cycle: -2.0V cathodic 1s; -0.4V anodic; 25 cycles.

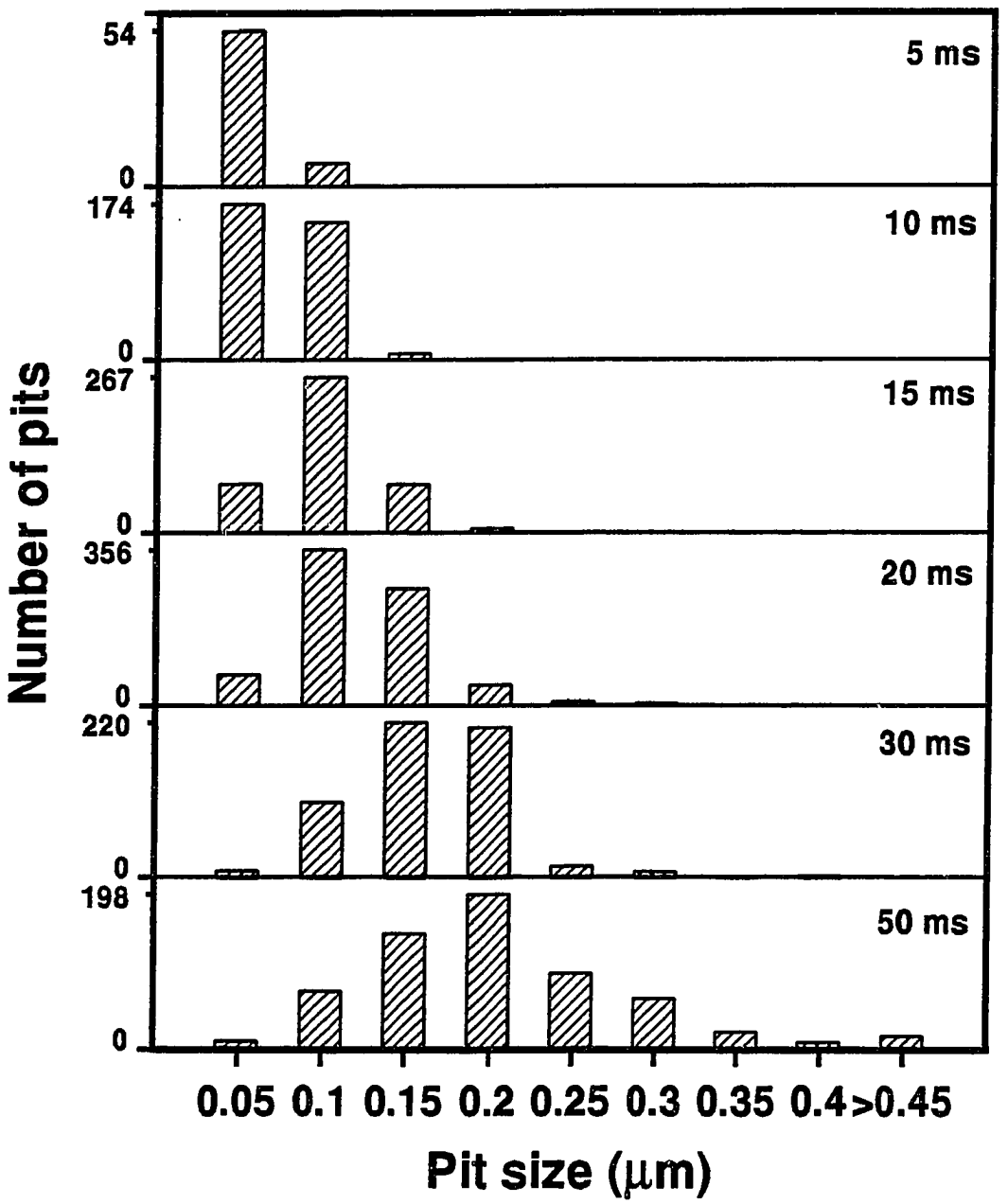

Figure 6. Pit size distributions during anodic polarization following cathodic polarization as function of anodic time; 0.1M HCl, room temperature. Applied potential cycle: -2.0V cathodic 1s; -0.4V; 25 cycles.

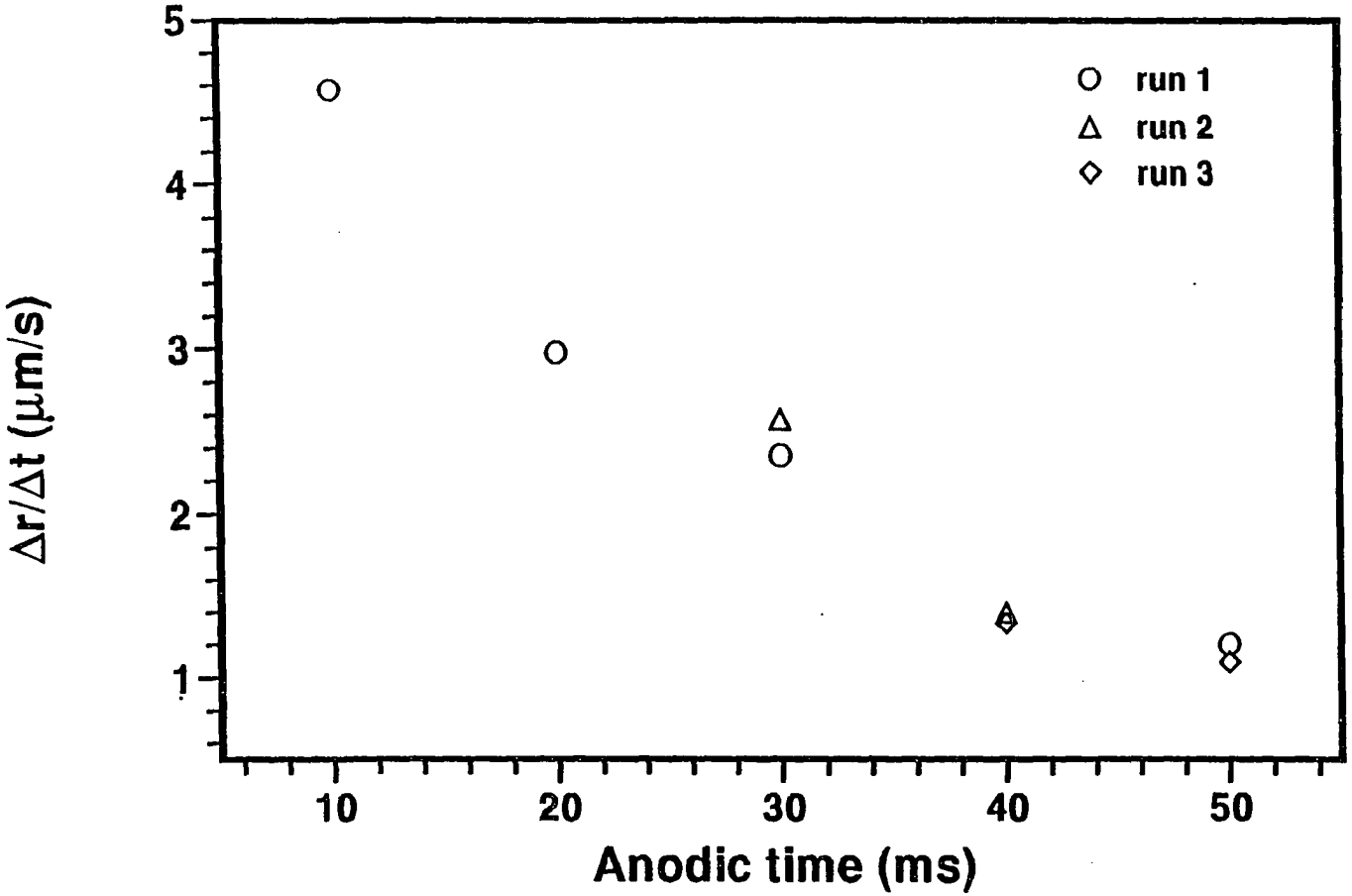

Figure 7. Representative pit growth rates during anodic polarization following cathodic polarization as function of anodic time; 0.1M HCl, room temperature. Applied potential cycle: -2.0V cathodic 1s; -0.4V anodic; 25 cycles.

structures of pits were obtained by anodizing the etched samples, and then dissolving the remaining aluminum (8). Fig. 2b shows a micrograph of an oxide replica of pits. The width and depth of pits were measured from the oxide replica, using the atomic force microscope, and are shown in Fig. 8. The ratio of pit depth to width is 0.41, which was obtained from the slope in Fig. 8. The intercept in Fig. 8 is 112 nm which is the thickness of the anodic oxide film of the replica. Total pit volumes were calculated from pit number densities and size distributions, by assuming that pits have square cross-sections,

$$V_{pit} = \sum_i n_{pit}\, w_i^2 (0.41 \times w_i) \qquad [2]$$

where w_i is pit size in Fig. 6. The equivalent anodic charges for metal dissolution (Q_{pit}) were calculated from the measured pit volumes, assuming that removal of one Al atom corresponds to three anodic electrons

$$Q_{pit} = \frac{3F\rho_{Al}}{M_w} V_{pit} \qquad [3]$$

Figure 9 shows that Q_{pit} was small during the first 15 ms and then increased approximately linearly with anodic time, while the electrochemical charges (Q) increased from zero time. The pit current (slope of Q_{pit} in Fig. 9) was constant after 10-15 ms, but zero at 5 ms (since the pit density was zero). Therefore the rising current at times between 5-10 ms in Fig. 1 can be attributed to pitting dissolution. The charge difference is 30.3 $\mu C/cm^2$ at 5 ms and increases to 101.2 $\mu C/cm^2$ at 20 ms. The charge difference was approximately constant after about 10-20 ms, which indicates that the

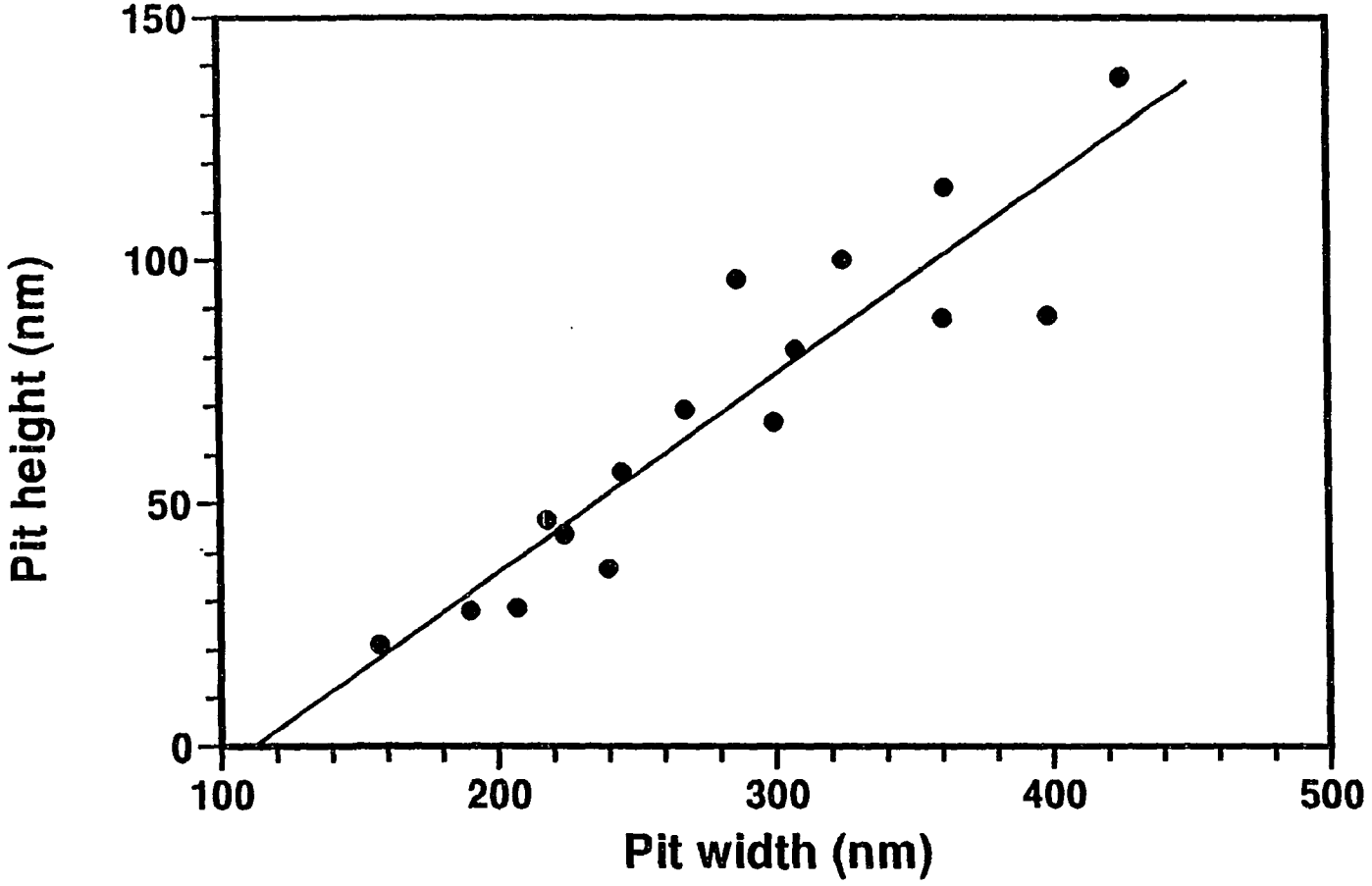

Figure 8. Pit height as function of pit width measured from the oxide replica of the etched sample, using the atomic force microscope. Applied potential cycle: -2.0V cathodic 1s; -0.4V, 40ms; 25 cycles.

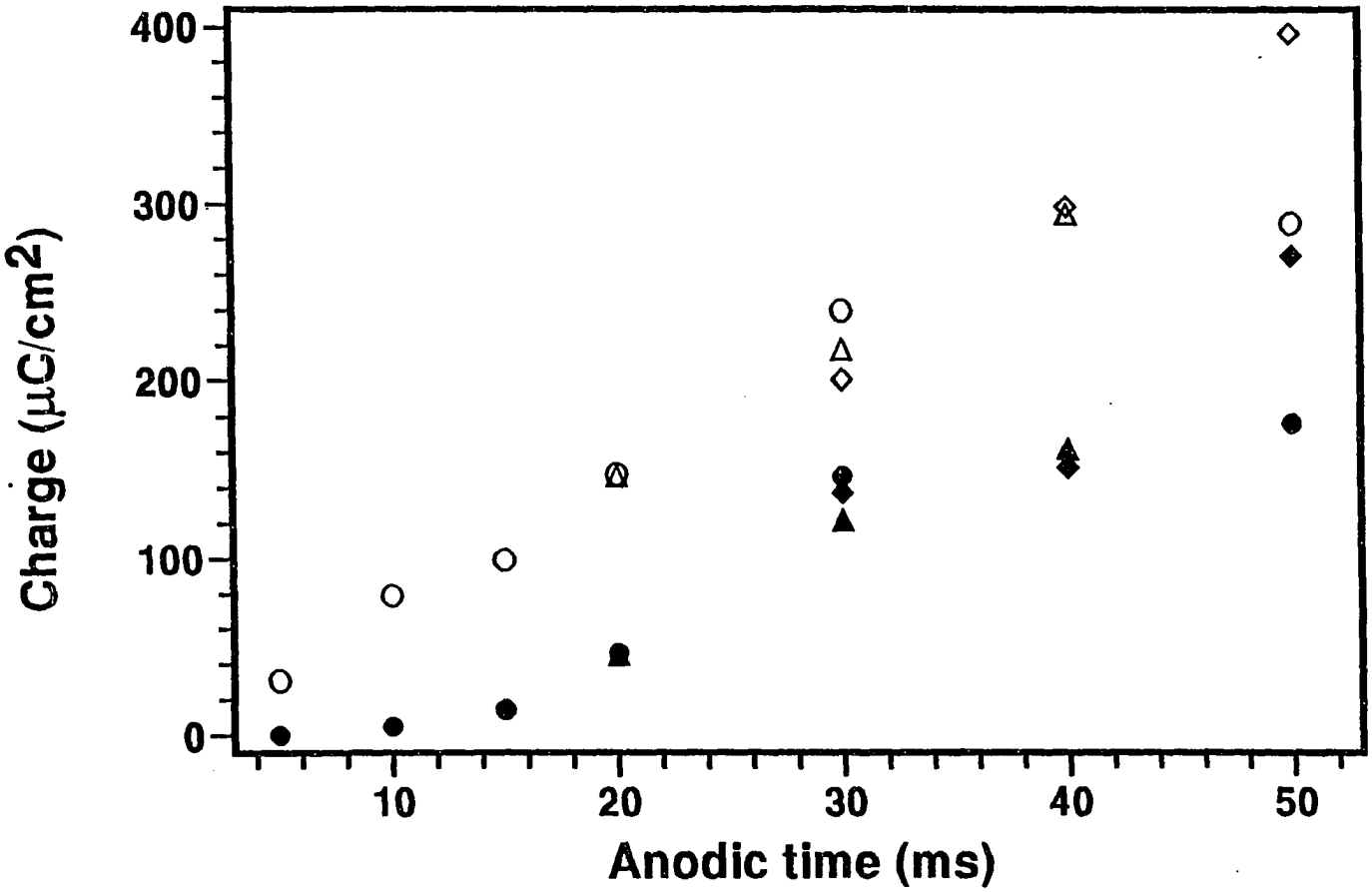

Figure 9. Comparison of electrochemical charges (Q) and the equivalent charges calculated from pit volume (Q_{pit}). Applied potential cycle: -2.0V cathodic 1s; -0.4V anodic; 25 cycles. The charges had been averaged for one cycle. Open markers Q, closed markers Q_{pit}.

anodic current at later times was mainly due to pitting corrosion. The discrepancy between Q_{pit} and Q indicates that, during early stage of anodic period, a large fraction of anodic charge was not contributed from metal dissolution. Previous study has shown that cathodic polarization induces rapid oxidation reactions, when the electrode potential was subsequently stepped near the open circuit potential (6). Figure 1 shows that similar oxidation reactions occurred at the anodic potential of -0.4V and were predominant at times earlier than about 20 ms. Therefore, the difference between Q and Q_{pit} may be associated with a cathodically-induced oxidation reaction.

Although direct measurement of oxidation current is difficult in the presence of simultaneously pitting, the oxidation charge may be inferred from experiments carried out in 0.1M H_2SO_4 solution. In Ref. (6), at the cathodic charge of 11.3 mC/cm^2, the anodic charge during the first 20 ms was 37.8 μC/cm^2 (capacitive charging current excluded), at -0.9V in 0.1M HCl solution. Also from Ref. (6), in 0.1M H_2SO_4 solution, the initial anodic current was 2.4 and 6.5 mA/cm^2 at the anodic potentials of -0.9V and -0.4V respectively. The ratio for these two current is 2.6. Since the oxidation current depends on film resistance (6), the current at -0.4V can be inferred from the current at -0.9V. The anodic oxidation charge, in HCl solution at -0.4V, could then inferred from the charge at -0.9V and the current ratio of 2.6 for the initial currents at -0.4 and -0.9V in H_2SO_4 solution. The anodic oxidation charge at -0.4V thus estimated is 98.3 μC/cm^2. This charge is close to the charge difference between Q and Q_{pit} of about 101 μC/cm^2 at 20 ms in Fig. 9. Thus, it is concluded that charge differences between Q

and Q_{pit} were due to oxidation reaction induced by prior cathodic polarization, which occurred in the first 20 ms of the anodic period.

The ohmically limited current for the experiments in Fig. 1 can be calculated by

$$\frac{E_{applied} - E_R}{AR_\Omega} = i_\Omega \qquad [4]$$

Where $E_{applied}$ is -0.4V, E_R is the repassivation potential, -0.67V, and the solution resistance AR_Ω, is 37 Ω-cm^2. The limiting current density from Eq. [4] is 7.3 mA/cm^2. Figure 1 shows that this current is reached in most of the AC cycles. Therefore, in this case, the rise time of the current to the plateau cannot be given special significance as the time period of rapid pit nucleation and pit growth. The time of pit nucleation must be inferred from SEM measurements.

Effect of cathodic charging on pitting current transients.- The effect of cathodic charging on pitting current transients is shown in Fig. 10. Figure 10 shows the anodic current transients, at times less than 100 ms, for samples with prior cathodic charging at a constant potential of -2.0 V, followed by anodic polarization at -0.4V. The figure shows that for cathodic charge below 7.18 mC/cm^2, the anodic currents rose more rapidly with increasing cathodic charge. This trend is the same as that found previously on aluminum foils (3), for which similar current transients were observed. It has been shown from Fig. 9 that the rising anodic currents were supplied by metal dissolution from pits. Figure 10 shows that the ohmically limited current is reached only in cases 4 and 5. Thus, in all other experiments in Fig. 10, the rise time of the current to the

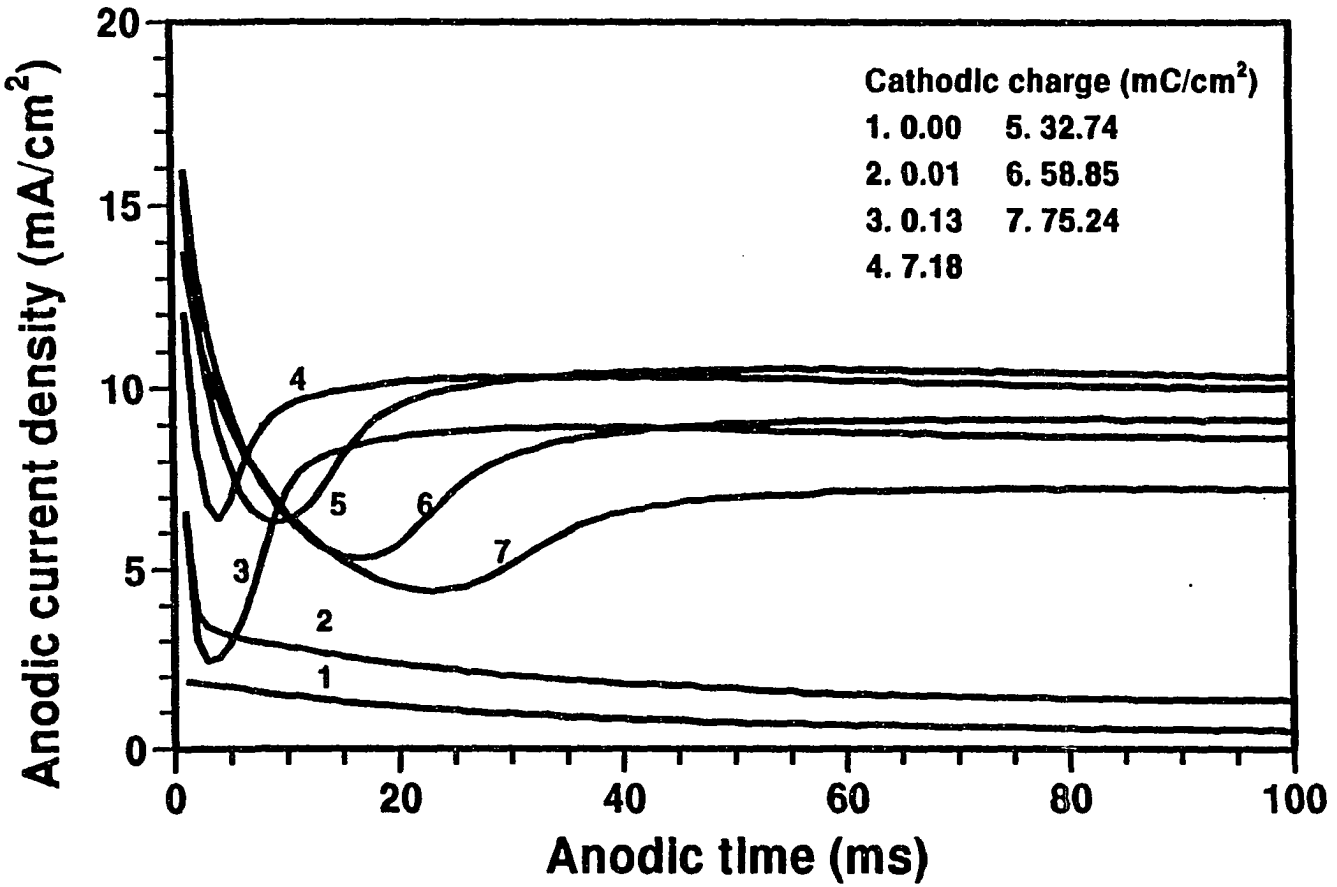

Figure 10. Effect of cathodic applied charges on anodic current transients at constant cathodic potential; 0.1M HCl room temperature. Cathodic charges as indicated. Cathodic applied potential -2.0V; anodic potential -0.4V, 0.1s.

plateau can be identified as the time period of rapid pit nucleation, which is enhanced by prior cathodic charging. It should be noted here that the electrode area for experiments in Fig. 10 and Fig. 12 was smaller (A=0.28 cm^2, i_Ω=8.9 mA/cm^2), so the limiting currents were higher than those in Fig. 1. For cathodic charges larger than 32.74 mC/cm^2, the anodic currents in Fig. 10 rose less rapidly with greater cathodic charge. Figure 10 shows that both the times for the initial current decays and for the anodic currents to rise to steady-state values increase with cathodic charge.

A similar dependence on cathodic charge is displayed by the time period of the oxidation reactions below the pitting potential. In Fig. 11, the rise time of the pitting current from Fig. 10 is compared to the decay time of the faradaic current below the pitting potential. The rise time is defined as the time for the current at -0.4V to increase to 85% of its peak value; the decay time is the time needed for the current at -0.9V (after subtraction of the capacitive current) to decay by 85% of the initial current. The agreement between the rise time and the decay time suggests that the rates of initiation and early growth of pits, which determine the pitting current transients in Fig. 10, are controlled by the same factors as those which determine the rate of the cathodically-induced oxidation processes below the pitting potential. It was shown in Ref. (6) that the oxidation current at -0.9V decreases with time because the film resistance increases as the film is converted from a hydroxide to an oxide. The time period of this conversion increases linearly with film mass.

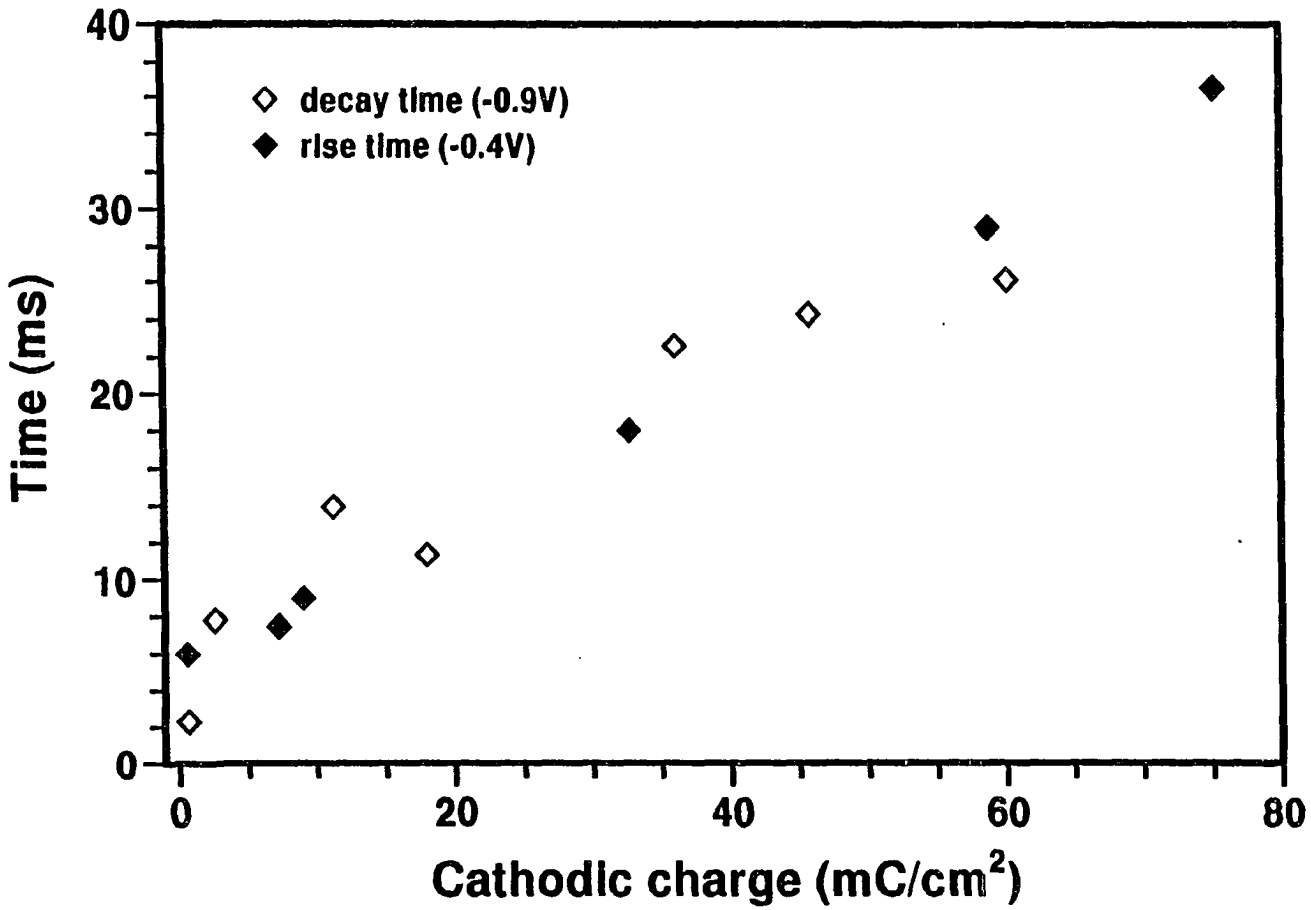

Figure 11. Comparison of the rise times of the pitting current at -0.4V and the decay times of the anodic current at -0.9V. Cathodic potential -2.0V.

The connection between anodic oxidation below the pitting potential, and cathodically-stimulated pitting current, was further investigated in experiments in which, after cathodic charging, the potential was held for a period of time at -0.9V, and then stepped to a value above the pitting potential (-0.4V). The intermediate potential of -0.9V, which is between the open circuit potential and the pitting potential, was also the potential used above to investigate uniform oxidation processes. During the time at -0.9V, oxidation reactions took place which changed the film composition from hydroxide to oxide and increase the transport resistance of the film (6). Figure 12 shows that the acceleration of pitting current clearly diminishes for interruption times greater than 20 ms. The rise time of the anodic current continuous to increase up to an interruption time of 3s, after which it is constant. The current transients at 3s and 5s interruptions may be taken to represent the anodic current where no cathodic charging had been applied. The interruption time of 3s corresponds to the total time required for the transient reactions below the pitting potential (6).

It is concluded from Fig. 12 that when uniform oxidation reactions were allowed to take place before the potential was stepped above the pitting potential, the cathodic acceleration of pitting was significantly attenuated. This result suggests that pitting is accelerated at -0.4V by the same factors which control the oxidation reactions which occur during polarization at -0.9V. The anodic current densities at -0.9V were 7, 0.87, 0.33 mA/cm^2 at the times of 1, 20 and 100 ms respectively. The anodic current decays to a steady state corrosion current of about 10 $\mu A/cm^2$ at the time of 1s. Since

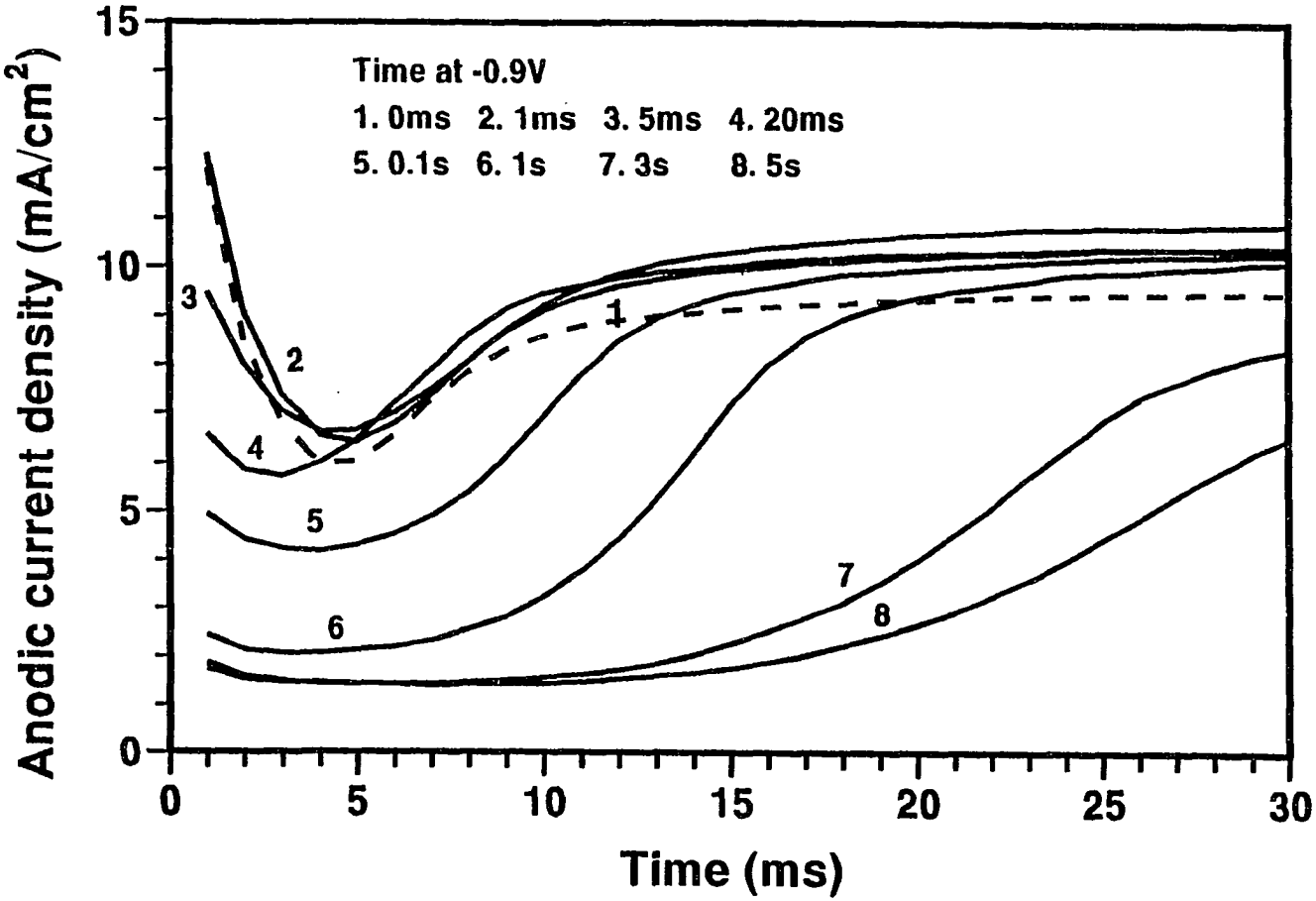

Figure 12. Effect on anodic pitting currents of interruption time between cathodic and anodic polarization. Cathodic potential -2.0V, cathodic time 5s, interruption potential -0.9V, anodic potential -0.4V. Average cathodic charge 14.7 mC/cm^2. Interruption time as indicated.

the anodic current at these times is a measurement of film "conductivity"; so the decrease of anodic current with time indicates that the film resistance increases. According to the anodic currents at -0.9V, the film resistance increases by three orders of magnitude for an interruption time of 1s, which results in less enhancement on pitting corrosion at -0.4V as shown in Fig. 12. The pitting currents in Fig. 12 could not be distinguished for interruptions smaller than 20 ms, though the resistance has increased by about an order of magnitude prior to this time. However, it was observed in etching of Al foils that, for an interruption of 20 ms at -0.9V, the number of pits nucleated at -0.4V was much smaller while the pit size was much larger, compared to those without interruption. Thus, for interruption smaller than 20 ms, the effect of film resistance on the rate of pit initiation may not reflect on the initial pitting current such that shown in Fig. 12. It is often assumed that the induction time for pit initiation corresponds to the time required to penetrate or break down the passive film (8); therefore, Fig. 12 may provide further evidence that the induction time for pitting is directly related to film resistance.

DISCUSSION AND CONCLUSIONS

The effect of cathodic charging has been found to "activate" aluminum surface through change of film composition, i.e., from aluminum oxide to aluminum hydroxide (4). The film resistance was reduced dramatically after cathodic charging, and ion transport in the film followed Ohm's law. In the present work, results of pit number densities, pit size distributions and pit volume measurements show that both the oxidation current and the pitting current were enhanced by prior cathodic charging during the first second at potentials above the pitting potential. Thus, the observed enhancement of pit initiation and pit growth rates, through cathodic charging, may be explained by the decrease of film resistance for ion transport.

In Ref. (6), the decay of anodic current was attributed to increase of film resistance, which was considered to be a consequence of chemical reactions involving water which had been stored in the film during cathodic charging. In Fig. 5 and Fig. 7, the rate of pit initiation and pit growth were found to diminish at about 30 ms. Thus, increase of film resistance may be responsible for the decrease of rates of pit initiation and growth. The effect of oxidation reactions and, therefore, film resistance can be illustrated further by interruption experiments. As shown in Fig. 12, the critical interruption time to diminish initial oxidation current and pitting current was between 20 and 100 ms, and for interruption greater than 3s, there is no cathodic enhancement of pitting. The later time agrees with the time for reaction of Al with H_2O (6). Thus,

during the interruption, most of the water in the film had been consumed during the oxidation reaction at -0.9V, which resulted in a decrease in film conductivity.

Figure 11 shows that both the rise time and the decay time increased with cathodic charge. In Ref. (6), the increase in decay time was shown to be due to increase of cathodic film mass. The thicker film would require longer time for excess water in the film to be consumed, and thus, a longer time for the film resistance to increase. Accordingly, the period of time when the film has low resistance is longer for greater film mass, so pits can initiate over a longer period of time, as shown in Fig. 10. Figure 10 also shows that the rate of pit initiation is slower with thicker film, which suggests a possible relationship between the rate of conduction and the rate of pit initiation.

The rates of pit initiation and growth during the first 30 ms are enhanced by prior cathodic charging significantly, as shown in Figs. 5 and 7. Similar observations were also found in a previous study on cathodically-enhanced pitting corrosion of aluminum foils (3). Based on the equivalence between cathodic charge and pit volume as well as on the enhanced initial pit growth rate, a vacancy diffusion mechanism was proposed for the cathodic enhancement (3). If pit initiation and pit growth were enhanced by vacancies, which would be produced by a chemical oxidation reaction such that occurs at potentials below the pitting potential, then Q_{pit} should be greater than the electrochemical charge (Q), since both vacancies and metal dissolution would contribute to pit volume. Also, if vacancies were produced during electrochemical oxidation at

potentials above the pitting potential, Q_{pit} should equal to or greater than Q. In the present study, however, the measured electrochemical charge (Q) is balanced by the oxidation charge and Q_{pit}, which provide no evidence for the vacancy diffusion mechanism. The increased pit initiation rate is understandable since cathodic charging reduces the film resistance. The enhanced pit growth rate, on the other hand, is more difficult to understand since once pits nucleated, metal dissolution occurs directly at pit site which would not depend on film resistance. It is possible that other oxidation reactions, which would not be detected in the present work, occur specifically at potentials above the pitting potential and contribute to pit growth through a process like vacancy diffusion.

ACKNOWLEDGMENTS

Financial support for this work was provided by KDK Corporation (Takahagi, Japan) through a fellowship to Mr. Lin. The authors appreciate Dr. James Anderegg for carrying out XPS measurement. The authors thank M. D. Porter for supplying the Edwards coating system, and E. R. Henderson and Y. Tak for assisting in AFM measurement.

REFERENCES

1. G. E. Thompson and G. C. Wood, *Corros. Sci.*, **18**, 712 (1978).

2. C. K. Dyer and R. S. Alwitt, *J. Electrochem. Soc.*, **128**, 300 (1981).

3. C.-F. Lin and K. R. Hebert, *J. Electrochem. Soc.*, **137**, 3723 (1990).

4. C.-F. Lin and K. R. Hebert, to be submitted.

5. C.-F. Lin, K. R. Hebert, and M. D. Porter, to be submitted.

6. C.-F. Lin and K. R. Hebert, to be submitted.

7. C. G. Dunn and R. B. Bolon, *J. Electrochem. Soc.*, **116**, 1050 (1969).

8. Z. Szklarska-Smialowska, "Pitting Corrosion of Metals," p. 103, NACE, Houston, Texas (1986).

PAPER V.

QUARTZ CRYSTAL MICROBALANCE FREQUENCY TRANSIENTS DURING CATHODICALLY-INDUCED PITTING CORROSION OF ALUMINUM

Quartz Crystal Microbalance Frequency Transients during Cathodically-induced Pitting Corrosion of Aluminum

Ching-Feng Lin and Kurt R. Hebert

Department of Chemical Engineering

Iowa State University
Ames, IA 50011

ABSTRACT

Cathodic charging of aluminum in acid solution induces a rapid current increase, at potentials above the pitting potential, which is accompanied by a complex quartz crystal frequency transient. Without prior cathodic charging, the vibration frequency increases continuously with anodic time, and is mainly due to metal dissolution. The cathodically-induced complex frequency transient was resolved by AT-cut and BT-cut quartz, and simultaneous mass increase and tensile stress increase during the early stage of pitting corrosion were observed. There is a linear relationship between the mass change and stress change. Interruptions of pit growth did not affect the transients, so they are not associated with electrode roughening.

INTRODUCTION

The effects of cathodic charging on the surface film composition and pitting corrosion resistance of aluminum have been reported previously (1-5). The effect of cathodic polarization is to reduce the film resistance for ion transport (2). Formation of surface film at the potential where the film resistance reduced (around -1.65V *vs.* Ag/AgCl/4M KCl) was also detected by *in-situ* quartz crystal microbalance technique and by *ex-situ* infrared reflection spectroscopy (2,3). The film contains appreciable amounts of water and has relatively "open" structure. The pitting corrosion resistance was shown to be reduced dramatically by prior cathodic charging (1,5).

In Ref. (4), cathodic charging was found to induce anodic oxidation reactions accompanied by electrode mass increases, at potentials below the pitting potential in acid solutions. Also, cathodically-induced compressive stress changes accompanying oxidation reactions were also observed from experiments carried out on both AT-cut and BT-cut quartz crystals. In the present work, the effects of cathodic charging on the vibration frequency of quartz crystals as well as on pitting current transients at potentials above the pitting potential are reported.

EXPERIMENTAL

Al film samples used in this study were evaporated from a pure source (99.99% Al foil, provided by KDK corporation, Japan) onto quarz disks. The pressure in a cryopumped coating system (E360A, Edwards, West Sussex, England) was < $1x10^{-6}$ torr and the base pressure was < $4x10^{-7}$ torr. The detailed procedures for deposition of Al films have been described in a previous paper (2). The evaporated aluminum films were exposed in laboratory ambient for 24 hours.

The electrochemical quartz crystal microbalance (QCM) system utilized was the same as those employed in previous studies (6-9). Potentiostatic control and current measurement were accomplished by interfacing the QCM to a personal computer using a Lab-PC data acquisition board (National Instruments). The frequency was measured with a Hewlett Packard 5334b frequency counter interfaced with a GPIB-PCII board. A QuickBasic (Microsoft) program was developed to drive the two boards simultaneously. The frequency was measured at the rate of 18 ms per reading.

Aluminum film samples were evaporated onto both sides of planar (1 inch diam), overtone-polished, AT-cut quartz crystal (Valpey-Fisher). In some experiments, 5 MHz, BT-cut crystals were used. The films, which were deposited using a standard keyhole design (10), were ca. 0.25 μm thick and 0.34 cm^2 electrode area. The crystals were operated at the fundamental frequency of 5 MHz with the mass sensitivity of 17.67 $ngHz^{-1}cm^{-2}$, according to Sauerbrey relationship (10,11). The crystal was mounted in

the wall of the electrochemical cell using an O-ring joint and two O-rings. Prior to polarization experiments, the Al film was allowed to contact with the electrolyte for 5 minutes at open circuit condition.

The reference electrode was a commercial Ag/AgCl/4M KCl electrode (Fisher). All reported potential values were referred to this reference electrode. The counter electrode was A Pt wire insert into the cell. Cathodic polarization was at constant potential of -2.0V. Anodic potentials varied from -0.9V to -0.4V. In all experiments the electrolyte were 25 ml aqueous 0.1M HCl solutions and the temperature was ambient ($25^{o}C$).

RESULTS AND DISCUSSION

Frequency transients during polarization.- Figure 1 shows the QCM frequency transient for an aluminum film on AT-cut quartz crystal, during cathodic polarization followed by anodic polarization above the pitting potential. Figure 1 shows that there was an initial period of about 1-2s during which there was no significant frequency change. After this initial period, the frequency decreased linearly with time, which had been previously shown to be due to formation of a surface aluminum hydroxide film (2). The corresponding cathodic current, which is shown in Fig. 2, rose rapidly during the first 2s, then increased slowly. The simultaneous film growth and cathodic current increase was due to an increased film conductivity, as described in detail in previous work (2).

Figure 1 also shows that, when the potential was stepped from the cathodic potential to -0.4V, which is above the pitting potential, a complex frequency transient was initiated. The pitting potential is -0.65V, which was determined from the polarization curve shown in Fig. 3. Detailed frequency transients during anodic polarization, after cathodic charging, can be seen in Fig. 4. The cathodic conditions were 5s, -2.0V, and the cathodic frequency decreases ranged from 1-7 Hz. Since the cathodic conditions were the same, the figure shows that the basic features of the anodic frequency transient are reproducible. The frequency increased rapidly up to about 0.1s after the potential was stepped to -0.4V. After staying at an approximately constant

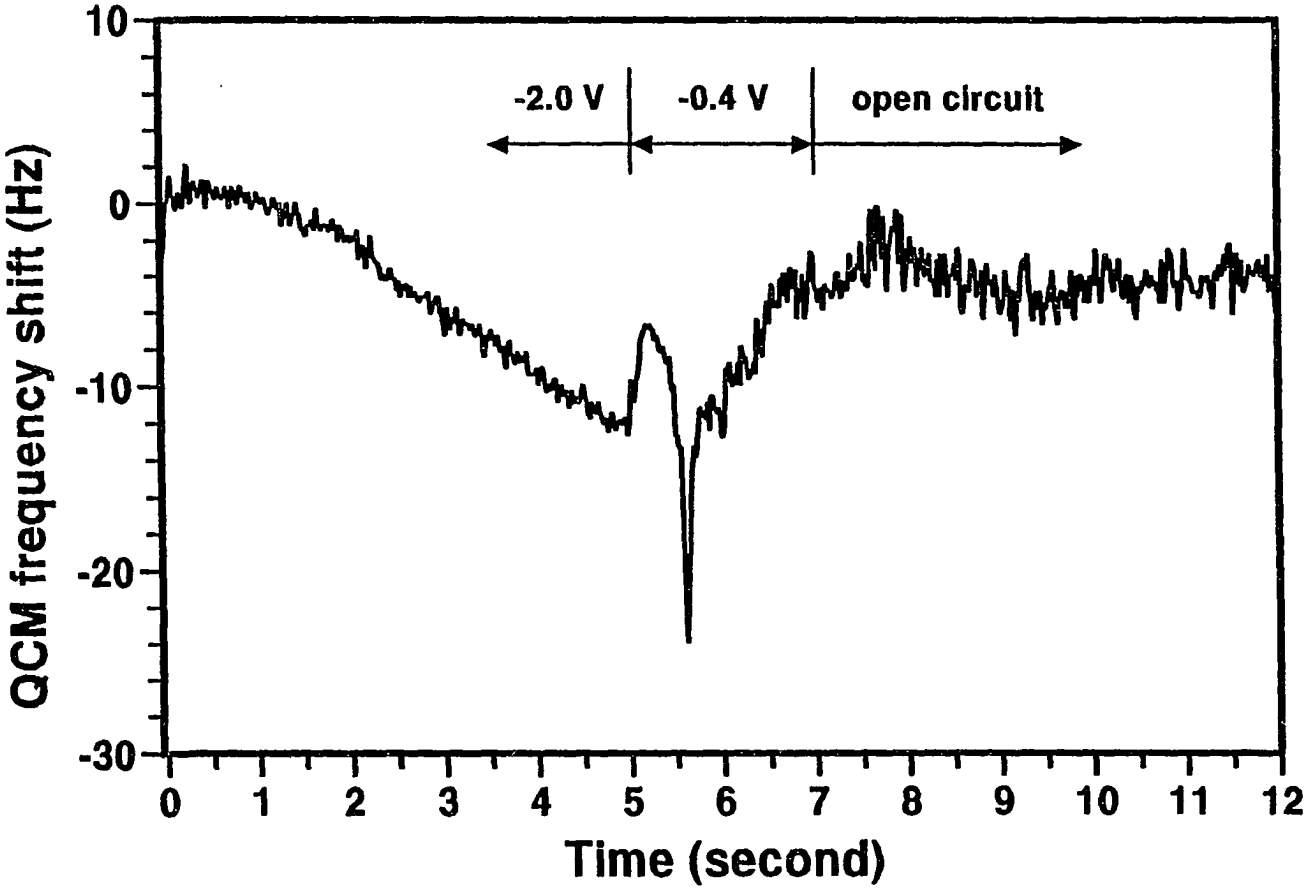

Figure 1. Quartz crystal frequency shift obtained during cathodic-anodic polarization of Al on AT-cut quartz crystal; 0.1M HCl, room temperature. Cathodic applied potential -2.0V, cathodic time 5s, anodic applied potential -0.4V, anodic time 2s.

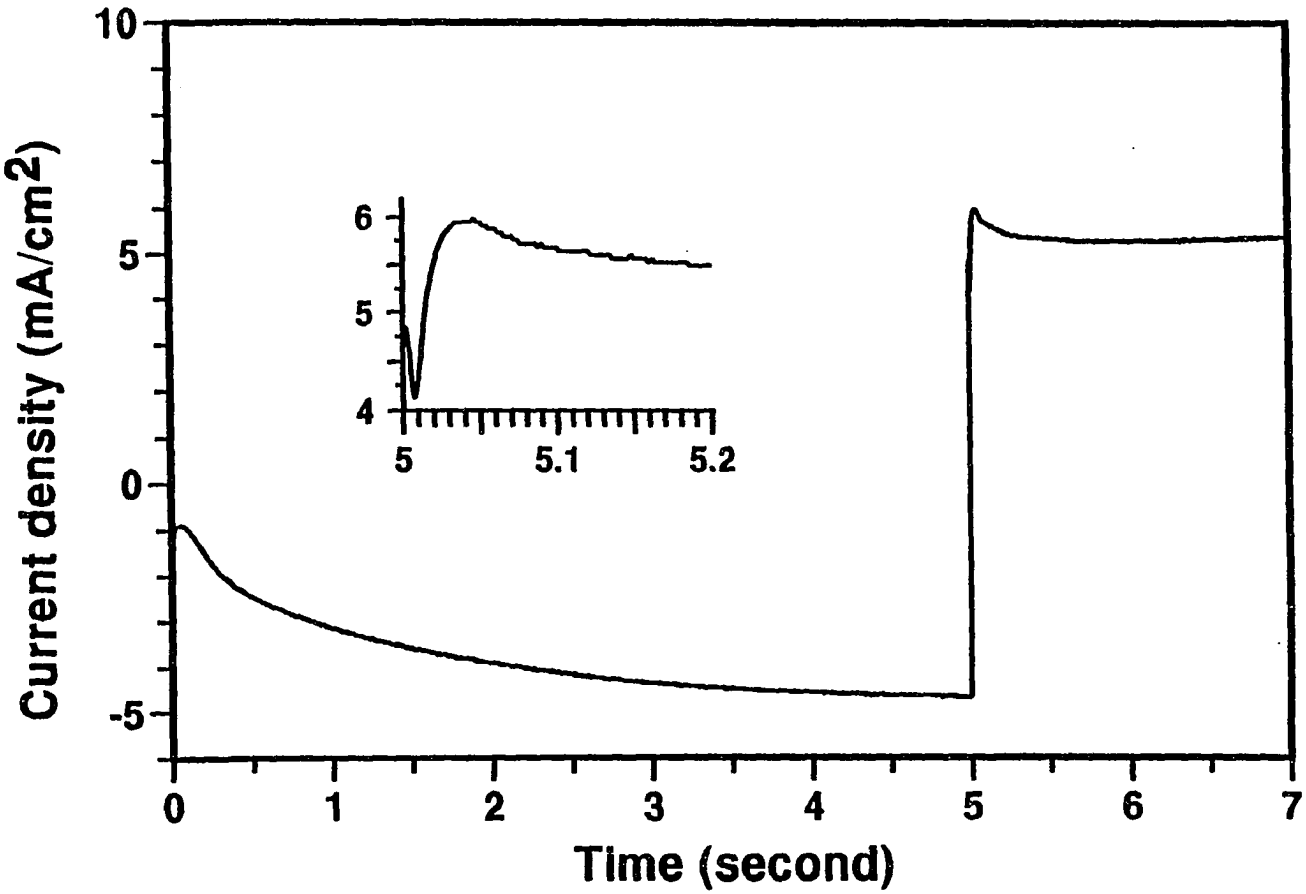

Figure 2. Current transients obtained during cathodic-anodic polarization of Al on AT-cut quartz crystal. Current and frequency shift (see Fig. 1) obtained simultaneously. Inset, initial anodic current transient. Cathodic applied potential -2.0V, anodic applied potential -0.4V.

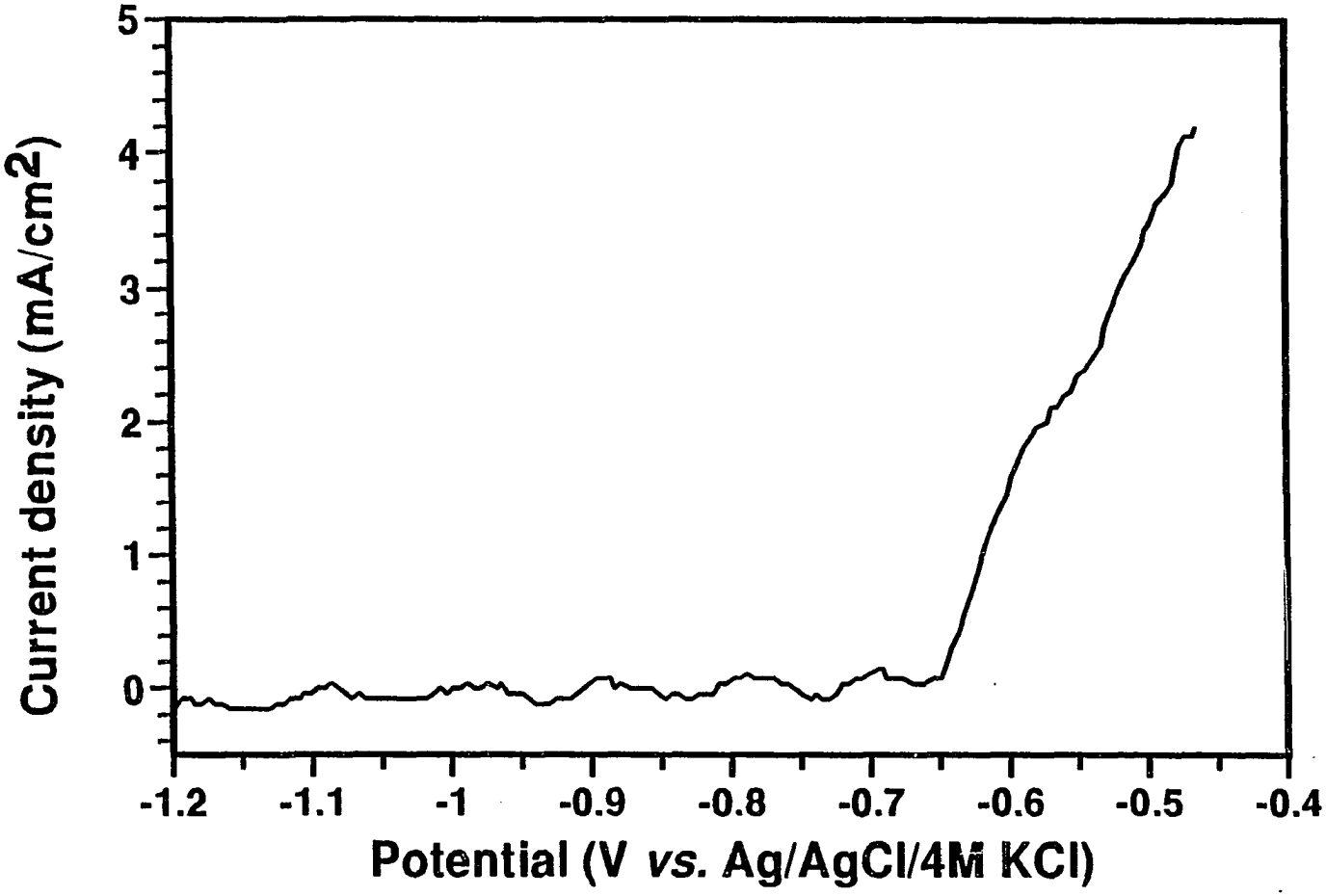

Figure 3. Anodic polarization curve for Al film in 0.1M HCl at room temperature. Potential scan rate 10 mV/s.

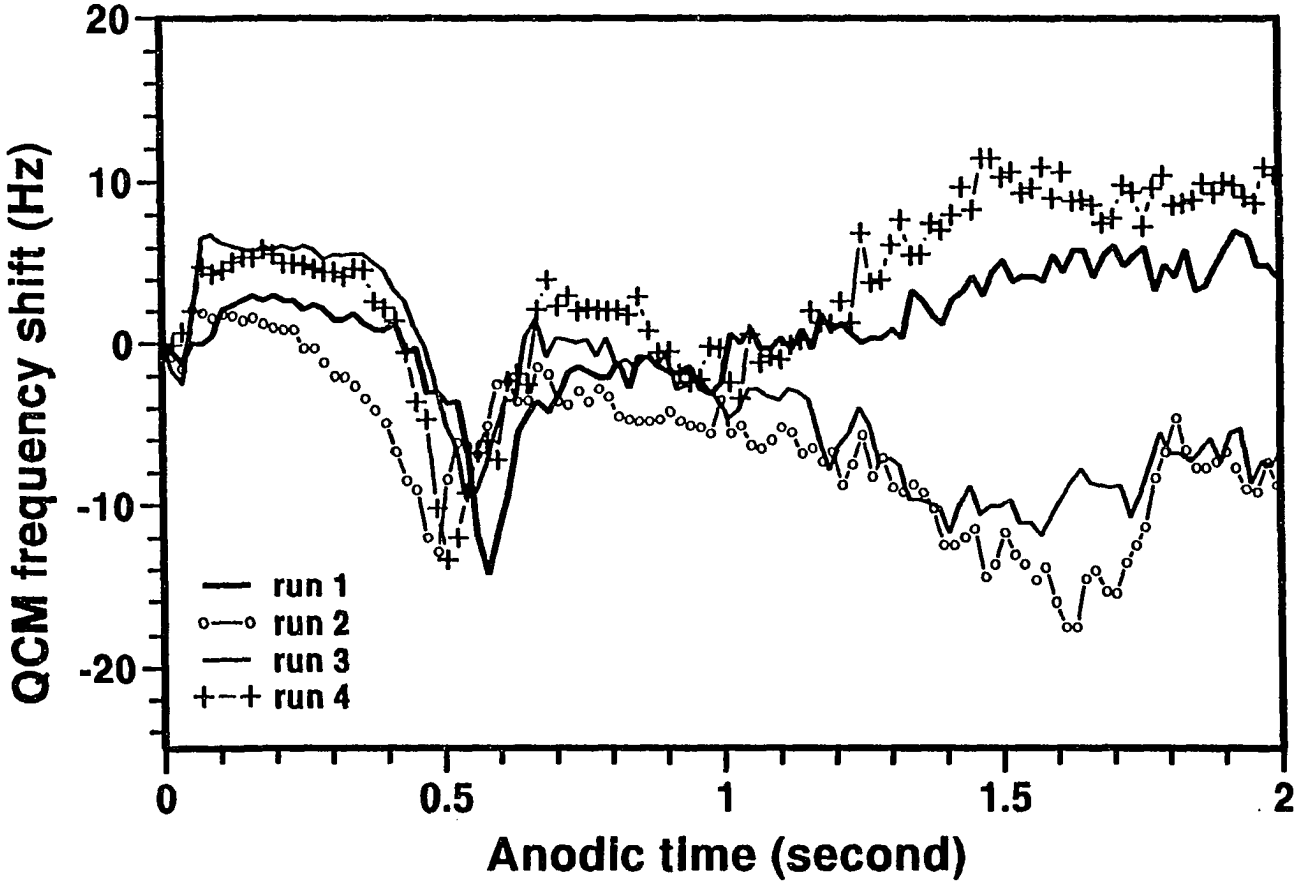

Figure 4. Quartz crystal frequency transients obtained during anodic polarization following cathodic polarization of Al films on AT-cut crystals; 0.1M HCl solution, room temperature. Cathodic potential -2.0V, cathodic time 5s.

value for another 0.2s, the frequency began to decrease, and eventually reached a minimum at about 0.5s. After reaching the minimum value, the frequency rose rapidly and then increased or decreased slowly. The anodic current, which is shown in Fig. 2, reached a maximum at about 40 ms. After the maximum, the anodic current decreased rapidly for 0.2s and then decayed slowly to a constant value. It has been shown that, during the rapid current rise period, the rates of pit initiation and pit growth were rapid, having been enhanced by prior cathodic charging (1,5). Therefore, the anodic frequency transient may be associated with electrode phenomena accompanying rapid pitting corrosion.

Effect of anodic potential.- The relationship between the complex frequency transient and pitting corrosion is demonstrated in Fig. 5. The cathodic conditions were the same for both experiments; they have the same cathodic frequency transient. The anodic potentials were chosen to be just above (-0.6V) and just below (-0.7V) the critical pitting potential of -0.65V (see Fig. 3). As the potential was stepped to different anodic potentials, the corresponding frequency transients were different. Figure 5 shows that, when the potential was stepped to -0.7V, the anodic frequency decreased continuously for about 3s, then remained constant. This frequency transient is similar to ones which had previously been measured at -0.9V, and is due to absorption of water into the surface film (4). On the other hand, a complicated frequency transient, similar to that observed in Fig. 1, was obtained when the potential was stepped to -0.6V.

Figure 6 compares anodic current transients for both potentials. A typical anodic

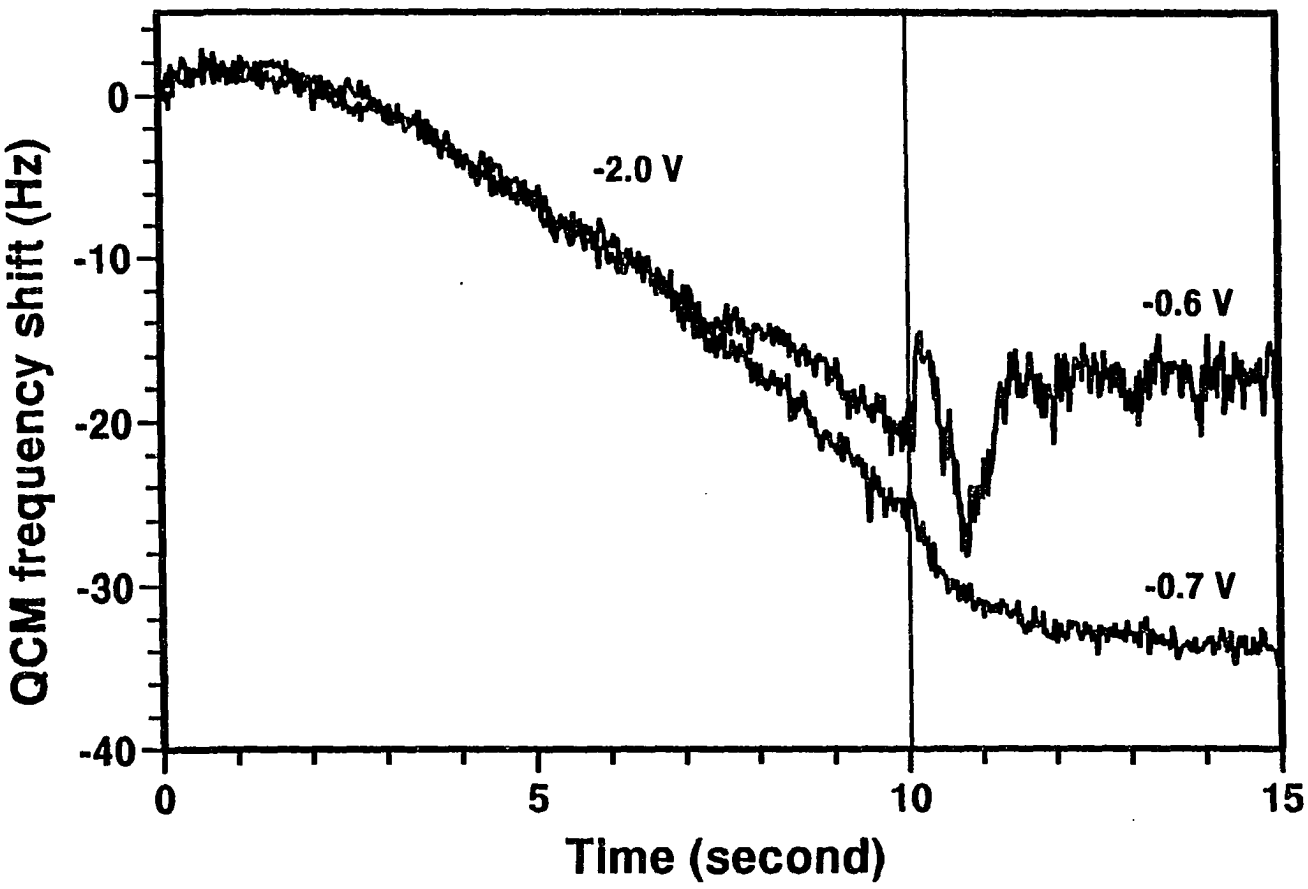

Figure 5. Comparison of anodic frequency transients at different applied anodic potentials; AT-cut quartz crystals. Cathodic potential -2.0V, cathodic time 10s. Anodic potentials as indicated.

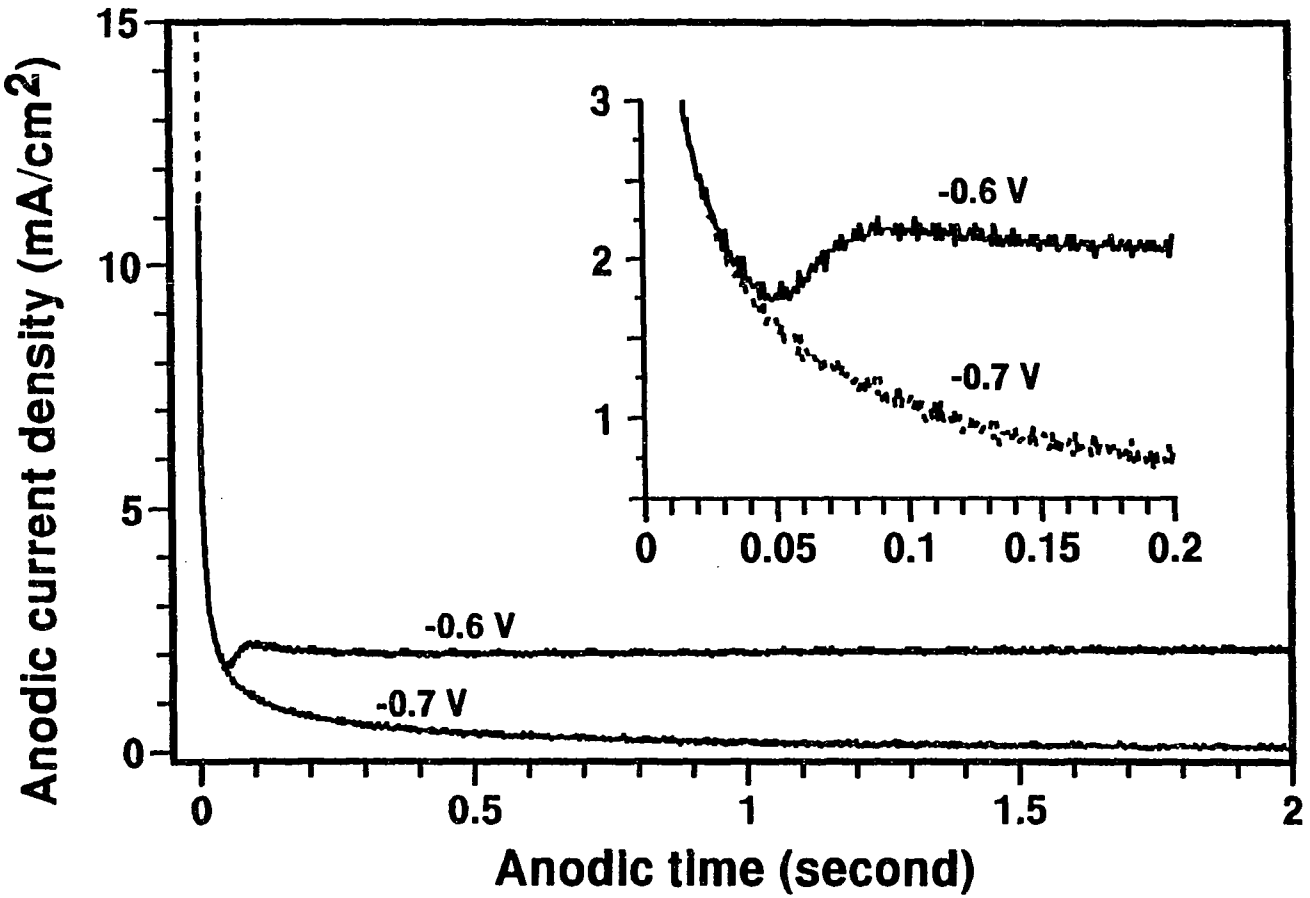

Figure 6. Comparison of anodic current transients at different applied anodic potentials. Cathodic potential -2.0V, cathodic time 10s. Anodic potentials as indicated.

current decay was found for the potential of -0.7V, which is due to oxide film formation induced by prior cathodic charging (4). At the potential of -0.6V, the current decreased initially for about 50 ms and then increased. The current transient at -0.6V, similar to that observed at -0.4V, was due to pitting because pits were observed on sample surface. Therefore, the complex frequency transients in Fig. 4 are associated with pitting corrosion.

Possible factors influencing the frequency transients include: attached foreign mass change (9-10), surface roughness (9,10,12), stress (9,13-16), electrolyte solution density changes caused by gas evolution (9,17), and surface tension changes caused by double layer charging (10). Changes in electrolyte solution density near the surface due to hydrogen evolution might occur during both cathodic and anodic polarization; nevertheless, no complicated frequency transients were observed during cathodic charging, as show in Fig. 1 and Fig. 5, as well as in previous studies (2,4). Therefore, changes of solution density accompanying gas evolution are likely not the cause for the complex anodic frequency transient above the pitting potential. Double layer charging was found to occur within 1 ms of potential step (4), which is much shorter than the time for initial frequency increase of about 0.1s. Further, no frequency increase was observed in experiment where the potential was stepped from -2.0.V to -0.7V (Fig. 5). Therefore, double layer charging is not a likely cause for the frequency transient.

Experiments were carried out to examine the possible effect of surface roughness changes due to pitting on the anodic frequency transient. For this purpose, anodic

polarization above the pitting potential was interrupted partway through the complex frequency transient causing the pits to passivate. For the experiment in Fig. 7, the anodic potential was reduced from -0.4V to -0.9V at 0.3s. Both the frequency transient and the corresponding anodic current are shown. The pitting current was abruptly reduced to zero when the potential was stepped. On the other hand, the frequency transient is essentially the same as those without interruption. Since surface roughness does not further change when the pitting current is zero, the complex frequency transient is apparently not related to electrode roughening. It follows that there must be some processes other than surface roughness change, which account for the frequency behavior.

QCM transient without cathodic charging.- Figures 5-6 showed that the complicated anodic frequency transient was related to pitting. It was of interest to investigate whether the same anodic frequency transient can be induced by pitting corrosion, without the influence of prior cathodic charging. Figure 8 shows the frequency transient as well as charge applied during anodic polarization at -0.4V, without prior cathodic charging. Both frequency and charge increased simultaneously with time indicating that the frequency increase was due to metal dissolution. The frequency increased smoothly without any complex transient like that found in Fig. 1. The corresponding anodic current was also different as can be seen from Fig. 9. The current decreased initially and stayed at zero current for about 3s. The current then began to increase slowly suggesting that rates of pit initiation and pit growth were slow.

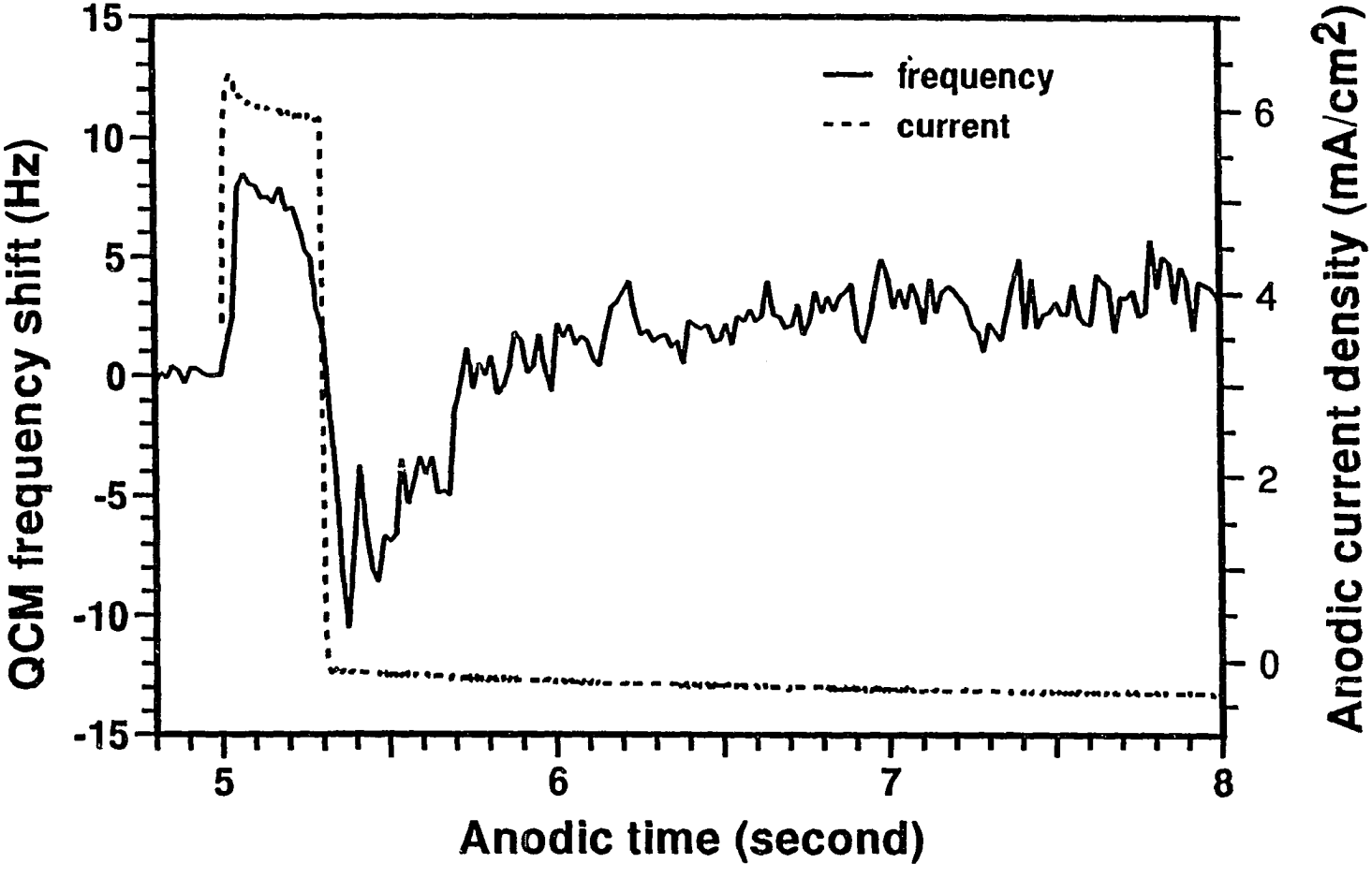

Figure 7. Quartz crystal frequency shift and anodic current transient obtained during anodic polarization following cathodic polarization. AT-cut crystal. Cathodic potential -2.0V, cathodic time 5s. Anodic potentials 5-5.3s -0.4V, 5.3-8s, -0.9V.

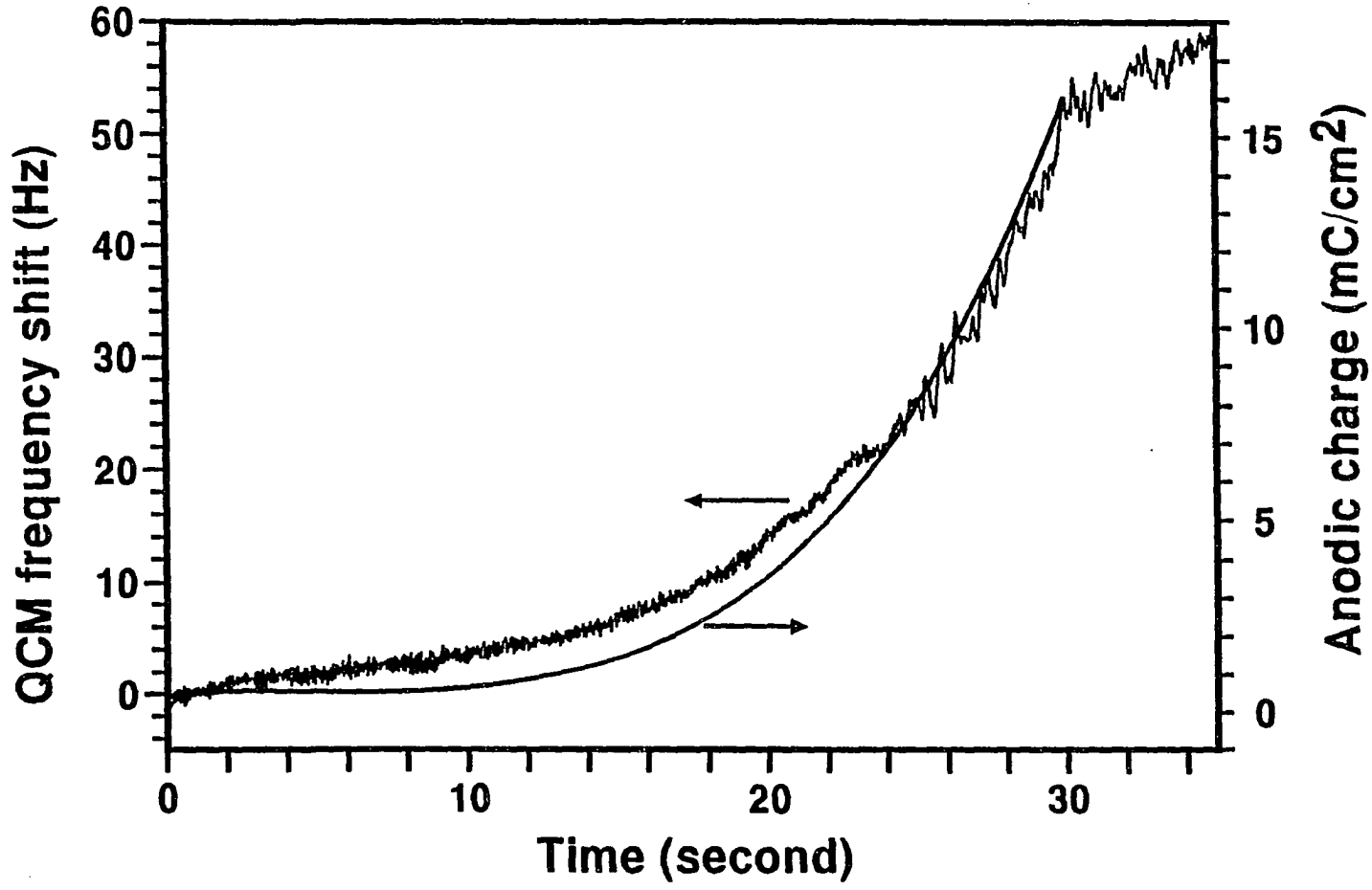

Figure 8. Quartz crystal frequency shift and accumulated anodic charge obtained during anodic polarization; no prior cathodic polarization. AT-cut crystal. Left axis frequency transient, right axis anodic charge.

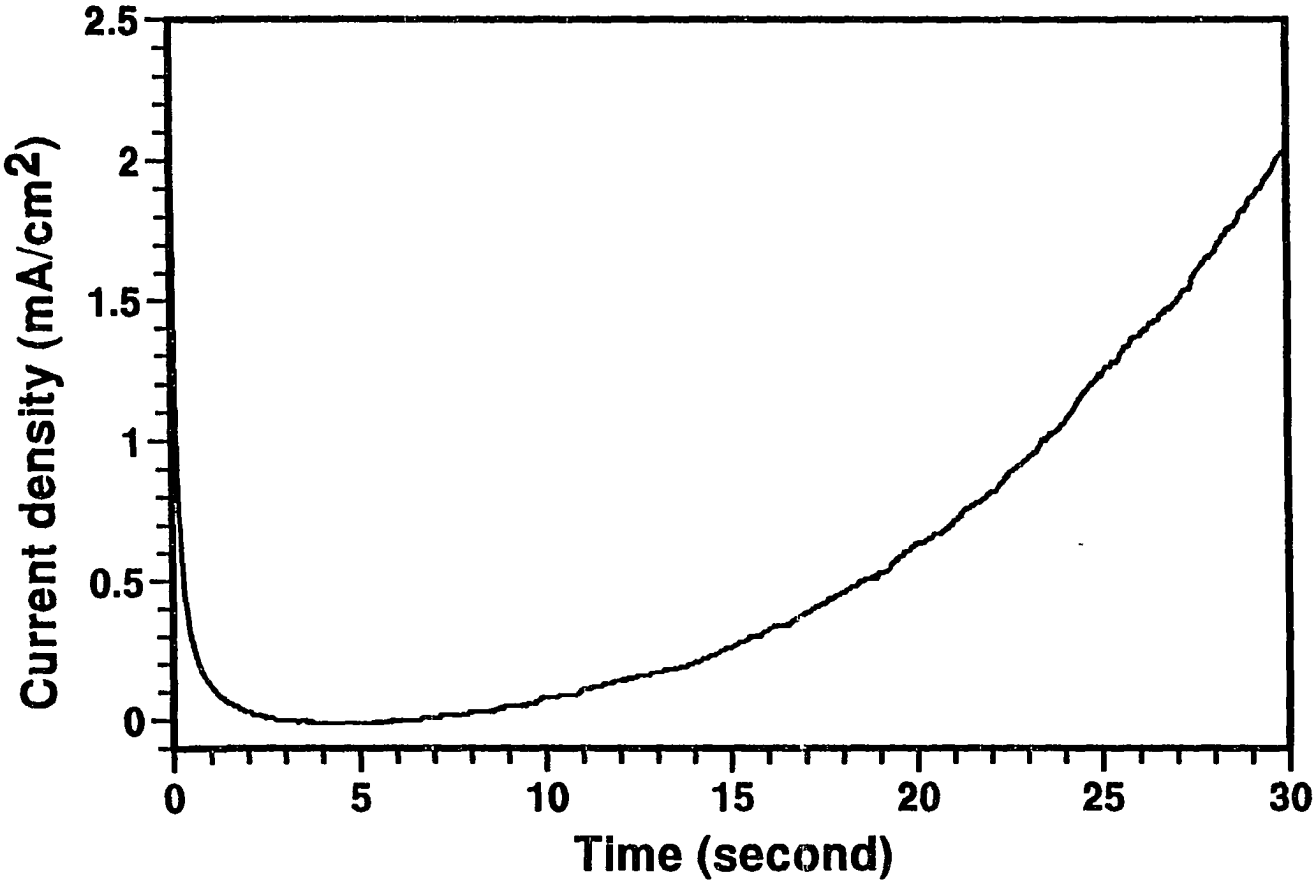

Figure 9. Anodic current transient obtained during anodic polarization; no prior cathodic polarization. AT-cut crystal.

For 5 MHz quartz, the thickness of the solution layer whose mass is coupled to the quartz is on the order of 1 μm (10), which is much larger than the metal film thickness of 0.25 μm. Therefore, recognizing that the void left by aluminum dissolution from the pits was replaced by solution, the total weight change for the electrode can be calculated from the measured anodic charge,

$$W = V_{Al} (\rho_{Al} - \rho_{solution}) \times \frac{Q}{3F} \qquad [1]$$

Where V_{Al} is the molar volume of Al (10.0 cm^3/mole), ρ_{Al} the density of Al (2.7 g/cm^3), and $\rho_{solution}$ the density of 0.1M HCl solution (1.0 g/cm^3), Q the anodic charge and F Faraday's constant. The weight change calculated is 945.6 ng/cm^2, which, according to the Sauerbrey Equation (10,11), corresponds to a frequency increase of 53.5 Hz for 5 MHz AT-cut crystal. This value is the same as the measured frequency change of 53.5 Hz, indicating that the frequency increase in Fig. 8 is due to metal dissolution from pits. The frequency transient in Fig. 8 together with the current transient in Fig. 9 suggests that the complex anodic frequency transient in Fig. 1 is unique only for cathodically-enhanced pitting corrosion.

Determination of stress change.- The frequency transient may partly associated with changes of film stress. Therefore, experiments with AT-cut and BT-cut quartz were conducted to examine any stress change in the film. AT-cut and BT-cut quartz crystals have the same mass constant but opposite stress constant (13) and have been used in the study of stress changes due to electrochemical loading of hydrogen and

deuterium atoms in palladium (15). In order to calculate film stress change, aluminum films were evaporated onto both AT-cut and BT-cut crystals. Cathodic-anodic polarizations were then carried out at the same experimental conditions. The cathodic potential was -2.0V and the cathodic time was 5s. The anodic frequency transients for AT-cut crystals are shown in Fig. 4, and, for BT-cut crystals, in Fig. 10. The frequency shifts were referenced to the first anodic frequency readings of each curve. Figure 10 shows that, in contrast to those of AT crystals, the frequency transients on BT crystals show two peaks with much larger frequency shifts.

The four AT frequency transients in Fig. 4, as well as the four BT frequency transients in Fig. 10, were averaged together to obtain one AT and one BT transient. Stress changes were then calculated from the two averaged frequency transients, according to the method of EerNisse using the following equation (13,15),

$$\Delta S = (K^{AT}-K^{BT})^{-1}\left[\tau_q^{AT}\,\Delta f^{AT}(f^{AT})^{-1} - \tau_q^{BT}\,\Delta f^{BT}(f^{BT})^{-1}\right] \qquad [2]$$

The stress coefficients K^{AT} and K^{BT} have the values 2.75×10^{-12} cm^2/dyne and -2.65×10^{-12} cm^2/dyne, respectively (13,15), the quartz plate thicknesses τ_q are 0.033 cm (AT) and 0.045 cm (BT). Figure 11 shows film stress changes as well as mass changes calculated from Eq. [2]. The figure shows that, during early stage of pitting of about 0.4s, film stress and electrode mass increased simultaneously. After reaching maximum values, both stress and mass decreased. The positive sign indicate that the stress in the metal film is tensile in nature (15). The process was then repeated and a second peak was reached at about 0.8s. Figure 12 shows that there was a linear relationship between

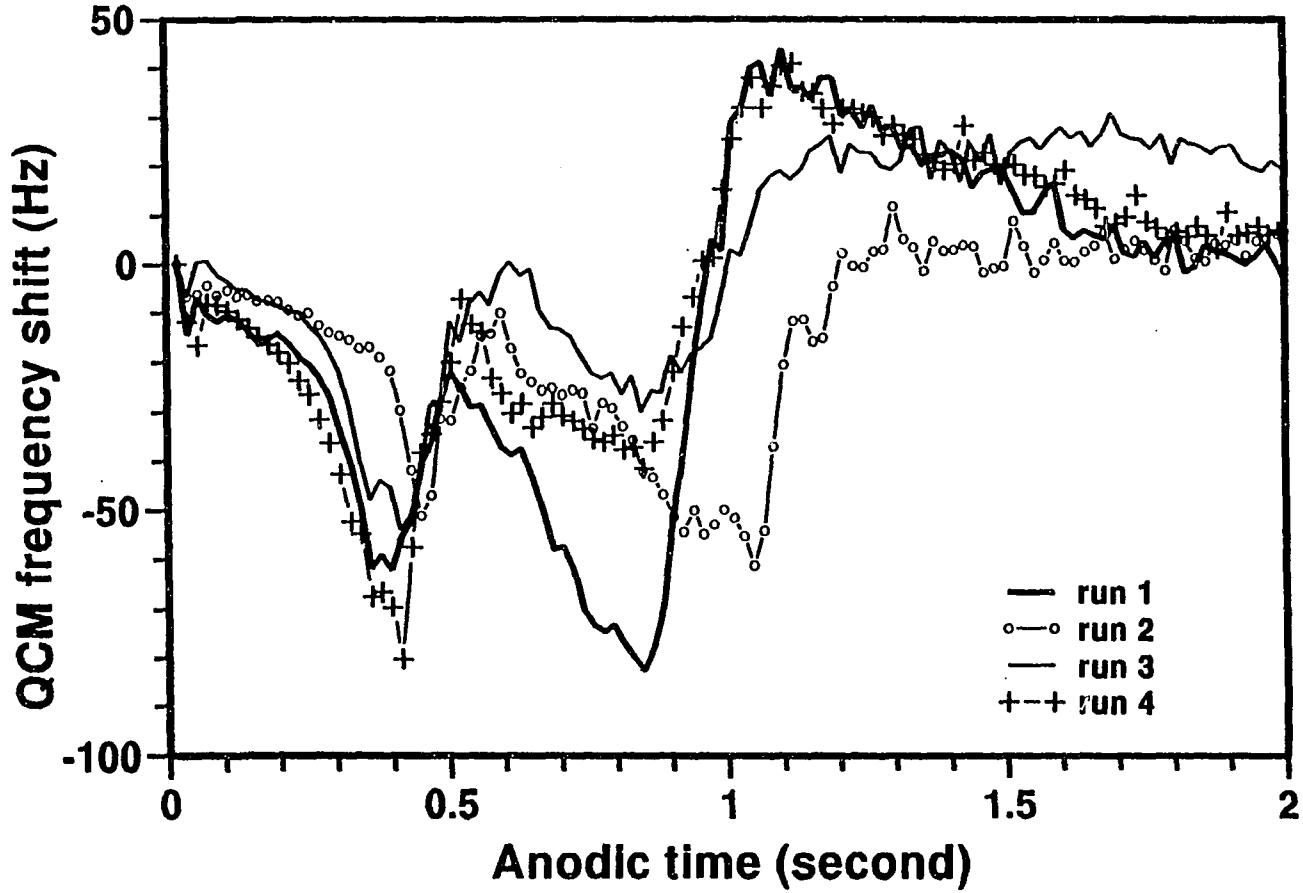

Figure 10. Quartz crystal frequency transients obtained during anodic polarization following cathodic polarization of Al films on BT-cut crystals; 0.1M HCl solution, room temperature. Cathodic potential -2.0V, cathodic time 5s.

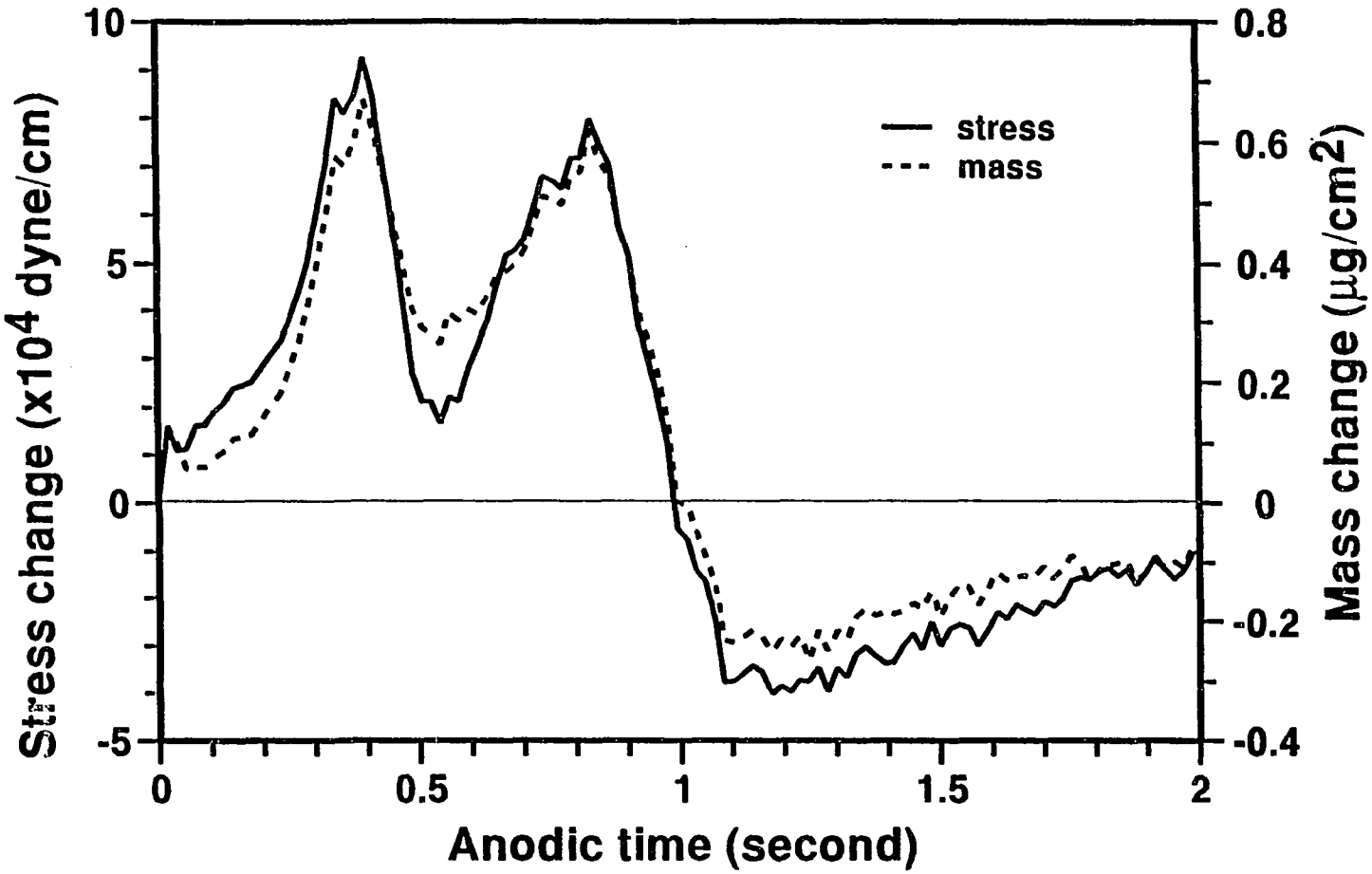

Figure 11. Stress changes and mass changes during anodic polarization following cathodic polarization. Stress change and mass change were calculated from average AT and BT frequency transients in Fig. 4 and Fig. 10 (see text).

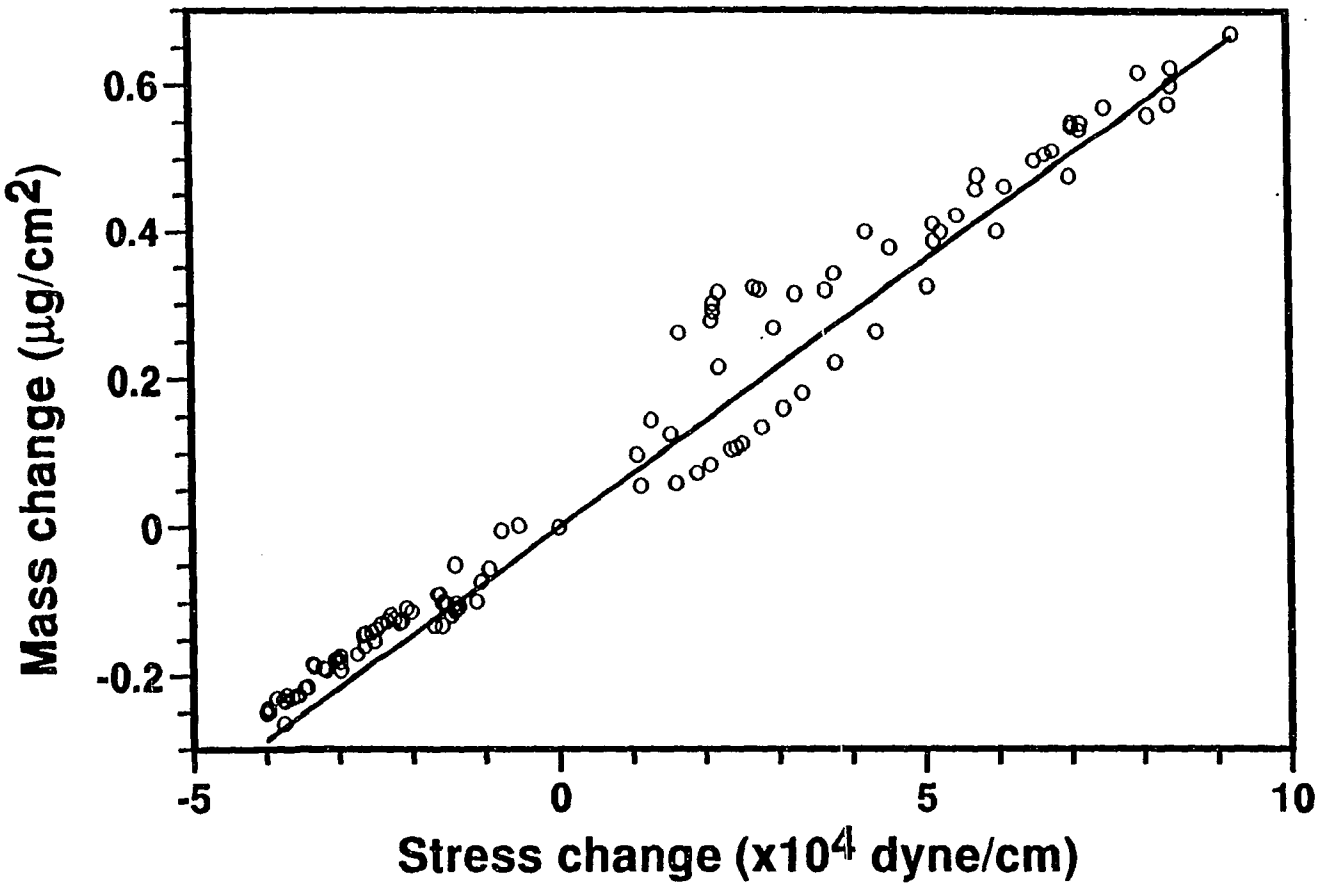

Figure 12. Dependence of mass change on stress change during anodic polarization following cathodic polarization. Stress changes and mass changes obtained from Fig. 11.

mass change and stress during the transient, suggesting that the mass change may be related to "defects" each of which also carries stress. Specific reasons for the simultaneously stress change and mass change, as well as their mutual relationship, can not be given at this time.

DISCUSSION AND CONCLUSIONS

Cathodically-induced pitting corrosion is accompanied by a complex frequency transient of quartz crystal. No complicated frequency transients was observed for pitting corrosion which had not been enhanced by cathodic charging. During early stage of the cathodically-induced pitting corrosion, the electrode mass and film stress increase simultaneously.

The simultaneous mass increase and tensile stress increase are interesting. The frequency decreases during the 5s cathodic polarization varied from 1-7 Hz (about 0.018-0.12 $\mu g/cm^2$) for those experiments in Fig. 4 and Fig. 10. The air-formed oxide film thickness was determined to be 3.1 nm, which corresponds to 0.93 $\mu g/cm^2$ in mass assuming that the film has a density of 3.0 g/cm^3 (2,18). The electrode mass increase about 0.68 $\mu g/cm^2$ during the first 0.4s, which is significant compared to the original film mass and the mass increase due to cathodic film growth. Since the complex transients are specifically found under conditions leading to pitting corrosion, the mass increase in Fig. 11 is likely associated with of Cl^- ions.

The Cl^- ions may be adsorbed on the film and then enter and penetrate the film. The effect of cathodic charging on the rapid pitting current has been shown due to reduce of film resistance, i.e., from more oxide to more hydroxide (2). It is possible that reduce of film resistance allows the transport of Cl^- ions in the film. Cl^- ions may displace OH^- ions or H_2O in the film because the Cl^- ion is a stronger Lewis base than

either OH^- or H_2O (19). Replacement of hydroxide or water by Cl^- would result in changes of chemical bonding of the film. Consequently, the film stress may be changed.

Figure 10 shows that after reaching maximum, both the mass and the stress decrease. If Cl^- ions are absorbed during early stage of pitting corrosion, then decrease of mass implies desorption of Cl^-. As discussed in a previous paper, chemical transformation of the cathodic film from hydroxide to oxide takes place when the potential is stepped from cathodic to anodic (4). The transformation process takes about 3s, which is much longer than the frequency transient period of about 1s. Thus, the simultaneous mass and tensile stress decrease at around 0.4s could possibly due to replacement of Cl^- by oxygen.

Alternatively, since the mass increase is relatively large compared to the film mass and since the process is reversible, it is possible that most of the Cl^- ions are adsorbed on the film surface. If one considers that the anodic charge applied (2.56 mC/cm^2) during the first 0.4s was mainly due to metal dissolution, and the Al^{+3} ions then react with Cl^- to form $AlCl_3$, then a increase of mass of 942 $\mu g/cm^2$ would be expected. This value is an upper limit. The salt film may not stable and may be dissolved at later time. The precipitation/dissolution process of $AlCl_3$ may repeat until the anodic time of about 1s.

ACKNOWLEDGMENTS

Financial support for this work was provided by KDK Corporation (Takahagi, Japan) through a fellowship to Mr. Lin. The authors thank M. D. Porter for supplying the Edwards coating system.

REFERENCES

1. C.-F. Lin and K. R. Hebert, *J. Electrochem. Soc.*, **137**, 3723 (1990).

2. C.-F. Lin and K. R. Hebert, to be submitted.

3. C.-F. Lin and K. R. Hebert, and M. D. Porter, to be submitted.

4. C.-F. Lin and K. R. Hebert, to be submitted.

5. C.-F. Lin and K. R. Hebert, to be submitted.

6. O. Melroy, K. Kanazawa, J. G. Gordon II, and D. A. Buttry, *Langmuir*, **2**, 697 (1986).

7. G. S. Ostrom and D. A. Buttry, *J. Electroanal. Chem.*, **256**, 411 (1988).

8. L. A. Larew, J. S. Gordon, Y.-L. Hsiao, D. C. Johnson, and D. A. Buttry, *J. Electrochem. Soc.*, **137**, 3071 (1990).

9. D. A. Buttry, in "Electrochemical Interfaces," H. D. Abruña Editor, p. 531, VCH Publishers, New York (1991).

10. S. Bruckenstein and M. Shay, *Electrochim. Acta.*, **30**, 1295 (1985).

11. G. Sauerbrey, *Z. Phys.*, **155**, 206 (1959).

12. R. Schumacher, J. G. Gordon and O. Melroy, *J. Electroanal. Chem.*, **216**, 127 (1987).

13. E.P. EerNisse, *J. Appl. Phy.*, **43**, 1330 (1972).

14. A. Grzegorzewski and K. E. Heusler, *J. Electroanal. Chem.*, **228**, 445 (1987).

15. G. T. Cheek and W. E. O'Grady, *J. Electroanal. Chem.*, **277**, 341 (1990).

16. L. Gräsjo and M. Seo, *J. Electroanal. Chem.*, **296**, 233 (1990).

17. C. Gabrielli, F. Hute, M. Keddam and R. Torresi, *J. Electroanal. Chem.*, **297**, 515 (1991).

18. D. R. Lide, "CRC Handbook of Chemistry and Physics," 71st ed., p. 4-41, CRC press, Boston (1990).

19. P. Fugassi and E. G. Haney, in " Titanium Science and Technology," R. I. Jaffee and H. M. Burte, Editors, p. 2611, Plenum Press, New York (1973).

GENERAL CONCLUSIONS

In this dissertation, the effect of electrochemical reaction on the surface film composition and corrosion resistance of aluminum in acid solutions have been studied. The effect of cathodic charging on the surface aluminum oxide film have been studied through polarization curves as well as *in-situ* weight change measurements. Results from polarization curves studies showed that cathodic charging "activates" the aluminum surface at the potential around -1.65V, where the hydrogen evolution rate increases abruptly and film growth begins. The effect of cathodic charging is to reduce the oxide film resistance for ion transport, through change of the film composition from oxide to hydroxide. A 5 minutes immersion of the sample in the electrolyte solution, prior to cathodic charging, is also necessary for the cathodic activation. It was shown that pH, instead of the anion, is responsible for the effect of pretreatment on cathodic activation.

The mass of the electrode begins to increase at the potential where the hydrogen evolution kinetics changed. The mass increase was shown due to formation of surface oxide film. Change of pH on the electrode surface was shown to be insignificant, which indicates that the film is unlikely produced through a precipitation mechanism. The rate of proton conduction was found to follow Ohm's law, and the conductivity of the film has the same order of magnitude as precipitated aluminum hydroxide. The composition of the cathodically produced film was determined to be containing at least four oxygen atoms for every aluminum atom, which indicates that at least one water molecule per Al

atom. Appreciable amount of water in the film was considered to be responsible for the increase of film conductivity.

The cathodic film composition and structural information were further studied using *ex-situ* infrared reflection spectroscopy. The cathodic product detected by infrared spectroscopy is an aluminum oxide or hydroxide which contains water. The peak areas for three major bands increased linearly with cathodic charge suggesting that the film maintains an approximately uniform composition as it become thicker. The spectra for the cathodic products compare most favorably to that of the porous, amorphous oxide films formed by anodizing in acid solution. The OH groups or H_2O molecules of the film are readily accessible to exchange by D_2O indicating that the film has an "open" structure. The aluminum ions in the film are coordinated to hydroxyl groups.

The effect of cathodic polarization on anodic oxidation processes were investigated using the quartz crystal microbalance technique. Cathodic charging of aluminum in acid solution induced an anodic current transient accompanied by an electrode mass increase, which was primarily due to water absorption into the film. The anodic current decay is due to an increase of film resistance by three order of magnitude. Change of film composition during cathodic charging was responsible for the observed anodic current and mass transients. Chemical reactions in the film involving water which had been stored in the film during cathodic charging were considered to be responsible for the dependence of anodic mass increase, anodic charge and anodic current decay on cathodic film mass. Excess water in the hydroxide film

reacts with the aluminum metal to produce aluminum oxide, thus increasing the film resistance. As chemical reaction proceeded, the film resistance increased which resulted in decreases of anodic current and the rate of water absorption.

The effect of cathodic charging on pitting corrosion resistance of aluminum films in acid aqueous solution was also studied using electrochemical methods and scanning electronic microscopy. Prior cathodic polarization induced rapid oxidation reaction during the first 20 ms of anodic polarization at -0.4V. The rates of pit initiation and pit growth were also enhanced by cathodic charging during the first 30 ms. The effect of cathodic charging was to reduce film resistance for ion transport, which was considered to be responsible for the increased rates of pit initiation and pit growth. Pits initiate over a longer period of time with greater oxide film mass. The pitting current diminished if oxidation reaction was allowed to take place more than 20 ms at -0.9V before the potential was stepped to -0.4V. The film resistance increased three order of magnitude after an 1s of oxidation at -0.9V. Increase of film resistance was responsible for the decreased rates of pit initiation and pit growth.

Finally, observations of the effect of prior cathodic charging on the quartz crystal microbalance frequency transient during anodic polarization at potentials above the pitting potential were reported. Cathodic charging of aluminum in acid solution induces a rapid current increase, at potentials above the pitting potential, which is accompanied by a complex quartz crystal vibration frequency transient. Without prior cathodic charging, the vibration frequency increases continuously with anodic time, which is

mainly due to metal dissolution. The cathodically-induced complex frequency was resolved by AT-cut and BT-cut quartz, and simultaneous mass increase and tensile stress increase during the early stage of pitting corrosion were observed. It is believed that further understanding of the mutual relationship between stress change and mass change during anodic polarization following cathodic polarization will provide information important in understanding pitting corrosion.

REFERENCES

1. A. T. Fromhold, Jr., in "Passivity of Metals," R. P. Frankenthal and J. Kruger, Editors, p. 59, the Electrochemical Society, Inc., Princeton, NJ (1977).

2. J. R. Galvele, in "passivity of Metals," R. P. Frankenthal and J. Kruger, Editors, p.285. The electrochemical Society, Princeton, New Jersey (1978).

3. H.-H. Strehblow, *Werkst. Korros.*, **35**, 437 (1984).

4. Z. Szklarska-Smialowska, "Pitting Corrosion of Metals," p. 337-401, NACE, Houston, Texas (1986).

5. H. Bohni, in "Corrosion Mechanisms," F. Mansfeld, Editor, p. 285-323, Marcel Dekker, Basel, New York (1987).

6. J. Tousek, "Localized Corrosion of Metals", p. 1, Trans Tech Publications Ltd, Switzerland (1985).

7. C.-F. Lin and K. R. Hebert, *J. Electrochem. Soc.*, **137**, 3723 (1990).

8. C.-F. Lin, M.S. Thesis, Iowa State University, Ames, IA(1989).

9. G. C. Wood, *Corros. Sci.*, **11**, 901 (1971).

10. B. J. Wiersma and K. R. Hebert, *J. Electrochem. Soc.*, **138**, 48 (1991).

11. A. K. Vijh, *J. Phys. Chem.*, **72**, 1148 (1968).

12. J. O'M Bockris, *Chem. Rev.*, **43**, 525 (1948).

13. J. O'M. Bockris in "Modern Aspects of Electrochemistry," Vol I, J. O'M. Bockris and B. E. Conway, Editors, Butterworth and Co., Ltd., London, 1954, Chapter IV.

14. B. E. Conway and M. Salomon, *Electrochim Acta*, **9**, 1599 (1964).

15. B. E. Conway, *Trans. Roy. Soc. Can.*, **54-III**, 19 (1960).

16. A. K. Vijh, *J. Phys. Chem.*, **73**, 506 (1969).

17. J. Krunze. *Corros. Sci.*, **7**, 723 (1967).

18. J. Radoševič, M. Kliškič, P. Dabič, R. Stevanovič and A.Despič, *J. Electroanal.Chem.*, **277**, 105 (1990).

19. H. Kaesche, in :Localized Corrosion," R. W. Staehle *et al.* Editors, p. 516, NACE, Houston (1974).

20. E.P.G.T. ven de Ven and H. Koelmans, *J. Electrochem. Soc.*, **123**, 143 (1976).

21. W. Vedder and D. A. Vermilyea, *Trans. Faraday Soc.*, **65**, 561 (1969).

22. M. J. Pryor and D. S. Krie, *J. Electrochem. Soc.*, **102**, 605 (1955).

23. F. H. Haynie and S. J. Ketcham, Corrosion, **19**, 403t (1963).

24. C. W. Goulding and T. C. Downie, *Metallurgia*, **68**, 93 (1963).

25. J. W. Diggle, T. C. Downie and C. W. Goulding, *Corros. Sci.*, **8**, 907 (1968).

26. K. Nisanciouglu and H. Holtan, *Corros. Sci.*, **19**, 537 (1979).

27. A. R. Despič, D. M. Dražič, J. Balakšina, Lj. Gajič-Krstajič, and R. M. Stevanovič, *Electrochim. Acta*, **35**, 1747 (1990).

28. G. E. Thompson and G. C. Wood, *Corros. Sci.*, **18**, 721 (1978).

29. C. K. Dyer and R. S. Alwitt, *J. Electrochem. Soc.*, **128**, 300 (1981).

ACKNOWLEDGMENTS

First of all, I am sincerely grateful to my research adviser, Professor Kurt R. Hebert, for the support he gave me during the whole program. It is hard to imagine that this dissertation could be completed without his patient guidance. I hope I can find a better word than "thanks" to express my gratitude.

I would like to thank KDK Corporation (Takahagi, Japan) for their financial support for this work through a fellowship to me.

I would like to thank Drs. Terry S. King, Marc D. Porter, John D. Verhoeven and Gordon R. Youngquist for serving on my advisory committee.

I would also like to thank former and current group members: Bruce Wiersma, Yongsug Tak, Isamu Obi, Xiaolin Wu, Joe Isaac, Mei-hui Wang and Mark Aspengren for their help and friendship.

I would especially like to thank my wife, Chiu-guei, for her patience and support which have made my graduate studies easier. Special thanks give to my little son and daughter, Jeff and Joyce, for their love and spiritual support.

Finally, I would like to thank and to dedicate this work to my family for their encouragement all the time so far away from home.

APPENDIX.

A THERMODYNAMIC MODEL FOR THE ALUMINUM ELECTRODE IN ACIDIC SOLUTIONS

A Thermodynamic Model for the Aluminum Electrode in Acidic Solutions

K. R. Hebert and C.- F. Lin

A model for the aluminum/solution interface in acidic aqueous solutions is described. The model includes thermodynamics and kinetics of processes at the metal/oxide film interface (hydrogen evolution, aluminum oxidation) and at the film/solution interface (hydrogen, aluminum, and oxide ion transfer, and water absorption). In addition, thermodynamic equilibria within the film between oxide, hydroxide, and hydrogen ions and water molecules are considered, as well as transport of hydrogen and aluminum ions through the film. The formalism of macroscopic thermodynamics is followed. The model is believed to be the first model for an oxide-covered metal, which considers cathodic as well as anodic processes, and predicts changes in the film composition as a result of electrochemical reactions.

The model equations, together with the available kinetic data, are used to obtain a semi-quantitative explanation for variations in film composition during cathodic and subsequent anodic polarization of aluminum in acid solution. These composition changes caused by electrochemical reactions induce profound changes in the film's electrical resistance and consequently its influence on corrosion rate. The observations to be explained are: (1) Upon cathodic polarization below about -1.63V NHE, the resistance of the film is greatly diminished over a period of a few seconds, and, after about 2 seconds, a film begins to grow on the electrode surface. (2) After the potential is then

stepped into the passive region below the pitting potential (e. g., -0.68V NHE), the anodic current is initially much larger than the passive current (about 10 mA/cm^2) and then decays over a period of about 5 seconds to values of about 10 $\mu A/cm^2$. This anodic current transient is accompanied by an electrode mass increase, which is primarily due to water absorption into the film.

Reactions.- The chemical and electrochemical reactions which are included in the model are indicated in Fig. 1. The reactions at the metal/film interface are aluminum oxidation and hydrogen evolution,

$$Al \rightarrow Al^{+3}_{(film)} + 3e^- \qquad [1]$$

$$H^+_{(film)} + e^- \rightarrow \frac{1}{2} H_2 \qquad [2]$$

Both these reactions are considered to be irreversible. Aluminum, hydrogen and oxide ions can be transferred between the film and the solution at the film/solution interface,

$$Al^{+3}_{(film)} \rightleftharpoons Al^{+3}_{(solution)} \qquad [3]$$

$$H^+_{(film)} \rightleftharpoons H^+_{(solution)} \qquad [4]$$

$$O^{-2}_{(film)} + 2H^+_{(solution)} \rightleftharpoons H_2O_{(solution)} \qquad [5]$$

Also, water molecules may be transferred between the film and solution,

$$H_2O_{(film)} \rightleftharpoons H_2O_{(solution)} \qquad [6]$$

The major constituents of the film are considered to be aluminum, oxide and hydroxide

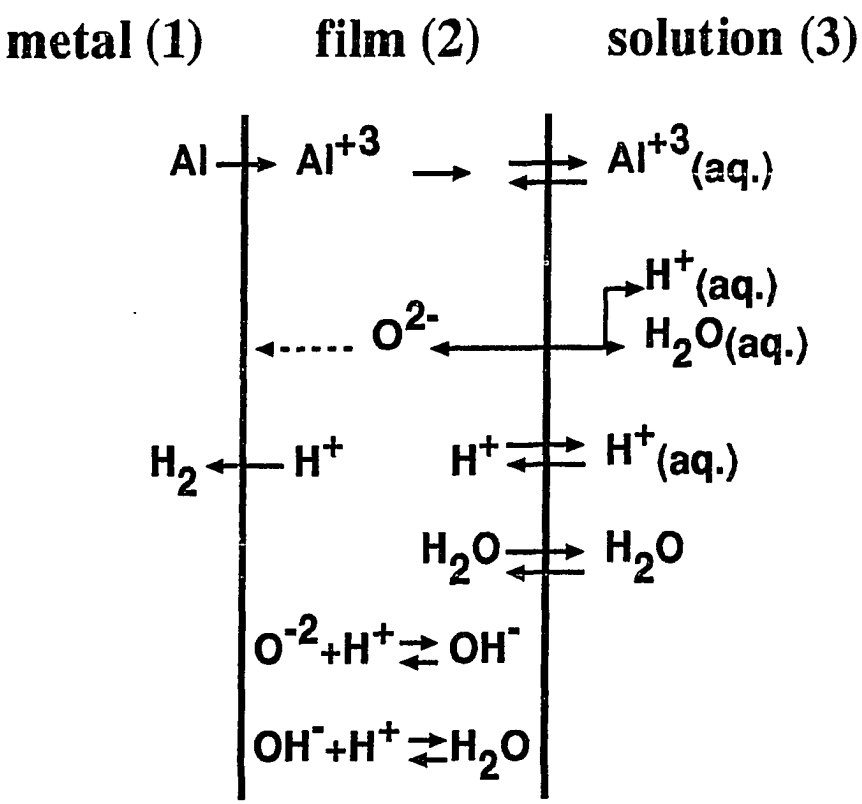

Figure 1. Schematic representation of chemical and electrochemical reactions at the metal/film interface, in the film and at the film/solution interface.

ions, and water. Hydrogen ions are also present, but their concentration is assumed to be insignificant compared to those of the other species. Two hydration reactions involving protons are considered to proceed in the film,

$$O^{-2} + H^{+} \rightleftharpoons OH^{-} \qquad [7]$$

$$OH^{-} + H^{+} \rightleftharpoons H_2O \qquad [8]$$

These homogeneous reactions are assumed to be at equilibrium. Because hydrogen ions are in equilibrium with water both in the film and in the solution, it can be seen that reactions [4] and [5] are thermodynamically equivalent to reaction [6]. However, since reaction [6] is a physical or chemical absorption process, its kinetic driving force is different from those of the electrochemical reactions [4] and [5]. Therefore, water absorption is included as a distinct reaction.

Cell potential.- The experimentally measured cell potential is taken with respect to a hydrogen reference electrode in equilibrium with the cell electrolyte solution. The cell potential can be decomposed into a series of overpotentials,

$$V = \eta_H^{12} + \eta_H^{2} + \eta_H^{23} + \eta_H^{3} \qquad [9]$$

$\eta_H{}^{ij}$ is the hydrogen overpotential between points i and j,

$$F\eta_H^{ij} = \mu_{H^+}^{i} - \mu_{H^+}^{j} \qquad [10]$$

so that if $\eta_H{}^{ij}$ is positive, the current due to hydrogen ion transfer is anodic. In Eq. [9], the superscript 12 refers to overpotential across the metal/film interface; 2 to

overpotential across the film, between the film side of the metal/film interface and the film side of the film/solution interface; 23 to overpotential across the film/solution interface; and 3 to overpotential between the solution side of the film/solution interface, and the reference electrode. The superscripts on electrochemical potentials refer to the phases in which the ionic species are found: 1, 2, and 3 correspond to the metal, film, and solution respectively. The overpotential across the metal/film interface can be written as

$$F\eta_H^{12} = \frac{1}{2}\,\mu_{H_2}^{21} - \mu_{e^-}^{1} - \mu_{H^+}^{21} \qquad [11]$$

Superscripts of the type ij on chemical or electrochemical potentials specify phase i near its interface with phase j. The chemical potential of hydrogen gas is assumed to be constant throughout the system, so that the cell potential is independent of hydrogen pressure. The solution overpotential η_H^3 contains concentration and ohmic overpotentials.

An equation for the cell potential V can also be written in terms of the overpotentials for aluminum ion transfer,

$$\begin{aligned} 3FV = {} & (3/2\ \mu_{H_2} - \mu_{Al}) + (\mu_{Al^{3+}}^{32} - 3\mu_{H^+}^{32}) \\ & + 3F(\eta_{Al}^{12} + \eta_{Al}^{2} + \eta_{Al}^{23}) + 3F\eta_H^3 \end{aligned} \qquad [12]$$

The overpotentials for aluminum are defined in a way analogous to Eq. [2],

$$3F\eta_{Al}^{ij} = \mu_{Al}^{i} - \mu_{Al}^{j} \qquad [13]$$

The first term in parentheses in Eq. [12] is zero, since both hydrogen and aluminum are in their standard states. The second term in parentheses depends on the solution composition at the film/solution interface (superscript 32),

$$\mu^{32}_{Al^{+3}} - \mu^{32}_{H^{+}} = RT \ln \left[\lambda^{\theta}_{Al^{+3}} / (\lambda^{\theta}_{H^{+}})^3\right] + RT \ln \left[m_{Al^{+3}} / (m_{H^{+}})^3\right] + RT \ln \left[\gamma_{Al^{+3}} / (\gamma_{H^{+}})^3\right] \quad [14]$$

where λ_i^{θ} represents the secondary reference state, m_i is molality, and γ_i is the molality-based activity coefficient. If the system is in equilibrium with all components in their standard states, the only non-zero term in the cell potential is the term in Eq. [14] containing secondary reference states; this term is then related to the standard potential of the aluminum electrode, and has the value -1.663V x 3F (1).

All the overpotentials in Eqs. [9] and [12] are related to the rates (currents) for the corresponding reactions by the appropriate kinetic expressions.

Film composition. - The overpotentials in Eqs. [1] and [4] depend on the electrochemical potentials of ions in the film. In order to draw relations between these overpotentials, it is necessary to define the model's assumptions about the surface film composition.

It is convenient to write the thermodynamic equations for the film in terms of the chemical potentials of neutral rather than charged species. The neutral ionic compounds which contain the ions in the film are aluminum hydroxide and aluminum oxide. The chemical potentials of these compounds are related to the electrochemical potentials of the ions by dissociation equilibria,

$$\mu_1 = \mu_{Al_2O_3} = 2\mu_{Al^{+3}} + 3\mu_{O^{-2}} \quad [15]$$

$$\mu_2 = \mu_{Al(OH)_3} = \mu_{Al^{+3}} + 3\mu_{OH^-} \quad [16]$$

In addition, it is assumed that hydrogen ions in the film are in equilibrium with hydroxide ions and water,

$$\mu_3 = \mu_{H_2O} = \mu_{H^+} + \mu_{OH^-} \quad [17]$$

and that hydrogen ions are also in equilibrium with oxide and hydroxide ions,

$$\mu_{OH^-} = \mu_{H^+} + \mu_{O^{-2}} \quad [18]$$

Eqs. [15] - [18] can be combined to obtain an equilibrium relationship between the chemical potentials of the constituent neutral species of the film,

$$2\mu_{Al(OH)_3} = 3\mu_{H_2O} + \mu_{Al_2O_3} \quad [19]$$

The chemical potentials of neutral species depend only on composition, and not on the electrical state of the material (i. e., the electrostatic potential). As a first approximation, the film is considered to be an ideal mixture of aluminum hydroxide, aluminum oxide, and water. Accordingly, the chemical potential of one of the neutral components is

$$\mu_i = \mu_i^o + RT \ln x_i \quad [20]$$

for i = 1, 2, 3. μ_i^o is the standard chemical potential of component i and x_i is the mole fraction. The standard chemical potentials of aluminum oxide and aluminum hydroxide

are taken to be the same as the bulk compounds (1). The standard chemical potential of water may differ from that of bulk water, by the absorption (either chemical or physical) energy of water in the oxide film.

Since the mole fractions of the three components must add to unity, Eq. [19] implies that there is only one compositional degree of freedom for the film. Thus, large water chemical potentials imply that the hydroxide content of the film is high compared to the oxide content. When the water chemical potential is small, the film composition is predominantly aluminum oxide. Alternatively, low ratios of moles of oxygen to moles of aluminum are associated with relatively anhydrous oxide films, while high ratios of moles of oxygen to moles of aluminum imply hydrated hydroxide films.

Relationships between overpotentials.- The equilibria in the film relate the electrochemical potentials of ionic species in the film. For this reason, overpotentials of different reactions proceeding at the same interface are not independent. For example, at the metal/film interface, the overpotentials for aluminum oxidation and hydrogen evolution can be related through Eqs. [15] and [16],

$$3F\eta_H^{12} = 3F\eta_{Al}^{12} + (\mu_1^{21} - \mu_2^{21}) \qquad [21]$$

At the film/solution interface, a relationship exists between the overpotentials for aluminum ion and hydrogen ion transfer,

$$3F\eta_{Al}^{23} = 3F\eta_H^{23} + (\mu_1^{23} - \mu_2^{23}) + (3\mu_{H^+}^{32} - \mu_{Al^{+3}}^{32}) \qquad [22]$$

Also at the film/solution interface, aluminum ion transfer is coupled to transfer of oxide ions, whose overpotential is

$$2F\eta_O^{23} = \mu_3^3 - 2\mu_{H^+}^{32} - \mu_{O^{-2}}^{23} \qquad [23]$$

The relationship between these two overpotentials is

$$3F\eta_{Al}^{23} = 3F\eta_O^{23} + 1/2\ \mu_1^{23} - 3/2\ \mu_3^3 + (3\mu_{H^+}^{32} - \mu_{Al^{+3}}^{32}) \qquad [24]$$

The overpotentials driving transport of hydrogen and aluminum ions through the film are also related. The hydrogen transport overpotential can be related to the overpotential for aluminum ion transport and the film composition through Eq. [15], [16], and [18],

$$3F(\eta_H^2 - \eta_{Al}^2) = (\mu_2^{21} - \mu_1^{21}) - (\mu_2^{23} - \mu_1^{23}) \qquad [25]$$

Eqs. [21], [22], [24] and [25] can be thought of as statements that the driving forces for different electrochemical processes at an interface are coupled through their common dependence on the electrical potential difference across the interface. These equations also indicate that changes in the driving force for an interfacial reaction are brought about by changes inthe electrical potential difference at the interface, or by changes in the film composition.

References

1. M. Pourbaix, "Atlas of Electrochemical Equilibria in Aqueous Solutions," p. 168, Pergamon Press, Oxford (1966).